AD-A268 394

WL-TR-93-3058

AN EXPERIMENTAL STUDY OF FLUCTUATING WALL
PRESSURES IN A HIGHLY SWEPT, SHARP FIN-
INDUCED, MACH 5 SHOCK WAVE/TURBULENT
BOUNDARY LAYER INTERACTION

John D. Schmisseur

Final Report for Period August 1990 to May 1992

DTIC
ELECTE
S AUG 2 4 1993
B   D

Approved for public release; distribution is unlimited

FLIGHT DYNAMICS DIRECTORATE
WRIGHT LABORATORY
AIR FORCE MATERIEL COMMAND
WRIGHT-PATTERSON AIR FORCE BASE, OHIO 45433-7562
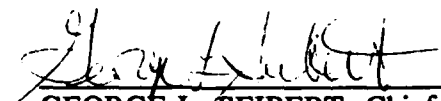
93 8 23 134

93-19630

NOTICE

When Government drawings, specifications, or other data are used for any purpose other than in connection with a definitely Government-related procurement, the United States Government incurs no responsibility or any obligation whatsoever. The fact that the government may have formulated or in any way supplied the said drawings, specifications, or other data, is not to be regarded by implication, or otherwise in any manner construed, as licensing the holder, or any other person or corporation; or as conveying any rights or permission to manufacture, use, or sell any patented invention that may in any way be related thereto.

This report is releasable to the National Technical Information Service (NTIS). At NTIS, it will be available to the general public, including foreign nationals.

This technical report has been reviewed and is approved for publication.

JOHN D. SCHMISSEUR
Aerospace Engineer
Experimental Facilities Research Branch

GEORGE L. SEIBERT, Chief
Experimental Facilities Research Branch
Aeromechanics Division

DENNIS SEDLOCK, Chief
Aeromechanics Division
Flight Dynamics Directorate

If your address has changed, if you wish to be removed from our mailing list, or if the addressee is not longer employed by your organization please notify WL/FIME, WPAFB, OH 45433-7562 to help us maintain a current mailing list.

Copies of this report should not be returned unless return is required by security considerations, contractual obligations, or notice on a specific document.

REPORT DOCUMENTATION PAGE

Public reporting burden for this collection of information is estimated to average 1 hour per response, including the time for reviewing instructions, searching existing data sources, gathering and maintaining the data needed, and completing and reviewing the collection of information. Send comments regarding this burden estimate or any other aspect of this collection of information, including suggestions for reducing this burden, to Washington Headquarters Services, Directorate for Information Operations and Reports, 1215 Jefferson Davis Highway, Suite 1204, Arlington, VA 22202-4302, and to the Office of Management and Budget, Paperwork Reduction Project (0704-0188), Washington, DC 20503.

1. AGENCY USE ONLY (Leave blank)	2. REPORT DATE Jan 93	3. REPORT TYPE AND DATES COVERED Final for August 1990 to May 1992

4. TITLE AND SUBTITLE An Experimental Study of Fluctuating Wall Pressures in a Highly Swept, Sharp Fin-Induced, Mach 5 Shock Wave/Turbulent Boundary Layer Interaction	5. FUNDING NUMBERS PE: 62201F PR: 2404 TA: 13 WU: 21
6. AUTHOR(S) J.D. Schmisseur	

7. PERFORMING ORGANIZATION NAME(S) AND ADDRESS(ES) Flight Dynamics Directorate Wright Laboratory Air Force Materiel Command Wright-Patterson AFB OH 45433-7562	8. PERFORMING ORGANIZATION REPORT NUMBER WL-TR-93-3058

9. SPONSORING/MONITORING AGENCY NAME(S) AND ADDRESS(ES) Flight Dynamics Directorate Wright Laboratory Air Force Materiel Command Wright-Patterson AFB OH 45433-7562	10. SPONSORING/MONITORING AGENCY REPORT NUMBER WL-TR-93-3058

11. SUPPLEMENTARY NOTES

12a. DISTRIBUTION AVAILABILITY STATEMENT Approved for Public Release; Distribution is Unlimited	12b. DISTRIBUTION CODE

13. ABSTRACT (Maximum 200 words)

Fluctuating wall pressure measurements have been made beneath the shock wave/turbulent boundary layer interaction generated by a sharp, unswept fin at angle of attack. Tests were conducted at Mach 5 with a freestream unit Reynolds number of 47.88×10^6 /m. The boundary layer developed naturally on the tunnel floor under approximately adiabatic temperature conditions. From visual inspection and standard time series analysis of fluctuating wall pressure signals, it has been shown that the separation shock wave undergoes a translating, intermittent type motion for fin angles between 16 and 28 degrees. Both the mean wall pressures and higher order moments are quasi-conically symmetric when collapsed in a conical coordinate system. Finally, the maximum wall pressure standard deviation in the intermittent region has been shown to scale with the sweep of the interaction and not with the inviscid pressure rise as has been previously suggested in the literature.

14. SUBJECT TERMS Shock Wave, Boundary Layer, Turbulent Interaction, Interaction Unsteadiness	15. NUMBER OF PAGES 149
	16. PRICE CODE

17. SECURITY CLASSIFICATION OF REPORT Unclassified	18. SECURITY CLASSIFICATION OF THIS PAGE Unclassified	19. SECURITY CLASSIFICATION OF ABSTRACT Unclassified	20. LIMITATION OF ABSTRACT Unlimited

NSN 7540-01-280-5500

Table of Contents

List of Figures

List of Tables

Foreword

The following report is the author's Master of Science in Engineering thesis, submitted to the Graduate School of the University of Texas at Austin. During the research the author was supported by the Air Force Palace Knight program. The author would like to acknowledge the guidance of his advisor, Dr. David S. Dolling, and his Palace Knight Mentor and Supervisor, Dr. George L. Seibert.

Nomenclature

C_f	skin friction coefficient
f	frequency
f_m, f_c	zero-crossing frequency
G	power spectral density coefficients
H	boundary layer shape factor
Li	inception length
M	Mach number
Mn	normal Mach number
P_1	pressure upstream of shock
P_2	pressure downstream of shock
P_0	total pressure
$\bar{P}_w$	mean wall pressure
P_∞	freestream static pressure
q_∞	freestream dynamic pressure
$q(Mn)$	dynamic pressure calculated using normal Mach number
Re_∞	freestream unit Reynolds number
Re_θ	Reynolds number based on boundary layer thickness
T_0	total temperature
VCO	virtual conical origin
U_∞	freestream velocity
X, Xs	coordinate normal to the inviscid shock trace
α	sharp fin angle of attack
β	angle in conical coordinates
β_0	inviscid shock angle
β_{ui}	upstream influence angle
β_s	separation line angle
g	intermittency
δ	undisturbed boundary layer thickness
δ^*	boundary layer displacement thickness
θ	boundary layer momentum thickness
σ_p	wall pressure standard deviation
ϕ	azimuthal angle in spherical/polar coordinates

1. Introduction

1.1 General Motivation

With the increasing prominence of hypersonic vehicles in our national agenda, interest in the field of high Mach number aerodynamics has recently been rekindled. Fundamental to progress in high-speed aerodynamics is our understanding of shock wave/turbulent boundary layer interactions. Shock wave/turbulent boundary layer interactions are responsible for generating excessive heating rates and fluctuating surface pressures which in turn are critical to the prediction of aeroacoustic loads and structural fatigue. In order to optimize aerodynamic design of high-speed aircraft, especially with regard to inlets and control surfaces/body junctions, an understanding of the dynamics of the shock wave/turbulent boundary layer interaction is essential.

Significant progress has been made toward understanding the time averaged aspects of shock wave/turbulent boundary layer interactions, through both experimental and computational means. Computational fluid dynamics has contributed considerably to our understanding of time averaged flow structure, but there are still aspects of the flow that computational methods do not predict well (i.e., fluctuating loads, heat transfer).

Thus, unsteady measurements in shock wave/turbulent boundary layer interactions are needed in order to improve our physical understanding. Documenting the dynamics of the interaction can aid investigators not only in interpreting mean measurements and in developing more meaningful models of the time averaged flowfield, but also in providing the empirical data for urgently needed correlation methods for fluctuating loads.

1.2 Interaction Classification

Interactions are classified using dimensional analysis according to the effect of the shock generator on the flowfield. Interactions in which the shock generators impose no length scale on the interaction are called *dimensionless*, while interactions whose dimensions scale with the shock generator dimensions are referred to as *dimensional* interactions. If the dimensions of the

1

shock generator are sufficiently large that a further increase in the dimensions does not affect the interaction, the generator is described as being *semi-infinite*. Finally, interactions for which the shock generator is not semi-infinite are called *protuberance* or *non-semi-infinite* interactions. The different types of interaction classifications are shown in Figure 1. As seen in Figure 1, the interaction generated by a sharp, unswept fin is semi-infinite and dimensionless.

1.3 Sharp Fin-Induced Interactions

One of the most commonly studied swept shock wave/turbulent boundary layer interactions is that caused by a sharp fin at angle of attack, α, mounted perpendicular to a flat plate. This interaction, called the sharp fin or glancing shock interaction, is perhaps the simplest of the interactions, at least geometrically. Such interactions are typical of those found in box-type engine inlets and at fin/body junctions. Although much has been learned about the general time averaged flowfield of the sharp fin interaction, many questions remain regarding the unsteadiness of the separation process and global flowfield.

The dominant inviscid feature of the sharp fin-induced interaction is the planar shock wave attached to the leading edge. The property changes across the inviscid shock are immediately known from inviscid shock theory given the Mach number and angle of attack. A standard measure of the interaction strength is the *normal Mach number*, defined as the upstream Mach number normal to the inviscid shock. Due to the conical nature of the external inviscid flow and the dominance of the inviscid flow on the interaction, far from the fin leading edge the interaction wave structure and surface features approach *quasi-conical symmetry*. Quasi-conically symmetric flowfields exhibit a conical behavior in the interaction farfield. As a result, the most appropriate coordinate system for studying the interaction is that of a spherical/polar coordinate system with the origin located near the fin leading edge (Figure 2). Angles are defined as the angle between the feature of interest and the freestream direction.

Figure 3 shows the pertinent interaction surface features and their corresponding nomenclature. As seen in Figure 3, the inviscid shock bifurcates into a frontal, separation shock and a rear shock. Bifurcation is observed in all but the weakest interactions. In the region of the separation shock foot the flow is first disturbed from its incoming conditions. The *upstream*

2

influence line is the line along which the incoming flow is first disturbed. On surface flow visualization patterns the upstream influence line is the line along which the incoming streamlines initially deviate from the freestream direction. This initial deflection of the surface streamlines correlates well with the initial increase in mean pressure. In the conical coordinate system used to describe the interaction, the angle of the upstream influence line is given by either β_{ui} or β_u.

The surface features and paths of surface streamlines in the sharp fin interaction are shown in Figure 4. The *separation line*, downstream of the upstream influence line, is defined as the line along which the boundary layer separates due to the adverse pressure gradient behind the separation shock. In surface flow visualization results the separation line appears as a coalescence of streaklines. For extremely weak interactions the boundary layer does not separate, but for the majority of interactions it does. The angle of the separation line is defined as β_{s1} or just β_s. Beneath the separated boundary layer the flow forms a spiraling, helical vortex. The vortex is sketched in Figure 5 which shows two stream surfaces in the sharp fin interaction. These stream surfaces were determined for a Mach 3, 20 degree fin interaction computed by Narayanswami and Knight.[1] As seen from surface 2 in Figure 5, the flow near the floor rolls over into the spiraling vortex . The flow higher in the boundary layer, surface 1, turns toward the floor after passing through the shock system and attaches behind the helical vortex along the line of attachment, β_{A1}. A rarely seen flow feature noted on Figures 3 and 4 is the line of secondary separation, β_{s2}. Secondary separation appears to be the separation of the reverse flow in the vortex, although at this time very little is known of the phenomenon.

Since the interaction has significant viscous effects near the leading edge of the fin, a certain distance is required before the interaction assumes the conical nature of the external, inviscid flow. This distance is called the inception length, Li, and is a result of the dimension introduced into the flowfield by the incoming boundary layer thickness, δ. Due to the viscous effects which cause the inception length, the conical origin of the surface features in the interaction farfield is not coincident with the leading edge. The surface flow features in the quasi-conical region appear to emanate from a *virtual conical origin* just upstream of the fin leading edge along the inviscid shock trace. The inception length and virtual conical origin of the surface flow features are shown in Figure 4.

3

To the knowledge of the author, only two studies have been made of the unsteadiness of sharp fin interactions. Tran,[2] Tran, Tan, and Bogdonoff,[3] and Tan, Tran, and Bogdonoff,[4] at Princeton conducted a series of sharp fin experiments at Mach 3 and noted that the wall pressure signal near separation was characterized by large amplitude fluctuations, indicative of a translating separation shock wave. In contrast, Gibson[5] and Gibson and Dolling[6] at the University of Texas at Austin conducted experiments at Mach 5 which yielded wall pressure signals more indicative of a quasi-steady "shuddering" compression system as opposed to a translating separation shock wave. The apparent contradiction of the results of these two studies was in part the impetus for the current study.

1.4 Objectives

The current study is an attempt to resolve some of the questions that arose from the previous experiments of Tran and Gibson. The primary objectives of the current study are to answer the following questions.

1. Is the separation shock motion at Mach 5 characterized by a translating, intermittent type motion or a quasi-steady, shuddering type motion?

2. Is there a range of interaction sweep angles over which the shock motion exhibits a transition from intermittent to quasi-steady motion?

3. If it does undergo a change, over what range of flow sweepbacks does the change occur, and why? Can Tran and Gibson's work be understood within this framework?

4. Do the higher order moments of the fluctuating wall pressures, particularly the standard deviation, exhibit the same quasi-conical symmetry observed in the mean pressure distributions?

These questions are answered in Chapter 4 of this report.

2. Literature Review

The increased national emphasis on hypersonic flight over the last few years has made the study of shock wave/boundary layer interactions an important area of research. The majority of work has been with turbulent interactions since most practical applications involve turbulent boundary layers. The inherent unsteadiness and complexity of turbulent interactions make an analytical solution improbable, while the current state-of-the-art computational schemes can only model the interaction in a mean sense. Thus, because of the need for experimental data to evaluate computational predictions and the need for quantitative data on the unsteady aspects of the interaction, there is a need for experimental studies.

Since the technological capability to examine interaction unsteadiness relatively easily has only recently become available, a large part of the existing literature deals with the mean characteristics of the interaction. However, in the last few years, with the availability of high frequency pressure transducers and high speed data acquisition systems with large memories, several studies of the unsteadiness of turbulent interactions have been made.

Although this report is primarily concerned with the unsteadiness of the compression system near separation in the swept interaction generated by a sharp fin, the mean characteristics of the flowfield will be discussed briefly to familiarize the reader with the basic concepts and terminology used in the field. For more detailed, recent reviews of the mean flowfield and surface properties of the sharp fin interaction, the reader is referred to References 7 and 8.

2.1 Mean Characteristics of the Sharp Fin Induced Interaction

Before the unsteadiness of shock wave/turbulent boundary layer interactions may be understood, an understanding of the mean characteristics of the interaction is required. Because almost all of the studies of the sharp fin interaction have been of the interaction mean properties, the current state-of-the-art flowfield models only describe the time-averaged flowfield. The following section will introduce and discuss the major features of the sharp fin-induced

interaction.

2.1.1 Quasi-conical Symmetry

From Figures 2-4 it may be seen that as the distance from the fin leading edge increases, the distance from the inviscid shock trace to the upstream influence line also increases. This is due to the conical nature of the dominant external, inviscid flow. However, it has been shown by Inger[9], in an order of magnitude analysis of the governing equations, that near the fin leading edge the flowfield must have a physical scale which correlates with the dimension introduced by the incoming boundary layer thickness. The region in which this scaling occurs is called the inception region. Inger's calculations show that as the distance from the fin leading edge is increased the interaction approaches the conical behavior of the external flow. Because of this approach to conical symmetry far from the fin leading edge, the flowfield is commonly referred to as being *quasi-conically symmetric*.

2.1.1.1 The Inception Region

As discussed in the previous section, the interaction is not conically symmetric near the leading edge of the fin. An initial distance is required before the external, inviscid flowfield dominates the interaction. As noted above, this distance is called the inception length, Li, and is shown in Figure 4.

Lu and Settles[10] have investigated how the inception length varies for fin angles between 4 and 22 degrees and Mach numbers between 2.5 and 4. They determined the inception length from surface flow visualization by fitting an asymptote to the upstream influence line far from the fin leading edge. The end of the inception region and/or beginning of the quasi-conical region of the interaction was determined as the point at which the upstream influence line deviated from the farfield asymptote. Their results indicate that the inception length scales with the inviscid shock angle in the following way:

6

$$Li/\delta_0 \quad = \quad -43 \quad + \quad 1680 \: / \: \beta_0, \qquad 20° < \beta_0 < 35°$$
$$\approx \quad 3, \qquad\qquad\qquad \beta_0 > 35°.$$

As the strength of the interaction increases the inception length decreases until a minimum value is reached. Lu and Settles attribute this to the fact that as shock strength increases the inviscid parameters become increasingly dominant over the viscous parameters until some minimum value for the inception length is achieved.

2.1.1.2 The Virtual Conical Origin

As shown in Figures 3 and 4 the apparent origin of the surface flow features in the quasi-conical region is not coincident with the leading edge of the fin. If the inception length were not present the entire flowfield would be conical and the conical origin would be at the fin leading edge, as it is in the external, inviscid flow. However, because a finite distance is required to establish the conical nature of the interaction, the origin of the quasi-conical flow is at a point along the trace of the inviscid shock upstream of the fin leading edge called the Virtual Conical Origin (VCO). The VCO must be on the trace of the inviscid shock because the inviscid flow dominates the interaction and the inviscid shock wave is the primary feature of the external flow.

It should be noted that the VCO is not a physical phenomenon but rather a convenient tool developed to help understand the flow in a simple reference frame. Due to the variation of inception length with inviscid shock angle/shock strength and the dependence of VCO location on the inception region, the distance between the VCO and the fin leading edge increases as the shock strength decreases.

As may be seen in Figure 4 and as is discussed by Alvi and Settles[11], the fin surface itself cannot lie on a ray from the VCO. This is a consequence of the viscous dominated inception region which prevents the VCO from being coincident with the fin leading edge and the fact that near the surface of the fin the local flow is dominated by the presence of the fin itself.

7

2.1.1.3 Conical Scaling and Correlations of Surface Flow Features

For a conically symmetric flowfield properties are constant along a ray from the origin. As a result, the flow in the conical region can be treated as a two-dimensional problem. Consequently, analysis becomes considerably easier. One useful, practical implication of conical symmetry is that, once the characteristics of the interaction across a plane normal to a ray have been determined, the characteristics at any other parallel plane in the conical region may be determined. This is done by scaling the coordinates normal to the ray in the cross section with the known quantities to fit the coordinates normal to the ray in the cross section with unknown quantities. In other words, since flow properties are constant along a ray from the origin, any two parallel cross sections of the interaction will appear identical when expressed in conical coordinates. Figure 6 shows two Planar Laser Scattering (PLS) images in conical coordinates taken by Alvi and Settles[11] at different radial distances from the conical origin in a Mach 4 α = 20 deg. interaction. The Mach 5, α = 16 deg. mean pressure data of Rodi, Dolling, and Knight[12], also at two different distances from the origin, are shown in Figure 7. From these examples it can be seen that properties of the interaction at varying distances from the leading edge collapse in the conical region.

Using the fact that in the conical region the cross plane view of the interaction is solely a function of the angular coordinates, Lu, Settles, and Horstman[13] were able to show that the reduced upstream influence angle scaled with the reduced shock angle for Mach numbers between 2.5 and 4 and reduced shock angles between 0 and 20 degrees. The reduced angle is the actual value of the angle minus the Mach angle at the given freestream Mach number (e.g., $\Delta\beta_{ui} = \beta_{ui} - \mu_\infty$). The empirical correlation is given by:

$$\Delta\beta_{ui} = 2.2\Delta\beta_0 - 0.027\Delta\beta_0^2 \quad .$$

The validity of the correlation outside the Mach number range 2.5-4 is not clear. Gibson[5] found that the correlation seems to underpredict the upstream influence line by 5-8 degrees for Mach 5 fin interactions at fin angles of 16, 18, and 20 degrees.

A similar correlation was developed using surface oil flow patterns by Zheltovodov, Maksimov, and Shilein[14] for approximately the same Mach number and shock angle ranges as Lu, Settles, and Horstmann. Their correlation for upstream influence angle is given below:

8

$$\beta_{ui}\text{-}\beta_{ui}{}^* = 1.53 \ (\beta_0\text{-}\beta_0{}^*) \qquad .$$

In the above equation starred quantities refer to the values at incipient separation. Using a roughened surface beneath the interaction to trip the boundary layer, Zheltovodov, et al., developed correlations for the angle of the separation line, β_s, for both laminar and turbulent reverse flow in the interaction. For turbulent reverse flow the correlation is:

$$\beta_s \text{-}\beta_s{}^* = 2.15 \ (\beta_0\text{-}\beta_0{}^*) - 0.0144 \ (\beta_0\text{-}\beta_0{}^*)^2 \qquad .$$

In the case of laminar reverse flow the following correlation is applicable:

$$\beta_s \text{-}\beta_s{}^* = 1.94 \ (\beta_0\text{-}\beta_0{}^*) - 0.0154 \ (\beta_0\text{-}\beta_0{}^*)^2 \qquad .$$

The values of $\beta_s{}^*$ and $\beta_{ui}{}^*$ for the above correlations are found from the empirical formulas:

$$\beta_s{}^* = \beta_0{}^* \qquad\qquad \beta_{ui}{}^* = 1.22 \ \beta_0{}^* + 3.4 \qquad .$$

Table 1 below compares the predicted surface flow feature angles from both sets of correlations for a Mach 5 interaction.

Table 1. Predicted Surface Flow Feature Angles

α (deg)	Lu, et al.[13] β_{ui} (deg)	Zheltovodov[14] β_{ui} (deg)	Zheltovodov[14] β_s laminar (deg)	Zheltovodov[14] β_s turb. (deg)
16	36.9	38.1	34.2	36.8
18	39.94	41.5	37.6	40.7
20	42.81	44.8	41.0	44.5
22	45.49	48.3	44.3	48.4
24	47.96	52.0	47.5	52.2
26	50.19	55.8	50.7	56.0
28	52.15	59.8	53.7	59.8

As seen in Table 1, for fin angles below 24 degrees, both correlations agree to within about 3 degrees. For fin angles above 24 degrees the difference between the predicted values of the correlations starts to increase. Since both correlations were developed using data for Mach numbers between 2 and 4, the breakdown in agreement between the correlations in the relatively strong Mach 5 interactions is not surprising.

2.1.2 Mean Pressure Distribution and the Structure of the Interaction

The mean wall pressure distributions in a sharp fin generated interaction at Mach 5 are shown in Figure 7. The distributions were measured along two rows normal to the freestream. The distribution shows the typical shape in such an interaction: an initial rise at the upstream boundary of the interaction, a plateau in the separated region, and sharp final rise near the face of the shock generator.

The physics behind the shape of the mean pressure distribution become clear when the cross plane model of the interaction is examined. By taking advantage of the quasi-conical symmetry of the farfield interaction Alvi and Settles[11,15] were able to use both conical

10

shadowgraphy and conical Planar Laser Scattering (PLS) to develop a physical model of the cross plane structure of the interaction. The cross plane was taken normal to the inviscid shock. Some of the major features of the Alvi and Settles flowfield model are listed below. These flow features were observed for angles of attack between 7 and 25 degrees and at Mach numbers between 2.5 and 4. The corresponding normal Mach numbers ranged between 1.22 and 2.45. Figure 8 shows a shadowgraph, PLS image, and flowfield map for the Mach 4, 20 degree angle of attack interaction. All comments below refer to the interaction cross section taken normal to the inviscid shock.

1. For a normal Mach number of 1.22 no bifurcation is apparent in the shock wave. As the normal Mach number is increased the shock wave appears to bifurcate with the front of the lambda foot moving forward to form the separation shock wave.

2. Large scale separation seems to occur underneath the foot of the separation shock for normal Mach numbers above 1.22. A free shear layer appears to lift off the surface and, after being turned back toward the surface by the rear foot of the shock, impinges on the floor of the tunnel as a jet.

3. Impingement of the jet may be the cause of the peak pressure and heating rates near the base of the fin.

4. The separated shear layer forms the boundaries of a flattened vortex under the legs of the bifurcated shock wave.

5. A slipline forms at the triple point of the bifurcated shock and curves down into the junction of the fin and tunnel floor.

6. As the strength of the interaction increases the jet cross flow velocity may increase from subsonic to supersonic. Evidence for this is the appearance of "shocklets" in the jet which increase in strength to become a normal shock once the interaction strength is increased sufficiently.

7. For their strongest interaction, with a normal Mach number of 2.45, Alvi and Settles observed the appearance of a "shocklet," indicative of local supersonic cross flow, in the reversed flow of the vortex along the tunnel floor.

11

8.   Conical shadowgrams reveal the appearance of a "bulge" in the reversed flow of the separation bubble at moderate interaction strengths. Although there is no conclusive evidence, this may be indicative of secondary separation, a seldom seen phenomenon which appears at moderate interaction strengths and then disappears again as the interaction strength is increased.

Alvi and Settles observed that as the interaction strength is increased the separation shock extends further out in the interaction relative to the inviscid shock, while the impinging jet is compressed back in the narrowing region between the inviscid shock and the fin surface. This shift of the jet and inviscid shock position back in the interaction as the interaction strength is increased accounts for the more gradual initial pressure rises and steeper final pressure rises measured for relatively strong interactions when compared to the pressure distributions measured for weaker interactions.

2.2 General Comments on Interaction Unsteadiness

There have been very few studies of the unsteadiness of three-dimensional shock wave/turbulent boundary layer interactions. The majority of investigations have been made with two-dimensional interactions such as unswept compression ramps and forward facing steps and on the centerline of blunt fins and circular cylinders. In the following section the results of some of the studies of two-dimensional interactions will be discussed in order to introduce the reader to the concepts and terminology of this field.

With the advent of high frequency miniature pressure transducers and very high-speed data acquisition systems with large memories, it has become possible to examine fluctuating wall and pitot pressures in great detail. From the fluctuating wall pressure the behavior of the unsteady wave structure above the wall may be determined. This approach is particularly useful for examining the motion of the separation shock wave and/or compression system. A typical fluctuating wall pressure signal measured between the upstream influence and separation lines in a Mach 5 interaction generated by a 28 degree unswept compression ramp is shown in Figure 9a. From the figure it may be seen that the instantaneous pressure fluctuates between the range

12

of values associated with the undisturbed boundary layer and a higher value associated with the flow behind the moving separation shock wave. Essentially, the high frequency, low amplitude fluctuations associated with turbulence now have a set of high amplitude, low frequency pressure "pulses" superimposed on them. This "intermittent" wall pressure signal is indicative of the translating separation shock and is observed at all locations between the upstream influence and separation lines, in what is called the *intermittent region*.

Thus, the separation shock is not fixed in space but changes position, apparently randomly, over a region with a downstream boundary at the separation line and an upstream boundary near the upstream influence line. A useful parameter for describing the unsteadiness and describing the length scale of the shock motion is the intermittency, γ. The intermittency is defined as the percentage of time the separation shock wave is upstream of the transducer. That is, the percentage of time the transducer reads the relatively high pressure downstream of the separation shock as opposed to the relatively low pressure values associated with the undisturbed boundary layer. In contrast to the signals in the intermittent region, the fluctuating wall pressure histories in the undisturbed boundary layer and the separated region are essentially normally distributed. A typical wall pressure time-history and its corresponding amplitude probability density distribution in the separated region is shown in Figure 9b.

2.2.1 Interpretation of Surface Flow Features

Since it has been shown that the separation shock wave is unsteady, the question naturally arises as to what the surface flow features, such as the separation line, determined from the surface flow visualization actually signify. Because the kerosene-lampblack method has essentially zero frequency response, the surface flow visualization must be treated with caution. The following is a discussion of the meaning of the surface features determined from flow visualization for two-dimensional interactions.

By examining cross correlations between two wall pressure signals measured directly downstream of the translating separation shock in a Mach 5, cylinder induced interaction, Gramann and Dolling[16] concluded that the flow immediately behind the separation shock was separated. This conclusion was based on the presence of local peaks at negative time delay in

13

the cross correlation which indicated reversed flow. Thus, Gramann and Dolling deduced that the separation line determined from surface flow visualization is actually the furthest downstream position of instantaneous separation.

The time average interpretation of the upstream influence line from surface flow visualization is not quite as clear as that of the separation line and really hinges on what is meant by upstream influence. The upstream influence line determined by surface flow visualization correlates with the initial rise in mean wall pressure, and hence, the initial mean pressure rise is the conventional definition of upstream influence. However, as discussed by Dolling[17], other statistical properties of the pressure signal, such as the standard deviation and higher order moments, first deviate from the normally distributed incoming boundary layer values upstream of the upstream influence line. The deviation of the higher order moments, which are more sensitive to a few shock passages than the mean pressure, shows that the shock wave may occasionally travel upstream of the upstream influence line, even if relatively infrequently. Therefore, the name upstream influence line may be a misnomer. The mean pressure of the interaction first deviates from the boundary layer value at the upstream influence line, but the higher order moments have already been influenced by the shock motion.

2.2.2. Statistical Description of Wall Pressure Signals throughout the Interaction

The distributions of the standard deviation (rms) along the centerline for the interactions generated by an unswept compression ramp and a circular cylinder are shown in Figures 10 and 13, respectively. The spatial coordinate is normalized by the undisturbed boundary layer thickness for the unswept compression ramp data and the diameter of the cylinder for the cylinder data. The rms increases from the undisturbed value at the upstream influence line then sharply rises through the intermittent region until a peak is reached just upstream of separation. This rise and peak is generated by the intermittent, translating separation shock wave. Then the rms decreases slightly until just downstream of separation, beyond which the rms seems to increase at an approximately constant rate. The local mean wall pressure normalized by the freestream static pressure and the rms normalized by the local mean wall pressure for two unswept compression ramp interactions are shown in Figure 11. The Mach 5, 28 deg. ramp

14

data are that of Gramann and Dolling[18] while the Mach 3, 24 deg. ramp data are from Dolling and Murphy. The normalized rms increases at the upstream influence line and peaks in the intermittent region similarly to the unnormalized distribution. However, because of the increasing mean pressure in the interaction, the normalized value of rms decreases downstream of the intermittent region until a value close to the undisturbed boundary layer level is reached.

The amplitude probability density distributions of wall pressure signals in the undisturbed boundary layer, intermittent region, and separated region are shown in Figure 12 for the 28 degree compression ramp discussed earlier. In the undisturbed boundary layer and separated region, the PDDs are essentially normally distributed with the mean in the separated region larger than that of the undisturbed boundary layer, as should be expected. In contrast, in the intermittent region, the PDDs are either bimodal or highly skewed. The bimodal nature arises from the two distinct pressure levels in the intermittent signal.

The rms distribution and Power Spectral Densities (PSDs) for wall pressure signals measured through the interaction on the centerline upstream of a cylinder at Mach 5 are shown in Figure 13. For the undisturbed boundary layer, curve 1, the majority of the energy in the signal is at the higher frequencies associated with turbulence. Curves 2-4 indicate that in the intermittent region the major contribution to the signal variance shifts from higher frequencies to frequencies on the order of 1 kHz. Finally, as seen from curves 5-7, in the separated region the major contribution to the variance again shifts up to higher values. The shift in dominant frequencies to lower values in the intermittent region is due to the relatively low frequency motion of the separation shock wave in the intermittent region.

The intermittency distribution for the Mach 5, 28 degree, unswept compression ramp interaction (Reference 19) is shown in Figure 14. The intermittency curve strongly resembles the cumulative density distribution (CDD) for a Gaussian signal. The zero-crossing frequency, fc, is defined as:

$$f_c = \frac{1}{T_m} = \frac{1}{\frac{1}{N}\sum_{I=1}^{N} T_i}$$

15

where Ti is the shock period for the ith shock crossing and N is the number of shock crossings. The shock period is defined as the time between pressure rises generated by the shock passing over the transducer while moving upstream. Figure 15 illustrates the concept and defines the shock period, Ti. The zero-crossing frequency distribution for the unswept compression ramp interaction is shown in Figure 16. The maximum zero-crossing frequency occurs at intermittencies around 50 percent. This is intuitively logical since the pressure should fluctuate between the boundary layer value and the value behind the translating shock most rapidly at the point of 50 percent intermittency.

2.3 Investigations of Unsteadiness in Sharp Fin Induced Interactions

To the knowledge of the author, only two studies have been made of the unsteadiness of the interaction induced by a sharp fin. The first was made by Tran[2], Tran, Tan, and Bogdonoff[3] and Tan, Tran, and Bogdonoff[4] in the Princeton Mach 3 facility with a boundary layer thickness of 17 mm. Tran, et al. observed intermittent characteristics similar to those observed in the 2-D interactions discussed earlier; skewed probability density distributions (PDDs), a peak in the rms distribution near the upstream influence line and the appearance of "pulses" in the fluctuating wall pressure signal. The second study of interaction unsteadiness generated by a sharp fin was made by Gibson[5] and Gibson and Dolling[6] in the Mach 5 blowdown facility at the University of Texas at Austin. Gibson's experiment was made on a flat plate mounted on the centerline of the test section with a boundary layer about 6 mm thick. Gibson did not find any evidence of intermittent pressure signals. His rms distributions did not show a clear peak near separation and the PDDs in the intermittent region were approximately Gaussian. The apparent contradiction in the results of the two studies partly led to the current study. In order to understand the objectives of the latter better, the following sections will attempt to critically review the work of Tran, et al. and Gibson with the hope of shedding some light on why these two experiments have produced different results.

Tran, et al.'s mean wall pressure distributions normalized by the undisturbed boundary layer value along a line parallel to the freestream are shown in Figure 17. The Mach 3 measurements were made at fin angles of attack of 10, 12, 16, and 20 degrees. As shown in

Figure 14, as the fin angle is increased the initial and final pressure gradient are steeper and occur over a shorter distance and the plateau pressure increases. However, the decrease in spatial extent of the interaction with increasing fin angle shown in Figure 14 is misleading. Because Tran's transducers were located along a line parallel to the freestream direction, the orientation of the transducers with respect to the interaction changed with angle of attack. This change in orientation affects the distance from the inviscid shock to the flow features. In fact, as pointed out in the earlier discussion of the Alvi and Settles flowfield model, the spatial extent of the interaction increases as the strength of the interaction is increased.

The distribution of the wall pressure standard deviations for the same fin angles is shown in Figure 18. The rms is normalized by the undisturbed boundary layer value in Figure 18a and the local mean pressure in Figure 18b. Both distributions seem to follow the trends expected for a shock wave/boundary layer interaction. The rms peaks for angles of attack above 12 degrees would usually be interpreted as being indicative of intermittent shock motion. By inspection it may be seen that, in general, the magnitude of the pressure fluctuations increases as the fin angle is increased. The increase in rms for the distributions normalized by the local mean pressure indicate that the increase in rms levels is not simply a result of the increase in mean wall pressure. Also, when the rms is normalized by the local mean pressure it is seen that the magnitude of the fluctuations appears to reach another "equilibrium" level downstream of the inviscid shock (i.e., for $Xs/\delta_0 > \approx 2$ the ratio becomes approximately constant).

Gibson's rms distributions along a line perpendicular to the upstream influence line are shown in Figure 19. The rms distributions do not have the rms peak characteristic of an intermittent shock foot. On the other hand, they do demonstrate the same trends as Tran's data by showing a global increase in the magnitude of fluctuations as the fin angle is increased.

2.3.1 The Effect of Increasing Shock Strength on the Interaction

Although Tran stated that "... the data shows the strong dependence of the fluctuation, throughout most of the interaction, on the strength of the inviscid shock," and indeed by inspection these data do follow this trend, this conclusion cannot be supported by only one set of data. Consider that when the fin angle is increased both the inviscid shock strength and the

17

sweep of the interaction change. Hence, it is possible that the increase in rms levels as the fin angle is increased may be due to a change in the flowfield structure as the interaction sweep is decreased, the increase in inviscid pressure rise, or a combination of both parameters.

Tran tried to show that the upstream region of the interaction was a function of the inviscid pressure rise by comparing measurements made in the interactions generated by different geometries with the same inviscid pressure ratio. The geometries included a sharp fin at 17.5 degrees angle of attack, a 25 degree semi-cone, and two swept compression ramps, a 30-60 degree ramp and a 24-60 degree ramp. For the compression ramps the first number (i.e., 24 or 30) is the streamwise angle of the ramp face while the second number (60) is the sweep angle of the ramp corner line. The inviscid pressure ratio for all the generators is 3.2 except for the 24-60 degree compression ramp which had an inviscid pressure ratio of 3.0. The mean and rms pressure distributions are shown in Figures 20 and 21, respectively.

By using a coordinate stretching function Tran was able to match the location of the upstream influence line and inviscid shock for each interaction geometry and compare how the pressure distribution varied among the different geometries. From Figures 20 and 21, both the mean and rms pressure distributions are very similar between the upstream influence and inviscid shock trace lines. As is expected with a lower pressure ratio, the 24-60 degree swept compression ramp data fall slightly below the rest of the data.

From the above results Tran concluded that the inviscid shock strength was the primary governing parameter for such interactions. Another conclusion of Tran's was that because the pressure and rms distributions are the same for varying geometries, the fluctuations must be processed by the same mechanism.

Although the rms and mean pressures may be partially dependent on inviscid shock strength, the local flow structure, in the form of interaction sweep, may also play a role. When comparing unswept compression ramp and fin interactions, Tran noted that "... the rms peaks for the swept interactions are only about half the magnitude observed at similar shock strengths." Thus, the inviscid shock strength does not solely determine interaction pressure levels. This is not entirely surprising since the crossflow present in three-dimensional interactions creates a fundamental physical difference between three- and two-dimensional interactions. As reported by Settles and Kimmel,[25] the 17.25 deg. fin, 25 deg. semi-cone, and 30-60 degree compression

18

ramp all produce interactions with the same separation sweep angle. This similarity in local flow conditions may be one of the reasons the various interactions have the same mean and rms pressure levels.

2.3.2 The Effect of Spanwise Variation on the Characteristics of the Interaction

Tran compared the characteristics of the pressure signals at two spanwise distances from the fin leading edge. Tran's rms distributions at distances of 1.85 and 5.1 boundary layer thicknesses from the surface of the fin are shown in Figure 22. As may be seen from Figure 22, especially in part c where the length of the interactions has been scaled to match the upstream influence and inviscid shock positions, the two distributions appear almost identical. Thus, it appears that the standard deviation of the wall pressures are quasi-conically symmetric.

Gibson's rms distributions in the conical coordinates defined at the beginning of this chapter are shown in Figure 23. Although the distributions appear to collapse, scatter precludes a conclusion of quasi-conical symmetry, although other data support the idea. For example, the power spectral densities (PSDs) at various spanwise positions along a ray in the compression region, shown in Figure 24, indicate a quasi-conical flow. The similar shape of the curves points to the conical invariance of statistical properties along a ray in the conical region of the flow.

Although the PSDs and rms distributions of Figures 23 and 24 seem to indicate quasi-conical symmetry, Gibson suggested that the flow details may not be quasi-conical. Figure 25, which shows the contributions to the total variance of the various frequency bands at the different spanwise positions of Figure 24, indicates that there may be a shift from the higher frequencies to lower frequencies as the distance from the leading edge of the fin is increased. This is evident from the increase in the contribution to the variance from fluctuations in the 0-2 and 2-5 kHz ranges and the corresponding decrease in the 5-15 and 15-50 kHz ranges.

However, because of the difficulty of determining the exact location of the VCO, Gibson's row of transducers probably did not fall along a ray. As such, the changes in variance along the ray may be due to the change in position within the interaction that would occur along the survey line if it were, in fact, not coincident with a ray from the VCO. In the initial

19

compression region the rms increases and energy content of the fluctuations moves from high to low frequencies over a relatively short distance. If Gibson's transducer row were slightly misaligned, it is probable that the subtle evolution of the energy content of the signal shown in Figure 25 would be observed. Thus, this result must also be treated with caution.

2.3.3 Spectral Characteristics of Sharp Fin Interactions

Tran's power spectral densities (PSDs) along a line in the freestream direction located 5.1 boundary layer thicknesses from the fin for $\alpha = 20$ degrees are shown in Figure 26. Since the power is multiplied by the frequency and normalized by the total variance of the signal, the area under each curve is unity. Hence, this normalization allows comparison of the relative contributions of the various frequencies. The normalized PSDs at a given position in the interaction do not change significantly with fin angle; therefore, the 20 degree case shown will be sufficient to describe the spectral characteristics for all the interaction strengths. Similarly, the PSDs for Gibson's interaction at 18 degrees angle of attack are shown in Figure 27.

The evolution of the PSDs is seen to be very similar to the general picture presented in Section 2.2. The signal from the undisturbed boundary layer shows that most of the energy is at the relatively high frequencies corresponding to the incoming turbulence. In the intermittent region it may be seen that the dominant frequency shifts downward to lower frequencies with a center frequency in this case of about 2 kHz for Tran's data and about 7 or 8 kHz for Gibson's data. After the flow separates, in the plateau region, the power in the signal shifts back up to higher frequencies. Finally the PSDs shift back to shapes typical of the boundary layer spectrum toward the end of the interaction.

Figure 28, from Gibson, shows the contributions of various frequency bands to the variance of the signal as the position in the interaction is changed. Starting on the right hand side of the figure, which is in the undisturbed boundary layer, and moving to the left, into the interaction, it may be seen that the contributions of the 15-50 kHz range, which is the primary range of frequencies in the undisturbed boundary layer, decrease while the contributions of the lower frequency ranges increase. In the intermittent region, the third set of data points from the right-hand side, the dominant frequencies appear to be from the 5-15 kHz range while the 0-2

20

and 2-5 kHz ranges also increase in contribution to the variance while the 15-50 kHz range makes a minimum contribution. In the separated region the frequency contributions gradually relax to similar levels as in the undisturbed boundary layer.

The general trend of the evolution of frequency content through the interaction correlates for the data of both Tran and Gibson. Further experiment is needed in order to examine the change in center frequency for varying flowfield conditions.

2.3.4 Description of the Wall Pressure Signals

Time-histories and the corresponding PDDs at various positions in Tran's interaction are shown in Figure 29. Upon inspection the signals are obviously intermittent. The PDDs in the interaction upstream of separation are skewed which is indicative of the intermittent signal. In contrast to the compression ramp PDDs, the PDDs for Tran's intermittent signals are not bimodal. The reason the swept interaction does not have the high pressure mode associated with the flow behind the separation shock is not clear at this time.

From examination of Figure 29 it is now appropriate to bring up again the failure of surface flow visualization to satisfactorily predict the upstream influence line. The time-history upstream of the one marked UI (for the upstream influence line) shows a definite intermittent signal and skewed PDD.

In contrast to the data of Tran are the results presented by Gibson, shown in Figure 30. Gibson's time-histories show no evidence of an intermittent signal and the corresponding PDDs are approximately Gaussian, with only the slightest hint of skewness in the intermittent region. Although no explanation may be given for the discrepancy among the different experiments, the author feels that perhaps Gibson had a resolution problem caused by the relatively large transducer diameter compared to the boundary layer thickness. Figure 31 shows Gibson's skewness distributions for the 16 and 18 degree sharp fin interactions. The rise in skewness is consistent with that observed in intermittent interactions. The skewness distribution through an unswept compression ramp interaction is shown in Figure 32. To this author, the similarity of Figures 31 and 32 indicate that Gibson's signals may be intermittent.

Tran's intermittency distributions for angles of attack of 12, 16, and 20 degrees are

shown in Figure 33. Tran notes that for the higher angles the intermittency at the upstream influence line is 60 percent. This again may be due to the failure of the flow visualization to predict the upstream influence position or possibly some mistake in the interpretation of upstream influence on the flow visualization. In any case, the occurrence of 60 percent intermittency at the upstream influence line appears to be physically inconsistent with the definition of upstream influence.

2.3.5 Comparison of 2-D Compression Ramp and 3-D Sharp Fin Interactions

Although swept and unswept interactions apparently have different flowfield structures, Tran tried to correlate the peak rms values from three dimensional sharp fin interactions and two dimensional compression ramp interactions. The compression ramp data used was that of Dolling and Or.[21] The peak rms as a function of inviscid pressure rise is shown in Figure 34. It may be seen that the 2-D interactions produce a significantly higher peak rms than 3-D interactions of the same strength. This seems to invalidate Tran's comments earlier on the inviscid shock strength determining the rms levels.

The peak rms for both 2-D and 3-D interactions as functions of mean pressure gradient evaluated at the point of maximum rms and spatial extent of intermittency are shown in Figures 35a and 35b, respectively. The compression ramp and sharp fin interaction show opposing trends in both figures and it has been noted by Tran that the initial pressure gradient and spatial extent of intermittency must not be the appropriate parameters for determining peak rms values.

In a third attempt to produce a correlating parameter for peak rms values Tran tried to combine the mean pressure gradient and spatial extent of intermittency in a single parameter. The parameter, ΔP, is given at the bottom of Figure 36 which shows peak rms versus the parameter ΔP for both the compression ramp and sharp fin interactions. Although it appears that the combined parameter allows both sets of data to be combined on a single curve, only one point overlaps from each data set and no firm conclusions may be drawn from the data without further experiment.

22

2.4 Summary

The preceding chapter has attempted to briefly sum up the current knowledge of the interaction between a swept shock wave generated by a sharp unswept fin and a turbulent boundary layer. Since the routine capability to make unsteady pressure measurements beneath the interaction has only become available in recent years, the majority of our knowledge is of the time averaged flowfield structure and surface properties. The large body of work devoted to this end has resulted in a fairly sophisticated model of the time averaged interaction which is widely accepted. However, as far as is known, only two studies have been made of the interaction unsteadiness. Because of the importance of fluctuating pressure loads and heat transfer rates, the study of the interaction unsteadiness is an important research area in fluid dynamics.

The studies of interaction unsteadiness made by Tran[2] and Gibson[5] were reviewed in Section 2.3. The apparently contradictory results from these studies shows the need for further investigation of the interaction unsteadiness. Tran and Gibson's studies were made at different Mach numbers, thus, although the range of fin angles overlap, the inviscid pressure ratios and interaction sweep angles do not overlap. In the current study attention was focused on interactions with sweep angles that provided overlap with both Tran and Gibson's sweep angle ranges. The Mach number, 5, was the same as Gibson's experiment, but the boundary layer thickness was approximately the same as that of Tran's experiment. Hence, the current experiment is an attempt to study the unsteadiness of the interaction at flow conditions between the two extremes studied by Tran and Gibson. By examining the fluctuating wall pressure signals and using standard time series analysis, the questions posed in Chapter 1 have been addressed.

3. Experimental Program

In the current study fluctuating wall pressure measurements were made beneath the interaction generated by a sharp, unswept fin at 16, 18, 20, 22, 24, 26, and 28 degrees angle of attack at Mach 5. The experimental program consisted of two phases: a preparatory phase and a data acquisition phase. The objectives of the preparatory phase were (1) first "proofing" the models to ensure proper functioning in the wind tunnel and (2) obtaining surface flow visualization in order to obtain quantitative data on the flowfield scale and feature locations. Surface flow visualization results from the first phase of the experiment were used to position the pressure transducers at appropriate locations. The second phase consisted of making fluctuating wall pressure measurements from which the motion of the separation shock wave and details of the interaction unsteadiness were determined.

3.1 Test Facilities and Flow Conditions

Experiments were conducted in the Mach 5 blowdown tunnel at Balcones Research Center, Austin, Texas. The tunnel has a constant area test section which is 7 inches high by 6 inches wide and is located about 36 inches downstream of the nozzle throat. Two removable side doors allow access to the test section. A removable tunnel floor insert allows easy model installation and the means of optimizing the hardware locations for a given experiment.

Air for the tunnel is provided by a Worthington HB4 four-stage compressor and stored in external tanks with a volume of 140 cubic feet at a pressure of about 2500 psia. The stagnation pressure is regulated by a valve between the storage tanks and the stilling chamber. Stilling chamber temperature is regulated by two banks of nichrome wire heaters, each dissipating about 400 kW. The typical stagnation chamber pressure and temperature for the current work were 330 psia and 635°R, respectively. Nominal Mach number in the test section is 4.95. Table 2 lists the freestream conditions for the current experiment.

24

Table 2. Tunnel Freestream Conditions

Parameter	Metric	English
M_∞	4.95	4.95
Re_∞	$47.88 \times 10^6/m$	$14.59 \times 10^6/ft$
U_∞	766 m/s	2514 ft/s
P_0	2.275×10^6 Pa	330 psia
T_0	352 K	635 °R
δ_0	1.51 cm	0.59 inches

The experiment was conducted on the tunnel floor using the turbulent boundary layer which developed naturally on the wall. McClure[21] has made centerline pitot pressure and total temperature surveys of the undisturbed boundary layer at several streamwise positions in the test section and has shown that the velocity profile closely matches the law of the wall/law of the wake. Table 3 lists the properties of the boundary layer 3.74 inches from the junction of the nozzle and test section. This position is 1.3 inches downstream of the fin leading edge.

Table 3. Undisturbed Boundary Layer Parameters

δ_0	1.51 cm	0.59 in.
δ^*	0.67 cm	0.26 in.
Θ	6.6×10^{-2} cm	2.6×10^{-2} in.
Π	0.78	
H	10.2	
Re_Θ	3.17×10^4	
C_f	7.74×10^{-4}	

3.2 Shock Generator

3.2.1 Sharp Unswept Fin

The shock generator used for the current experiment was a stainless steel fin with an unswept, sharp leading edge mounted normal to the floor of the wind tunnel as shown in Figure 37. Two fins were built for the experiment since the design was improved between the first and second phases of the experiment.

In both cases the fins were maintained perpendicular to the tunnel floor by a 3/8-inch-diameter steel shoulder bolt. The bolt hole in the tunnel floor was located 3.44 inches downstream of the nozzle/test section junction and 1.69 inches from the right side of the tunnel when facing upstream. The bolt passed through the floor of the test section and threaded into the underside of the fin 1 inch from the fin leading edge. The shoulder bolt not only kept the fin in place and vertical, but also exerted a downward force on the fin ensuring that the fin remained in contact with the tunnel floor. Teflon tape was attached to the underside of the fin in order to prevent leakage between the high and low pressure sides when the fin was at angle of attack. The tape also prevented metal-to-metal contact as the fin angle of attack was changed.

At the maximum angle of attack of 28 degrees the leading edge of the fin was 1.44 inches from the right tunnel sidewall. The trailing edge of the fin was more than 1.5 inches from the left tunnel sidewall for all cases. Both distances were sufficient to prevent interactions of the fin with the sidewall boundary layer.

For the first phase of the experiment the fin was initially 6 inches in length, 4.5 inches in height, and 0.5 inches thick. With this fin the tunnel unstarted at an angle of attack of 23 degrees. In order to increase the angle of attack beyond 23 degrees, the fin length was decreased to 5 inches. The maximum angle of attack attainable subsequently increased to 26 degrees. Finally, the fin height was reduced to 3.75 inches which permitted tests at 28 degrees angle of attack. Because of the difficulty encountered in passing the tunnel startup normal shock through the test section, for large angles of attack the fin angle was decreased before tunnel startup to reduce tunnel blockage. After Mach 5 flow was established in the test section the fin angle was increased to the desired test angle. For the large fin used in the first phase of the experiment, all angles of attack over 24 degrees required a reduction in angle of attack for tunnel startup.

26

Another fin was built for the second phase of the experiment and was 5 inches long, 3 inches high, and 0.5 inches thick. It was smaller than the first not only to prevent tunnel stall until higher angles of attack, but also was small enough that the tunnel could be started at any required angle of attack. Thus no reduction in fin angle prior to tunnel start-up was needed.

3.2.2 Variable Angle of Attack Mechanism

An exploded view of the variable angle of attack mechanism is shown in Figure 38a. The mechanism is the same one used by Gibson[5] and Rodi[12] and consists of a stainless steel arm attached to an external mechanism made up of a collar, bolt, and block (see Figure 38a). The arm passed through a hole in the tunnel side door and was pinned to the collar whose opposite end had a hole threaded with left handed threads. The left hand threads of the yoke matched another set of left handed threads on the front section of the 0.5 inch stress-proof steel bolt. The part of the steel bolt near the head had right hand threads and a larger diameter than the front portion. The right hand threaded, large diameter section of the bolt mounted through the block which also had right hand threads. The block was attached to the external side of the wall of the test section. By turning the external end of the bolt a translation without rotation could be given to the arm via the two sets of opposing threads. In order to prevent the cavity inside the block from affecting the flow in the test section, two plates were bolted over the hole in the tunnel access door leading to the cavity in the block. A hole cut at the junction of the two plates was large enough for the arm to pass through unrestricted but not large enough to significantly affect the flow in the test section. The assembled angle of attack mechanism is shown in Figure 38b.

A side view of both fins is shown in Figure 39. The stainless steel arm attached to the fin at a height of 3 inches above the tunnel floor and 3.5 inches from its leading edge. In the case of the large fin used in the first phase of the experiment, the arm was attached to the leeward side by a pin that passed through a hole in the end of the arm. The end of the arm and attachment pin fit in the two slots in the side of the fin. The ends of the pin were held in the vertical slot by two plates that bolted onto the leeward side of the fin. The horizontal slot allows the fin to rotate with respect to the arm without contact between the arm and fin.

In the case of the smaller fin used in the second phase, also shown in Figure 39, the arm

27

was attached to the top of the fin using a steel shoulder bolt. As shown in Figure 39, the leeward side of the second fin had a shelf cut at the intersection of the leeward side and top of the fin. The shelf was needed in order to allow the arm to mount on the top of the fin while remaining horizontal.

3.3 Instrumentation

3.3.1 Transducer Specifications

Fluctuating wall pressure measurements were made using Kulite Semiconductor Products, Inc. model XCQ-062-15A and XCQ-062-50A miniature transducers. The transducers have a fully active four arm Wheatstone bridge diffused into a silicon diaphragm. The transducer has a pressure sensitive area 0.028 inches in diameter and an outer diameter of approximately 0.064 inches. The model XCQ-062-15A has a range of 0-15 psia and a natural frequency of about 250 kHz as quoted by the manufacturer. The model XCQ-062-50A has a range of 0-50 psia and a natural frequency of 500 kHz. Both types of transducers have perforated screens above the diaphragm to protect it from damage due to any dust particles in the flow. The protective screens limit the frequency response of both models to about 50 kHz. According to the manufacturer, both models have a nominal 100 mV full scale output and a thermal zero shift of approximately + 2% of full scale per 100 degrees Fahrenheit.

The transducers were calibrated statically using a Heise model 710A digital pressure guage accurate to within 0.001 psia. The calibrations were static since this is a much simpler procedure than dynamic and because it has been shown that static calibrations differ from dynamic calibrations by only 2-3 %.[22]

3.3.2 Instrumentation Plug

The transducers were mounted along two straight rows in a rotatable plug located underneath the swept interaction produced by the sharp fin. The locations of the plug and transducer ports relative to the fin are shown in Figure 40. The hollow circular plug was 3 inches in diameter with its center located 0.553 inches downstream and 1.729 inches toward the centerline of the tunnel from the fin mounting hole. Overall, the plug is 1.5 inches high, with

28

1 inch of plug shank passing through the 1 inch thick tunnel floor and a half-inch of plug with extensions on either side extending from the bottom of the tunnel on the outer surface. An isometric view is shown in Figure 41.

The plug was mounted in the floor of the tunnel as shown in Figures 37 and 40. The two three-quarter inch slotted flanges of 60 degrees arc on either side of the external surface are evident in Figure 41. Using these, the plug could be bolted to the external side of the tunnel floor. The plug surface had been machined flush with the tunnel floor but required shimming with masking tape before it was truly flush. To ensure no leakage between the plug and the tunnel floor, an O-ring was located on the shank of the plug in such a way that it would fill the gap between the tunnel floor and the plug when it was inserted in the tunnel floor. By using arced slots instead of bolt holes on the external flanges of the instrumentation plug, the plug could be rotated in the tunnel floor in order to position the rows of transducer ports as needed.

Transducers ports were located in two straight rows on the surface of the plug flush with the tunnel floor. Transducer locations on the plug are shown in Figure 42. When the plug is in its unrotated position, the transducer rows are at an angle of 55.5 deg. with respect to the freestream direction. As shown in Figure 42, rows B and C are 0.2 and 0.6 inches from the center of the plug, respectively, and are downstream of the center of the plug. There are 20 transducer ports on row C and 23 on row B. All transducer ports were spaced 0.115 inches apart. On row B the twelfth transducer is located on the diameter of the plug normal to the transducer row, while on row C the tenth transducer from the upstream region is on the diameter. Finally, the plug may be rotated 180 degrees and installed so that the transducer rows are at the same angle but upstream of the center of the plug. When the plug is in the fully rotated position, the transducer rows are closer to the leading edge of the fin. In the rotated position row C is renamed row A.

3.3.3 Signal Conditioning and Data Acquisition

Transducer voltage output was amplified by either Measurements Group Model 2311, PARC Model 113 or Dynamics Model 7525 amplifiers and low pass filtered by Ithaco Model 4113 or 4213 filters before being digitized. The amplification was optimized to produce the maximum range of output voltages within the limits of the data acquisition system while the

29

signal was filtered at cutoff frequencies of either 20 or 50 kHz depending on the sampling frequency. The analog to digital converters are two LeCroy Model 6810 Waveform Recorders with maximum sampling rates of 1 MHz/channel for 8 channels and an ouput of 4096 counts for 5 volts at the input. For the second phase of the experiment pressure data were taken on between 6 and 8 channels and at sampling rates of either 50 or 200 kHz per channel depending on the purpose of the run. For each run, 256 records of 1024 points were acquired. Typical noise on the data acquistion system was between ± 5-15 counts peak-to-peak.

3.4 Experimental Procedure
3.4.1 Determination of Fin Angle of Attack

Fin angle of attack was determined by placing a variable angle protractor against the windward face of the fin and then determining the angle between the fin face and the opposite sidewall of the test section. A feeler gauge was used to ensure that the surface of the protractor was flush with the fin face over the entire length of the fin and that there were no gaps between the fin and the tunnel floor. Using this method and accounting for a slight hysteresis in the arm mechanism, it is estimated that the angle of attack of the fin is accurate to within ± 0.5 degree.

3.4.2 Surface Flow Visualization

Before the surface pressure transducers could be properly positioned, the location and scale of the flow features had to be determined for each fin angle. This was accomplished via the kerosene-lampblack method of surface flow visualization[23].

The kerosene-lampblack method provides a full scale image of the mean surface streamlines. The mixture is painted on the test section floor upstream of the model prior to tunnel startup. As the flow establishes itself it is carried downstream and distributed by the mean wall shear stress. The carrier (i.e., the kerosene) evaporates, leaving behind the lampblack which traces the paths of the surface streamlines. After the tunnel has been shut down the surface pattern is lifted off the floor of the tunnel on a large piece of transparent tape.

Typically the lampblack is mixed with kerosene as the carrier but for this experiment the carrier was a mixture of kerosene and diesel fuel. The diesel fuel was added in order to delay the evaporation of the carrier until the mixture had been carried through the entire interaction.

30

No precise measurements of the quantities of diesel, kerosene, and lampblack used in the mixture were made. Rather the ingredients were added using a trial-and-error method until the mixture appeared to have a promising consistency. After the mixture had been tried in a tunnel run, the contents of the mixture were modified in order to try and produce better results. This iterative procedure was used until the mixture was judged satisfactory.

3.4.3 Fluctuating Wall Pressure Measurements

The fluctuating surface pressure in the interaction was measured using between six and eight pressure transducers along rows B and C of the instrumented plug. By rotating the plug 180 degrees it was possible to obtain data at four distances from the fin leading edge. In the following section the term "inner" refers to the condition where the plug has been installed with a 180 degree rotation, such that the transducer rows are upstream of the center of the plug. Also, when the plug is in the inner position the transducer rows are closest to the fin leading edge. Conversely, when the plug is in the "outer" position the transducer rows are downstream of the center of the plug and the rows are furthest away from the fin leading edge. The plug is shown in the outer position in the figures of the preceding sections. The majority of the data was collected with a sampling rate of 200 kHz, but since the number of data records acquired per run was constant, some runs were repeated using a sampling frequency of 50 kHz in order to obtain better resolution of the lower frequencies in the power spectrum.

Measurements were made perpendicular to the inviscid shock wave for all runs in which the transducer rows were in the inner position. When the transducer rows were in the outer position, measurements could be made normal to the inviscid shock for fin angles less than 22 degrees. Table 4 lists the orientation of the transducer rows with respect to normal to the freestream for all measurements made with the plug in the outer position.

Table 4. Orientation of Transducer Plug in Outer Position

Fin Angle (deg.)	Inviscid Shock Angle (deg.)	Transducer Row Angle (deg.)	Angle Between Transducer Row and Normal to Shock (deg.)
16	25.48	25.5	≈0
18	27.65	27.5	≈0
20	29.9	30	≈0
22	32.23	32	≈0
24	34.64	37 or 34.5	≈3 or 0
26	37.14	64	≈26
28	39.74	64	≈24

32

4. Results

4.1 Surface Flow Visualization

Originally, surface flow visualization was to be made during the first stage of the test program using a variation of the standard kerosene-lampblack technique.[23] However, due to the poor quality of some of the surface patterns obtained in the first stage, additional surface flow visualization was made at the end of the second stage of the test program.

Because of the low static pressure ($\approx$ 0.6 psia) in the Mach 5 tunnel, the kerosene in the standard flow visualization slurry evaporates before an adequate record of the streamlines can be obtained. For this reason diesel fuel was added to the mixture in order to delay the drying of the slurry and allow sufficient time for the lampblack to be deposited throughout the wall shear stress field. The key to employing this method of flow visualization is obtaining exactly the right mixture of diesel fuel, kerosene, and lampblack. If the mixture is too "wet", i.e., the ratio of diesel fuel to kerosene is too high, the slurry will not dry during the run and the backflow at tunnel shutdown will blur any features in the surface pattern generated by the interaction. Conversely, if the slurry is too "dry", i.e., with a low ratio of diesel fuel to kerosene, the slurry will dry before the surface pattern has been defined. This latter problem is the one typically encountered when the fin angle of attack must be reduced in order to decrease blockage for tunnel startup and then increased to the test angle after supersonic flow has been established in the test section.

Thus, in the first stage of the test program, which used the large fin, successful surface flow visualizations were obtained only for fin angles of 20, 22, and 24 deg. These angles were low enough so that the fin angle, α, did not have to be reduced for tunnel startup. Fin angles lower than 20 deg. exhibited a problem with the surface flow patterns not drying before they were distorted by the backflow at shutdown. Tests at fin angles higher than 24 degrees required a reduction in fin angle for tunnel startup and the slurry typically dried before the interaction surface pattern had a chance to form.

At the end of the second stage of the test program surface flow visualization was obtained using the smaller fin made for the second stage of the experiments. Satisfactory results were obtained for all fin angles studied because a reduction in fin angle was not required for

tunnel startup. Additionally, the slurry mixture was improved upon over that used in the first stage of the investigation, producing superior patterns. The quantitative results obtained using the second fin are practically identical to those obtained in the first stage.

A typical result of this method of surface flow visualization is shown in Figure 43. The upstream influence and separation lines are noted on the figure. The angle of the separation and upstream influence lines were determined by measuring the angle between the surface features outside of the inception region and a reference line in the freestream direction. The reference line was conveniently chosen as the line formed by the intersection of the tunnel floor insert and the tunnel floor and is noted in Figure 43. Finally, the virtual conical origin (VCO) was determined as the intersection point of a line drawn asymptotically to the separation line in the quasi-conical farfield and the inviscid shock trace extended ahead of the fin leading edge. Table 5 summarizes the results of the surface flow visualization made during both stages of the test program.

Table 5. Summary of Surface Flow Visualization Results

Fin Angle (deg)	Separation Line Angle (deg)	Upstream Influence Angle (deg)	Distance to VCO from fin L.E. (in)
16	34.5	- - - -	- - - -
18	41.5	- - - -	1.9
20	44	45	2.05
22	48	49	1.63
24	53	54	1.48
26	58.5	- - - -	1.2
28	64	66	0.81

The data presented in Table 5 are average values determined from between two and six surface flow visualization patterns for each angle of attack, with the exception of the results at α = 26 deg. for which only one surface pattern was obtained. A dashed line in the table indicates that results could not be determined for that case. The separation lines were clear for all angles except 16 degrees which had less well defined surface flow features, probably due to

34

the relatively weak strength and high sweep of the interaction.   For all fin angles for which multiple surface patterns were obtained the separation line angle was very repeatable (a maximum deviation of 2 degrees from the average value for the worst case).   In contrast, the upstream influence line was generally very difficult to discern in the surface flow patterns; no line was seen in any of the patterns taken at 16, 18, or 26 degrees.   For the angles for which upstream influence lines were observed, the upstream influence angle was greater than the separation angle by about 1 degree.

Finally, the distance from the fin leading edge to the VCO along the inviscid shock trace exhibited considerable scatter between the various patterns obtained at the same fin angle.   As shown in Table 5 above, for $\alpha \geq 20$ deg. the distance from the fin leading edge to the VCO decreases as the fin angle and, hence, the interaction strength, is increased.   This is the same trend observed in other investigations.[10]   No distance to the VCO was determined for the $\alpha =$ 16 deg. cases, and the $\alpha = 18$ deg. cases appear to be in the inception region.   This conclusion stems from the fact that the distance to the VCO is unrealistically small when compared with the results for higher fin angles.

Table 6 compares the results from the current study with the surface flow feature angles predicted using the correlations of Lu, Settles, and Horstmann[13] and Zheltovodov, et al.[14]   Both correlations were developed using the results of surface flow visualization.   The upstream influence angle correlations of Lu, Settles, and Horstmann were developed using data obtained at Mach numbers between 2.5 and 4 and for interactions with shock angles less than 20 degrees greater than the freestream Mach angle (i.e., $\beta_0 - \mu \leq 20$).   The correlations of Zheltovodov, et al., for upstream influence and separation angles were developed using data at similar Mach numbers and shock angles.   Chapter 2 provides a more complete description of both sets of correlations.

Table 6. Comparison of Results with Correlations

α (deg)	Lu, et al.[13] β_{ui} (deg)	Zhelt.[14] β_{ui} (deg)	Zhelt.[14] β_s lam. (deg)	Zhelt.[14] β_s turb. (deg)	Expt. β_{ui} (deg)	Expt. β_s (deg)
16	36.9	38.1	34.2	36.8	- - - -	34.5
18	39.94	41.5	37.6	40.7	- - - -	41.5
20	42.81	44.8	41.0	44.5	45	44
22	45.59	48.3	44.3	48.4	49	48
24	47.96	52	47.5	52.2	54	53
26	50.19	55.8	50.7	56.0	- - - -	58.5
28	52.15	59.8	53.7	59.8	66	64

From inspection of the table, both correlations reasonably predict the surface feature angles except for the strongest interaction where $\alpha \geq 26$ deg. This may result because the correlations were developed for Mach numbers between 2 and 4 and the Mach 5, $\alpha \geq 26$ deg. interactions are significantly stronger than any of those used to develop the correlations. For angles less than 28 deg. the separation angles determined experimentally show excellent agreement with those predicted via the Zheltovodov correlation. The correlation for turbulent reverse flow appears to best match the experimental results for $\alpha > 16$ deg., while for $\alpha = 16$ deg. the correlation for laminar reverse flow appears to provide the best prediction. In general, the experimentally determined surface flow feature angles showed good agreement with those predicted using correlations developed in other facilities. This indicates that the interactions generated in the current experiment are consistent with those studied in earlier work.

4.2 Fluctuating Wall Pressure Measurements

Fluctuating wall pressure measurements were made using up to eight high frequency pressure transducers simultaneously. Two data sets were compiled from these wall pressure measurements. The first, made at fin angles of 20, 24, and 28 degrees, consists of measurements made through the interaction from the undisturbed incoming boundary layer to

as close to the fin surface as was possible. Measurements were made at two distances from the fin leading edge using rows A and C. The second data set consists of measurements in the upstream region of the interaction from the incoming boundary layer to just downstream of separation. Data were obtained for fin angles of 16, 18, 20, 22, 24, 26, and 28 degrees measured on the outer radial row, row C. Exact transducer port and survey line locations with respect to the fin are given in Chapter 3.

Inviscid shock theory predicts a Mach reflection at the tunnel sidewall for $\alpha = 28$ deg. The corresponding surface flow visualization pattern is shown in Figure 44. The transducer ports on the outer row, C, appear to be quite near the sidewall interaction while the transducer ports on the middle row, B, appear to be outside and upstream of it. Power spectral densities (PSDs) for the transducer nearest the upstream influence line for all three radial positions in the 28 degree interaction are shown in Figure 45. The PSD near the upstream influence line for an unswept compression ramp interaction is also shown in Figure 45. It might be anticipated that the unswept compression ramp interaction would have similar features to the interaction produced by the essentially 2-D shock of the same strength impinging on the sidewall. The similarity of the PSD on row C to that of the unswept compression ramp, notably the low frequency components absent from the PSDs on rows A and B, confirm the suspicion that the outer row data near the tunnel sidewall are contaminated by the sidewall interaction. Surface flow visualization for the 26 degree sharp fin interaction is shown in Figure 46. The sidewall interaction in Figure 46 is significantly smaller and further downstream than that of the 28 degree interaction shown in Figure 44. From inviscid shock theory, the flow can be turned back to the freestream direction via a reflected shock for fin angles below 26 degrees. Hence, there appears to be no problem with interference from the sidewall interaction for fin angles below 26 degrees.

Due to the probable wall interference with the measurements made on row C at $\alpha = 28$ deg., additional 28 degree measurements were made on row B, closer to the fin leading edge. However, only measurements in the upstream region of the interaction were made in this case.

4.2.1 Mean Pressure Distributions

The mean wall pressure distributions through the interaction for $\alpha = 20$, 24, and 28 deg. are shown in Figure 47. The abscissa is measured normal to the inviscid shock trace. Hollow symbols denote measurements made on rows B and C while filled symbols denote measurements made on row A. As noted on the figure the distributions have been vertically offset so that the data for each fin angle may be clearly seen. The mean pressure has been normalized by the freestream static pressure and the distance from the inviscid shock trace has been normalized by the incoming boundary layer thickness. The location of separation determined from surface flow visualization is shown by the "S" near each distribution and the theoretical inviscid pressure level for each fin angle is indicated by the dashed line. Interference from the sidewall interaction does not appear to have significantly altered the mean pressures measured on the outer row of the 28 degree interaction.

As seen in Figure 47, the initial pressure rise moves upstream and steepens as the fin angle, and subsequently the interaction strength, increases. Figure 47 also shows the increase in interaction scale with radial distance from the fin leading edge; the initial pressure rise occurs further ahead of the inviscid shock as the distance from the fin is increased. The unnormalized mean wall pressure distributions in the upstream region of the interaction for all fin angles are shown in Figure 48. Each data point is the average of several measurements. It is again evident from Figure 48 that as the interaction strength is increased, the initial pressure rise moves further upstream with respect to the inviscid shock.

Since the focus of this investigation is on the fluctuating wall pressures and not on the mean wall pressures, high frequency transducers were used. The frequency range to be measured required transducers with stiff diaphragms, which have relatively large pressure ranges (i.e., 0-50 psia). Since they are not ideally suited to measuring the relatively low pressures encountered in these interactions, the scatter in the mean pressures in Figures 47 and 48 is to be expected. Overall though, the features and trends evident in the mean pressure distributions agree well with those measured by other investigators.

4.2.2 RMS Distributions

The standard deviation of the wall pressure signals through the entire interaction for α

= 20, 24, and 28 deg. measured on rows A and C are shown in Figure 49. Data measured on row B in the upstream region of the interaction is also included. From comparison with Figure 47 it is evident that the initial rise in rms occurs just upstream of the initial rise in the mean pressure. In contrast to the mean distribution, which exhibits a flat, plateau region after the initial rise, the rms distributions show a sharp initial rise after which they generally continue to increase towards the fin face. The peak in the rms distribution just after the initial rise that is typically associated with an intermittent separation shock wave is present in all distributions except α = 20 deg. on the inner row. For the α = 20 deg. interaction the peak in the rms distribution probably falls between the transducer ports and is, therefore, not seen in the distribution.

The rms distributions in the upstream region of the interaction for all fin angles are shown in Figure 50. It can be seen from Figures 49 and 50 that the rms levels increase globally as the fin angle is increased. Whether this is a function of the increased strength of the interaction (i.e., inviscid shock strength) or the decreased sweep will be commented on in a later section. Finally, from inspection of Figures 49 and 50, it appears that the interference from the sidewall interaction for α = 28 deg. has affected the rms of the outer transducers on row C. The fact that similar rms levels occur on rows A and B at α = 28 deg. seem to indicate that the higher rms levels seen on row C are not due to the interaction generated by the sharp fin, but rather, the tunnel sidewall interaction.

The standard deviation distributions normalized by the local mean wall pressure both through the interaction and in the upstream region are shown in Figures 51 and 52, respectively. The first point to note upon inspection of Figure 51 is the similarity with the results of Tran, shown earlier in Figure 18b. Although Tran's distributions do not have the large peak just in front of the inviscid shock, the present interactions are considerably stronger than those of Tran and it is possible that this phenomenon evolves as the strength of the interaction is increased. This conclusion is supported by Figure 11 which showed the normalized rms distributions for unswept compression ramps at Mach numbers of 3 and 5. The Mach 5 data exhibit a significant peak near the inviscid shock trace while in the Mach 3 data the peak is relatively small. Also similar to Tran's distributions are the relatively low normalized rms values reached near the fin surface (i.e., $\approx$ 0.05) by all the distributions. Figures 51 and 52 show that the normalized

39

standard deviation increases as the fin angle is increased. This indicates that the increase in standard deviation with increasing fin angle is not simply due to the increased mean pressures in the interaction. Finally, the influence of the sidewall interaction is seen again in Figures 51 and 52 where the rms levels measured on the outer row for α = 28 deg. are higher than the data taken on the inner two rows.

4.2.3 Characteristics of Pressure Signals

Samples of wall pressure histories for six transducers in the upstream region for α = 24 deg. and the corresponding probability density distributions (PDDs) and power spectral densities (PSDs) are shown in Figure 53. The latter are calculated from 256 records of 1024 points. The sample time-histories are plotted on the same scale in all cases so that direct, visual comparison of the fluctuating levels through the interaction can be made. The location of the transducers in the surface flow visualization pattern is shown in Figure 54. The spectral coefficients are multiplied by the frequency and normalized by the total variance of the signal so that the area under the curve is unity. The basic trends seen in these time histories, PDDs, and PSDs for α = 24 deg. are common to all other fin angles. Hence, the 24 degree data will be used as an example to demonstrate the trends seen in the upstream region.

Results from a transducer in the incoming undisturbed boundary layer are shown in Figure 53a. The wall pressure exhibits high frequency, very small amplitude fluctuations, the PDD is essentially normally distributed, and the PSD shows that the dominant frequencies are high as would be expected for the incoming boundary layer (i.e. $U_\infty/\delta \approx 50$ kHz). Data from a transducer located in the initial compression region are shown in Figure 53b. The time history shows a few small amplitude, one sided pulses when the separation shock foot crosses the transducer. Although the intermittent nature of the signal is not very evident from the time history, the slightly skewed PDD is characteristic of a translating shock wave with a low intermittency. Also, the obvious shift in power to lower frequencies shown by the PSD is characteristic of a signal that is weakly intermittent. The data from the third transducer, located between the upstream influence and separation lines as seen in Figure 54, are shown in Figure 53c. The data are now easily recognized as being intermittent. The PDD is now more skewed and the PSD has a clearly defined center frequency around 5 kHz. Figure 53d is based on data

40

from the fourth transducer which is just downstream of separation in the surface flow visualization. Upon visual inspection the pressure peaks in the raw pressure signal occur at approximately the same time as the pressure peaks on the previous two transducers. Because a well defined undisturbed boundary layer pressure level is not evident in the time history, it is unclear if this transducer is in the intermittent region. The PDD is slightly skewed to the left and the PSD still shows dominant frequencies around 5 kHz which would seem to indicate that the signal is still intermittent, however, probably very near 100 percent intermittency. The fifth and sixth plots on Figure 53 show the results from the transducers in the separated region. The PDDs for both channels are Gaussian, which is characteristic of separated flow, and the PSDs show a shift toward the higher frequencies associated with turbulent, rather than shock induced, fluctuations.

4.2.4 Intermittency

One of the primary questions addressed by this study was "Does the separation shock motion exhibit a transition from a translating, intermittent type motion to a quasi-steady, shuddering type motion, or does it remain the same for all sweepback angles?" The intermittent character of the fluctuating wall pressure signal was clearly evident in Figure 53c and could be discerned in Figures 53b. For all fin angles there were typically between two and three intermittent channels in the interaction. At this point the intermittency of the wall pressure signals as the angle of attack is increased will be examined.

Samples of the instantaneous wall pressure signals on the first intermittent channel in the interaction for α = 16, 20, 24, and 28 deg. are shown in Figure 55. The corresponding PDDs and PSDs are also shown. The intermittent character of the signals is evident from visual inspection of the signals. The skewed PDDs are also characteristic of an intermittent signal. For α = 20 and 28 deg. the PSDs show the distinct shift to lower frequencies. For the 16 and 24 degree cases the intermittency is lower and the evolution of the PSD from undisturbed boundary layer shape to the intermittent shape may be seen.

Samples of the wall pressure signals, PDDs, and PSDs for the second intermittent channel for α = 16, 20, 24, and 28 deg. are shown in Figure 56. In this case all the time histories are clearly intermittent and the corresponding PDDs are highly skewed. The PSDs are

41

all centered at the same low frequency ($\approx$ 5 kHz). This is because this second channel is well within the intermittent region for all angles and the dominant contributor to the power of the signal is the motion of the separation shock wave.

Intermittencies and zero crossing frequencies are shown in Figures 57 and 58. Because of the small scale of the intermittent region, the data set is necessarily sparse. Note, however, that the calculated zero-crossing frequency of between 3 and 4 kHz corresponds reasonably well with the dominant frequency of the intermittent PSDs described earlier. It is evident from Figures 57 and 58, as suggested by the time-histories discussed earlier, that the intermittent region is very small. If measurements were made at a greater radial distance from the fin leading edge the intermittent region would presumably be larger since the quasi-conical nature of the interaction in the farfield means that the interaction size grows linearly with distance from the virtual conical origin. However, in this study the transducers were located as far from the leading edge as possible without encountering interference from the sidewall interaction produced by the inviscid shock and the tunnel sidewall boundary layer. Hence, although the results show the fluctuating wall pressure signal is indeed intermittent, the length of the intermittent region is too small to obtain detailed distributions of the intermittency and zero crossing frequency through the interaction.

It is possible, however, to examine the increasingly intermittent nature of the fluctuating wall pressure by examining the skewness coefficient as a function of the fin angle of attack. The maximum skewness coefficient, which occurs just downstream of the upstream influence line, is plotted as a function of the inviscid shock angle in Figure 59. It can be seen that as the interaction sweep decreases, i.e., the shock angle increases, the maximum skewness increases. This increase is caused by the steepening pressure gradient behind the separation shock as the fin angle is increased. For low fin angles, such as 16 and 18 degrees that generate relatively weak interactions, the pressure downstream of the separation shock is not much higher than the pressure in the undisturbed boundary layer and the PDDs are only slightly skewed. In contrast, the higher fin angles which produce stronger interactions have a higher pressure behind the separation shock and the resulting PDDs are significantly skewed.

4.3 Conical Nature of the Mean Wall Pressure Field and Higher Order Moments

As discussed in Chapter 2, the surface flowfield features of sharp fin generated interactions have been shown to evolve quasi-conically in the farfield. Once the location of the VCO has been determined, the angular coordinates of surface features may be calculated. The VCO locations along the inviscid shock trace upstream of the fin leading edge, as determined by the intersection of the inviscid shock trace and the asymptote to the separation line in the farfield, were given in Table 5. Two other methods were also used to determine the VCO location. The first, a numerical method which made use of the mean wall pressure distributions, was not very successful due to scatter in the data. The second method, a variation of the graphical method used to determine the VCO distances in Section 4.2, produced consistent results with the same trends seen in earlier work.

The numerical method for finding the VCO position involved collapsing two mean wall pressure distributions measured at different spanwise positions. Since the mean wall pressure is known to be quasi-conically symmetric in the farfield, the VCO can be located by determining the VCO position that optimizes the collapse of the wall pressure distributions. However, because the measured mean pressures were always within the lowest 5-10% of the pressure range of the transducers used, there was considerable scatter in the data, as explained earlier. Thus, although a reasonable collapse of the distributions could be obtained (as will be shown later), this particular method did not generate realistic predictions of the VCO location.

The second method used the surface flow visualization and the measured rms distributions. Because the maximum rms in the initial compression region occurs close to the separation line, the transducer reading the peak rms value can be considered as lying along a ray which is approximately at the conical angle of the separation line in the flowfield. From geometry the distance from this transducer to the trace of the inviscid shock may be determined. By dividing this distance by the tangent of the difference in the angles of the separation line and inviscid shock, the distance from the survey line to the VCO may be calculated. Finally, by subtracting the distance between the fin leading edge and the survey line, the distance from the leading edge of the fin to the VCO may be determined. Using this method, referred to in Table 7 as the "Two-Point Method," the VCO position was calculated for all fin angles, although for some cases the fact that the survey line was in the inception region led to underpredicted VCO

43

positions. The results of all three methods are listed in Table 7. A dashed line in Table 7 denotes that a VCO position could not be determined for the given fin angle.

Table 7. Location of Virtual Conical Origin along Inviscid Shock Trace Ahead of Fin Leading Edge

Fin Angle (deg)	Graphical Method (in)	Numerical Method (in)	Two-Point Method (in)
16	- - - -	- - - -	3.69
18	1.9	- - - -	1.54
20	2.05	0.7	1.74
22	1.63	- - - -	1.66
24	1.48	0.8	1.22
26	1.2	- - - -	0.84
28	0.81	1.5	0.65

As seen in Table 7 above, both the magnitude and the trends in the results of the numerical method are in disagreement with the results of the graphical and two-point methods. The trends in the results of the graphical and two-point methods agree with the trends seen in the results of other investigators.[10] In light of the discussion of the physics behind the location of the VCO in Chapter 2, the trend observed in the numerical method of increasing VCO distance from the fin leading edge as the fin angle is increased is not logical. The only conclusion that may be made is that the numerical method is not reliable. In contrast, the results of the two-point and graphical methods agree well with each other and follow the trend in VCO position observed by other investigators. It should be noted, however, that the two-point and graphical methods are not completely independent. The conical angle of the separation line used in the two-point method is the average angle of the asymptote to the separation line used to determine the VCO position graphically. Although both the graphical and two-point methods give physically reasonable results, the wide use of the graphical method in the literature makes the results of that method the better choice for examining the conical collapse of the flow

properties.

The mean pressure distributions in conical coordinates for α = 20, 24, and 28 deg. are shown in Figure 60. As stated above, the virtual conical origins are those determined graphically. The location of separation, determined from surface flow visualization, and the theoretical inviscid shock location are noted on the figure as "S" and "β_0", respectively. The quasi-conical nature of the mean pressure distributions is quite evident by comparing Figure 60 with Figure 47 which shows the same data plotted versus distance normal to the inviscid shock trace. At a given fin angle, data at different radial distances from the virtual conical origin and with different physical dimensions collapse on what is essentially, given the unavoidable scatter in the data, a single curve.

The wall pressure standard deviation and the wall pressure standard deviation normalized by the mean wall pressure are plotted in conical coordinates in Figures 61 and 62. The VCOs are the same as those used in Figure 60. These figures answer one of the primary questions raised in the Introduction: "Does the standard deviation of the fluctuating wall pressure exhibit quasi-conical symmetry?" The distributions are not identical at both radial locations, but, for engineering purposes, little error would be incurred if the standard deviation distributions are considered quasi-conically symmetric. Note that the data for α = 28 deg. shows a very good collapse for rms values measured on the two inner spanwise rows, A and B. The rms levels on the outer spanwise row, C, are higher than the rms levels on the inner rows, probably due to the sidewall interaction and not the 28 degree fin interaction. This should be taken into account by the reader in the consideration of quasi-conical symmetry.

Quasi-conical symmetry is also present in the distributions of such sensitive parameters as the higher order moments (skewness and flatness coefficients) which are shown in Figures 63 and 64 for the α = 24 and 28 deg. interactions. Variations in magnitude at the locations of peaks in the distribution are due to slight differences in transducer location within the interaction. For the 28 degree interaction the first six data points on the outer row, C, have not been plotted since the interference from the sidewall interaction significantly alters the higher order moments.

4.4 Effect of Sweep on the Flowfield

Having shown that the mean and fluctuating wall pressure fields are quasi-conical in the sharp fin generated interaction, the next question to be addressed is "What effect does the flowfield sweep have on the interaction?" In this section three aspects of the change in flowfield characteristics with changing sweep will be discussed. First, two- and three-dimensional interactions under identical incoming flow conditions will be compared and contrasted, followed by a discussion of the effect of small changes in sweep. Finally, it will be shown that the sweep of the interaction is the determining factor affecting the maximum rms in the upstream region of the interaction.

4.4.1 Comparison of Two and Three-Dimensional Interactions

In this section, the 28 deg. unswept compression ramp data of Erengil[19] are compared with the 28 deg. fin data of the current study. Both studies were made in the same facility under practically identical conditions and the inviscid pressure rise of both interactions is the same.

The rms distributions for the unswept compression ramp and fin are shown in Figures 10 and 49, respectively. The first obvious difference in the two distributions is that the maximum rms level in the intermittent region for the unswept interaction is approximately twice that of the swept interaction. This difference in rms levels between 2-D and 3-D interactions of the same inviscid strength was also noted by Tran, as was the fact that the physical scales of the same "regions" of the interaction for both cases are different. For example, the unswept interaction has an intermittent region approximately 1.5 boundary layer thicknesses in length while the swept interaction has an intermittent region about a third of that length. Of course, it should be pointed out that the unswept flowfield has an essentially constant scale intermittent region due to the two-dimensionality of the interaction while the swept interaction grows approximately linearly in the farfield with distance from the fin leading edge. Finally, the rms distributions show that the maximum standard deviation occurs at different intermittencies in the swept and unswept interactions. In the unswept interaction the maximum rms occurs upstream of separation at an intermittency of 80-90%, with separation occurring after the rms has decreased from its maximum value. In contrast, the maximum rms of the sharp fin interaction occurs very near separation with an intermittency very close to 100%.

46

PDDs and PSDs at a low intermittency and at maximum rms in the upstream region for the compression ramp and sharp fin generated interactions are shown in Figure 65. The PDDs at low intermittencies are similar indicating that the flowfield structure and dynamics in the initial compression region are very similar for both interactions. However, at maximum rms the swept interaction has an approximately Gaussian PDD and the unswept interaction PDD is clearly bimodal. The PSDs for both interactions show that the two-dimensional interaction has significantly lower dominant frequencies than the unswept interaction at all positions in the intermittent region. Thus, towards the downstream end of the intermittent region the interaction structure is different for unswept and swept interactions. Although there is no supporting evidence, in the opinion of the author the lower rms levels and diminished size of the intermittent region in the sharp fin interaction are due to the sweep of the flowfield. The interaction sweep provides an exit for the fluid in the separated region analogous to the "three-dimensional relieving effect" seen in inviscid shock theory. Thus, the flow has another dimension to move in and the severity of the interaction is diminished.

4.4.2 Effect of Changing Sweep on Separation Shock Frequency

The changing sweep of the interaction does not appear to affect the spectral characteristics of the fin generated interaction. The power spectral densities at maximum standard deviation for fin angles of 16, 20, 24, and 28 degrees are shown in Figure 66. The sweep of the separation line changes 29.5 degrees over this range of fin angles. The PSDs at the position of the maximum measured skewness coefficient in the same interactions are shown in Figure 67. The similarity of the PSDs at maximum rms and skewness coefficient for all fin angles indicates that very little, if any, change in the interaction structure is occurring as the sweep of the interaction is changed. The magnitude of the fluctuations, as determined by the rms, increases as the sweep angle is decreased but, since the PSDs are normalized by the variance of the signal, the change of fluctuation magnitude is not reflected in the PSDs.

The spectral characteristics of the interaction appear to be relatively constant over the range of highly swept interactions examined in this study. Therefore, the change in the interaction frequency content, from the low frequency dominated fluctuations of the unswept interactions to the higher frequency content of the highly swept interactions, must occur in the

47

range of interactions with relatively low sweep angles.

4.4.3 Effect of Sweep on Maximum RMS Values and Intermittency

It was previously demonstrated, via Figures 50 and 52, that the maximum rms near separation increases with the fin angle. Because the sweep of the interaction decreases and simultaneously the strength of the interaction increases as the fin angle is increased, it is not readily apparent which parameter causes the change in the standard deviation. The effects of sweep and inviscid pressure rise could be decoupled if data were available for which the sweep of the interaction was the same but the inviscid pressure rise was different, and vice versa. Fortunately, the swept compression ramp data of Erengil[24] have recently become available and have been compared with the data of the present study. Both studies were made under practically identical flowfield conditions; hence, the only difference in the two studies is the geometry of the shock generator. For a given corner line sweep angle the inviscid pressure rise generated by the swept compression ramp is different than that generated by a sharp unswept fin at the same angle. This is due to the inclined face of the compression ramp. Erengil's swept compression ramps had a constant streamwise angle of 28 deg. and sweepback angles ranging from 0 to 50 deg.

The maximum standard deviation as a function of the overall inviscid pressure ratio for both data sets is shown in Figure 68. Inviscid pressure ratios for the swept compression ramps were calculated using the Mach number and deflection angle normal to the swept face of the ramp. No pressure ratio for the ramp with 50 deg. sweep was calculated because the shock was not attached to the ramp corner line. From inspection of Figure 68 it is clear that the maximum rms does not correlate with the inviscid pressure rise. Each geometry has an approximately linear increase in rms with increasing inviscid pressure ratio but with very different slopes. Thus the rms level is a function of local flowfield structure and not overall inviscid pressure rise.

The maximum rms for the interactions generated by both geometries as a function of separation line sweep angle is plotted in Figure 69. The smooth trend in the data indicates that, for fixed incoming flow conditions, the maximum rms is a function of interaction sweep. This conclusion agrees well with the findings of previous studies which indicated that the structures

within the interaction increased in intensity with increasing normal Mach number. The normal Mach number can be considered to be a measure of the sweep of the interaction.

Similar to maximum standard deviation, the maximum skewness coefficient measured in the interaction also scales with the sweep angle of the separation line. This is shown in Figure 70 for the data of Erengil and the current study. The scatter in Figure 70 is due to the fact that the finite transducer spatial resolution limits the ability to resolve the exact value of the peak skewness coefficient. The maximum skewness coefficient in the intermittent region may be used as a measure of the *intermittent intensity* of the interaction. As the pressure rise across the separation shock increases, the difference between the most probable (undisturbed boundary layer) pressure and the mean pressure increases. As a result the skewness coefficient also increases. Figure 70 shows that the intermittent intensity (the relative magnitude of the intermittent characteristics) scales with the sweep of the interaction.

4.5 Comparison with other Sharp Fin Experiments

One of the primary goals of this study was to determine the type of motion of the compression system upstream of separation, and, if possible, to explain and understand the results of Tran and Gibson in a common reference frame. The results of the current experiment clearly show that the interaction produces an intermittent separation shock wave for fin angles above 16 degrees. The questions that remain are therefore, "Why didn't Gibson observe the intermittency of the wall pressure signals?" and "Are Tran's results consistent with those of the current study?" The answers to these questions will be discussed in the following section.

Tran's results at Mach 3 indicated that the intermittent character of the wall pressure signal was first observable around $\alpha = 12$ deg., and that for $\alpha \geq 12$ deg. the intermittent characteristics of the signal increased in intensity as the fin angle was increased. When viewed in the larger framework which includes the current study, Tran's results appear to be consistent with the current data. Although Tran did not observe any intermittent characteristics for $\alpha = 10$ deg., a plausible argument why this was the case may be made using the results of the current study.

In Section 4.4 the intermittent intensity was shown to scale with the sweep of the interaction. Figure 71 shows the distribution of skewness coefficients as a function of local

49

conical angle for the $\alpha = 16, 20, 24$, and 28 deg. interactions of the current study. At $\alpha = 16$ deg. the skewness of the wall pressure signal and the size of the intermittent region have both become relatively small. The sweep of the inviscid shock at $\alpha = 16$ deg. is between the sweep angles of Tran's 10 and 12 deg. interactions. Coupled with the fact that Tran's interactions were significantly weaker than the interactions of the current study, it is plausible that the intermittent characteristics in Tran's interaction had not developed or were too small to be observed for Tran's $\alpha = 10$ deg. interaction.

The fact that Gibson did not observe intermittent wall pressures in his Mach 5 interactions can probably be attributed to a resolution problem with his instrumentation. Gibson's and the current study were made in the same facility with the same freestream conditions. The only difference in the two studies was that Gibson's was made on a flat plate with a boundary layer thickness of approximately 0.28 inches, while the current study was made on the tunnel floor with a boundary layer thickness of 0.59 inches. Both studies used the same transducer spacing, 0.115 inches. Thus, Gibson's ratio of transducer spacing to boundary layer thickness was about 0.4 while the current study had a ratio of about 0.2. Although the exact relation between boundary layer thickness and the intermittent region length scale is not known, it can be speculated that the latter should be determined to some extent by the boundary layer thickness. Section 2.1. discussed the inception region and the fact that the incoming boundary layer imposes a dimension on the flow which is the inception length. The inception length in turn affects the position of the VCO. Thus, when compared to the current study, Gibson's thinner boundary layer would result in a VCO closer to the fin leading edge. Since Gibson's transducer locations were at approximately the same distance from the fin leading edge as the transducers in the current study, then in a conical reference frame Gibson's transducer spacing would span a greater angular increment than the transducer spacing in the current study. Figure 72, which shows the skewness coefficient distributions for both studies for $\alpha = 18$ deg., supports this conclusion. The conical coordinates for the distributions are different because Gibson did not have surface flow visualization results for $\alpha = 18$ deg. and had to use the empirical data of Lu and Settles[10] to predict his VCO location. The scatter in Lu and Settles data, as well as the fact that Gibson had to extrapolate the correlation to Mach 5, make the location of Gibson's VCO questionable. Regardless of the exact conical coordinates, both

50

distributions show a peak in skewness near the upstream region of the interaction. The peak in Gibson's skewness coefficient distribution indicates that the pressure signals were intermittent. However, the lower values of the skewness coefficient in Gibson's interaction as well as the smooth trend of the data indicates that Gibson's transducers and/or spacing were probably too large for the interaction. Thus, it can be hypothesized with some measure of confidence that Gibson's pressure time-histories did not show any intermittent characteristics because the transducers were too far apart and too large when compared to the spatial extent of the pressure gradient in the interaction.

4.6 Spectral Characteristics Through the Interaction

To the knowledge of the author, the current study is the first to make fluctuating wall pressure measurements from the upstream influence line to near the surface of the fin. The spectral characteristics of the wall pressure signals under the separated region and near the fin surface are of interest because they may reveal what is happening in the flowfield above the wall. For the range of interactions studied (α = 16-28 deg.) the PSDs exhibited the same trends in all the interactions. Hence, the outer row data for the α = 24 deg. interaction will be used as an example to describe the general trends within the interactions.

PSDs from the undisturbed boundary layer through to the fin surface for the α = 24 deg. interaction are shown in Figure 73. The shift of power from the high frequencies associated with the incoming turbulence to the lower frequencies associated with the shock motion in the intermittent region was discussed in an earlier section. Downstream of separation, the power in the signal shifts again to the higher frequencies associated with turbulent fluctuations. In the separated region the PSDs assume an approximately constant shape with the center frequency between 10 and 20 kHz. Moving further downstream, the PSDs show another shift to lower frequencies just upstream of the inviscid shock location. The power in the signal shifts slightly down to a lower center frequency of about 10 kHz and the very low frequencies on the order of 100 Hz show a significant increase in power. Finally, between the inviscid shock and the fin surface, the dominant frequencies in the pressure signal increase to a center frequency between 15 and 20 kHz. In this region the PSDs strongly resemble the PSDs further upstream in the separated region with the only difference being that there is less power in the

51

5-10 kHz range near the face of the fin.

By comparing Figure 73 with the Alvi and Settles flowfield model, the frequency content of the wall pressure fluctuations may be seen to correlate with some of the structures in the flowfield. In the intermittent region the dominant low frequencies of the interaction are due to the unsteady motion of the separation shock. Moving further downstream in the interaction crossplane, there are no flow features in the Alvi and Settles model between the separation shock and the inviscid shock. Hence, the center frequency between 10 and 20 kHz in the separated region must be due to turbulent fluctuations in the separated boundary layer or the motion of the vortex beneath the separation bubble. Just upstream of the inviscid shock Alvi and Settles note the appearance of a "shocklet" in the reverse flow near the wall at an interaction normal Mach number of 2.45. The normal Mach number for the Mach 5, $\alpha = 24$ deg. interaction is about 2.8 and thus, should also have supersonic reverse flow. The PSDs in Figure 73 just upstream of the inviscid shock location show a slight shift in power to lower frequencies. This shift is probably due to the motion of the "shocklet" in the supersonic reverse flow. Finally, the Alvi and Settles flowfield model shows that the majority of the changes in flowfield occur after the inviscid shock. However, the PSDs in Figure 73 only show a shift in power back to a center frequency between 15 and 20 kHz. Either the impinging jet and corner vortex do not significantly affect the frequency of the wall pressure fluctuations or, more likely, the spatial resolution and proximity of transducers to the fin were not adequate to observe the effects of the impinging jet and corner vortex.

4.7 Influence of Incoming Boundary Layer Thickness on Compression System Frequencies

The effect of the incoming boundary layer on the sharp fin induced shock wave/turbulent boundary layer interaction may be examined by comparing the results of Gibson[5] with the current study. The power spectral densities at maximum wall pressure standard deviation for the 18 degree sharp fin interactions of Gibson and the current study are shown in Figure 74. While the power in the signal of the current study is centered around 5 kHz, the power in the fluctuations of Gibsons interaction is centered at a higher frequency, around 8 to 10 kHz. Gibson made fluctuating wall pressure measurements in the same facility as the current study with the only difference in the two experiments being that Gibson mounted the fin on a plate in

52

the center of the test section and in the current study the fin was mounted on the floor of the test section. Hence, the only difference in the two experiments is the incoming boundary layer thickness. The boundary layer on the floor of the test section, as discussed in Chapter 3, is approximately 1.51 cm thick. Gibson's boundary layer on the plate was only about 40 percent as thick as the floor boundary layer.

Originally, Gibson quoted a boundary layer thickness of 0.62 cm at a location about 3 inches ahead of his instrumentation plug and 1 1/2 inches off the tunnel centerline. Gibson's boundary layer survey was made 18.9 inches from the plate leading edge while his instrumentation plug was centered 22.1 inches from the plate leading edge. Assuming a linear boundary layer growth rate of about one hundredth of an inch per inch, the incoming boundary layer thickness over Gibson's instrumentation plug may be estimated to be about 0.72 cm.

Figure 75 shows the same power spectral densities plotted in Figure 74 only now the power in the signal is plotted as a function of the Strouhal number. The Strouhal number for these cases has been determined by dividing the frequency by the large eddy frequency of the incoming boundary layer. The large eddy frequency is approximated by dividing the incoming freestream velocity by the incoming boundary layer thickness. From Figure 75 it is evident that the center frequencies of both interactions seem to occur at a Strouhal number between 0.08 and 0.1. Figure 76 is the same as Figure 75 only now Tran's PSD at maximum standard deviation has been roughly sketched into the figure. From Figure 76 it appears that Tran's center frequency is not at the same Strouhal number. This may indicate a Mach number dependence on the center frequency of the PSDs.

4.8 Attempts to Correlate Peak RMS with the Flow Variables

A useful design tool would be a correlation that relates the maximum standard deviation in the intermittent region to the appropriate combination of flowfield variables. Using the Mach 3 data of Tran and the Mach 5 swept compression ramp data of Erengil[24] as well as the data of the current study, several attempts have been made to develop a correlation for maximum standard deviation in the intermittent region. Because Tran did not attempt to analyze his results in conical coordinates and did not report any VCO data, the conical coordinates of Tran's surface flow features were estimated from the dimensions of Tran's hardware (quoted in

53

Reference 2) and the VCO data of Lu and Settles.[10] Using this approach, Tran's upstream influence angles were estimated to within 3 degrees of those predicted using the correlation of Lu, Settles, and Horstmann.[13]

As noted in earlier sections, the maximum standard deviation does not scale with inviscid pressure rise, but rather with the sweep of the interaction. Figure 77 shows the maximum rms normalized by the freestream static pressure as a function of the separation line sweep angle. If scatter in the data and the fact that Tran's conical coordinates have been roughly estimated is taken into account, it appears that the data for both Mach numbers collapse in a smooth trend. Similar attempts were made by normalizing the maximum rms by the dynamic pressure, calculated using both the freestream and normal Mach numbers. As shown in Figures 78 and 79, neither approach collapsed the data.

5. Conclusions

Fluctuating wall pressure measurements have been made beneath the Mach 5 shock wave/turbulent boundary layer interactions generated by sharp, unswept fins at angles of attack of 16, 18, 20, 2, 24, 26, and 28 degrees. The experiment was conducted at Mach 5 under approximately adiabatic wall temperature conditions. Using standard time series analysis, the current study has attempted to answer several questions regarding the unsteadiness of the compression system near separation. Several of these questions are due, in part, to the seemingly contradictory results of the only two known previous studies of the unsteadiness of the sharp fin interaction. The results of the current study maybe summarized as follows.

1. The conical angles of surface flow features determined using the kerosene-lampblack method agree with the predicted values of the surface feature angles determined using the correlations of Lu, Settles, and Horstmann, and Zheltovodov, et al. Particularly good agreement is seen between the experimentally determined separation line angles and the correlation of Zheltovodov.

2. Visual inspection and time-series analysis of the fluctuating wall pressure signals between the upstream influence and separation lines indicate that the separation shock wave does generate an intermittent wall pressure signal, qualitatively similar to that seen in unswept interactions. This conclusion is supported by well defined peaks in the rms distribution in the intermittent region, skewed probability density distributions, and the appearance of large amplitude, low frequency "pulses" in the fluctuating wall pressure signal.

3. Using the virtual conical origin determined from surface flow visualization, it can be stated that within engineering accuracy both the mean pressure distributions and distributions of the higher order moments of the pressure signal collapse quasi-conically.

4. By comparing the results of the current study with the swept compression ramp results of Erengil, it has been shown that the maximum rms in the intermittent region correlates

with the sweep of the interaction and *not* with the inviscid pressure rise as had been suggested in the earlier literature. The maximum skewness coefficient measured in the intermittent region also scales with the sweep of the interaction.

5.   The earlier results of Tran and Gibson may now be explained within a common framework. The current study shows the intermittent characteristics of the interaction are weak and only just detectable as the interaction sweep angle increases beyond 60 degrees (i.e., the shock angle decreases below 30 degrees). For interaction sweep angles greater than 60 degrees neither Tran nor Gibson observed any intermittent characteristics. Since Gibson did not study any interactions with lower sweep angles and Tran observed intermittent characteristics in interactions with sweeps less than 60 degrees, the results of Tran and Gibson both agree with the findings of this study.

6.   Over the relatively small range of interaction sweeps studied in this experiment, the spectral content of the fluctuating wall pressure is approximately constant at the same relative position in the interaction. Thus, the experimentally observed change in the spectral content in the intermittent region from the low frequency ($\approx$ 1 kHz) dominated spectra in unswept interactions to the high frequency ($\approx$ 5 kHz) spectra seen in swept interactions must occur at lower interaction sweeps, and is not a continuous process with increasing sweep.

7.   Slight shifts to lower frequencies in the power spectra measured in the separated region near the inviscid shock trace may be due to the presence of "shocklets" in the reverse flow as seen by Alvi and Settles using conical shadowgraphy.

8.   The power spectra at maximum rms near separation for the $\alpha = 18$ degree interactions of Gibson and the current experiment collapse when plotted in terms of a Strouhal number based on freestream velocity and incoming boundary layer thickness. In contrast, Tran's normalized power spectra do not collapse with those at Mach 5, suggesting a dependence of the interaction frequencies on the Mach number.

56

9.   The maximum rms in the intermittent region, normalized by the freestream static pressure, measured under different freestream conditions, scales with the separation sweep angle. Normalizing the maximum rms by dynamic pressure does not collapse the data.

Although the results of the current study have certainly clarified some aspects of the unsteadiness of the sharp fin interaction, there are several points which require further investigation. Foremost of these is the effect of the incoming boundary layer thickness and Mach number on the unsteadiness of the interaction. A larger database of unsteady measurements is needed before any adequate conclusions may be reached.

6. References

[1]   Narayanswami, N., and Knight, D.D., "Viscous/Inviscid Effects in 3-D Shock
       Wave-Turbulent Boundary Layer Interactions," AIAA paper 89-0358

[2]   Tran, T.T., "An Experimental Investigation of Unsteadiness in Swept Shock
       Wave/Turbulent Boundary Layer Interactions," Ph.D. Dissertation, Mech. and Aero.
       Eng. Dept., Princeton University, March 1987.

[3]   Tran, T.T., Tan, D.K.M., and Bogdonoff, S.M., "Surface Pressure Fluctuations in a
       Three-Dimensional Shock Wave/Turbulent Boundary Layer Interaction at Various
       Shock Strengths," AIAA paper 85-1562, AIAA 18th Fluid Dynamics and Plasma
       Dynamics and Lasers Conference, Cincinatti, Ohio, July 1985.

[4]   Tan, D.K.M., Tran, T.T., and Bogdonoff, S.M., "Wall Pressure Fluctuations in a
       Three-Dimensional Shock Wave/Turbulent Boundary Interaction," *AIAA Journal*,
       Vol. 25, Jan. 1987, pp.14-21.

[5]   Gibson, B.G., "An Experimental Study of Wall Pressure Fluctuations Near Separation
       in a Mach 5, Sharp Fin Induced Turbulent Interaction," M.S. Thesis, Dept. of
       Aerospace Eng. and Eng. Mech., The University of Texas at Austin, August, 1990.

[6]   Gibson, Berry, and Dolling, D.S., "Wall Pressure Fluctuations Near Separation in a
       Mach 5, Sharp Fin-Induced Turbulent Interaction," AIAA paper 91-0646, AIAA 29th
       Aerospace Sciences Meeting, Reno, Nevada, Jan. 1991.

[7]   Settles, G.S., and Dolling, D.S., "Swept Shock Wave/Boundary-Layer Interactions,"
       in *AIAA Prog. in Astronautics and Aeronautics: Tactical Missile Aeordynamics*, edited
       by M. Hemsch and J. Nielson, Vol. 104, AIAA, Washington D.C., 1986, pp. 297-
       379.

[8]   Settles, G.S., and Dolling, D.S., "Swept Shock/Boundary-Layer Interactions -
       Tutorial and Update," AIAA paper 90-0375, AIAA 28th Aerospace Sciences
       Meeting, Reno, Nevada, Jan. 1990.

[9]   Inger, G.R., "Spanwise Propagation of Upstream Influence in Conical Swept
       Shock/Boundary-Layer Interactions," *AIAA Journal*, Vol. 25, Feb. 1987, pp. 287-
       293

[10] Lu, F.K., and Settles, G.S., "Inception Length to a Fully-Developed Fin-Generated Shock Wave Boundary Layer Interaction," AIAA paper 89-1850 , AIAA 20th Fluid Dynamics, Plasma Dynamics, and Lasers Conference, Buffalo, New York, June 1989.

[11] Alvi, F.S., and Settles, G.S., "A Physical Model of the Swept Shock/Boundary-Layer Interaction Flowfield," AIAA paper 91-1768, AIAA 22nd Fluid Dynamics, Plasma Dynamics, and Lasers Conference, Honolulu, Hawaii, June 1991.

[12] Rodi, P., Dolling, D.S., and Knight, D.D., "An Experimental/Computational Study of Heat Transfer in Sharp Fin Induced Turbulent Interactions at Mach 5," AIAA paper 91-1764, AIAA 22nd Fluid Dynamics, Plasma Dynamics, and Lasers Conference, Honolulu, Hawaii, June 1991.

[13] Lu, F.K., Settles, G.S., and Horstmann, C.C., "Mach Number Effects on Conical Surface Features of Swept Shock Boundary-Layer Interactions," *AIAA Journal*, Vol. 28, January, 1990, pp. 91-97.

[14] Zheltovodov, A., Private Communication, October 28, 1991.

[15] Alvi, F.S., and Settles, G.S., "Structure of Swept Shock Wave/Boundary-Layer Interaction Using Conical Shadowgraphy," AIAA paper 90-1644, AIAA 21st Fluid and Plasma Dynamics Conference, Seattle, Washington, June 1990.

[16] Gramman, R.A., and Dolling, D.S., "Detection of Turbulent Boundary Layer Separation Using Fluctuating Wall Pressure Signals," AIAA paper 88-4676, AIAA/NASA/AFWAL Conference on Sensors and Measurements Techniques for Aeronautical Applications, Atlanta, Georgia, September, 1988.

[17] Dolling, D.S., "Unsteadiness of Supersonic and Hypersonic Shock-Induced Turbulent Boundary Layer Separation," AGARD-FDP/VKI Special Course on "Three-Dimensional Supersonic and Hypersonic Flows Including Separation," Von Karman Institute for Fluid Dynamics, Brussels, July 1989.

[18] Gramman, R.A., and Dolling, D.S., "Dynamics of Separation in a Mach 5 Unswept Compression Ramp Flow," AIAA paper 90-0380, AIAA 28th Aerospace Sciences Meeting, Reno, Nevada, January 1990.

[19] Erengil, M.E., "Separation Shock Motion and Ensemble Averaged Wall Pressures in a Mach 5 Compression Ramp Interaction," M.S. Thesis, Dept. of Aerospace Eng. and Eng. Mech., The University of Texas at Austin, August, 1989.

[20] Settles, G.S., and Kimmel, R.L., "Similarity of Quasiconical Shock Wave/Turbulent

Boundary-Layer Interactions," *AIAA Journal*, Vol. 24, Jan. 1986, pp. 47-53.

[21]   McClure, W.B., Private Communication, November 1991.

[22]   Raman, K.R., "A Study of Surface Pressure Fluctuations in Hypersonic Turbulent
         Boundary Layers," NASA CR-2386, February 1974.

[23]   Settles, G.S., and Teng, H.Y., "Flow Visualization of Separated 3-D Shock
         Wave/Turbulent Boundary Layer Interactions," *AIAA Journal*, Vol. 21, March 1983,
         pp. 390-397.

[24]   Erengil, M.E., and Dolling, D.S., "Effects of Sweepback on Unsteady Separation in
         Mach 5 Compression Ramp Interactions," AIAA paper 92-0430, AIAA 30th
         Aerospace Sciences Meeting, Reno, Nevada, January 1992.
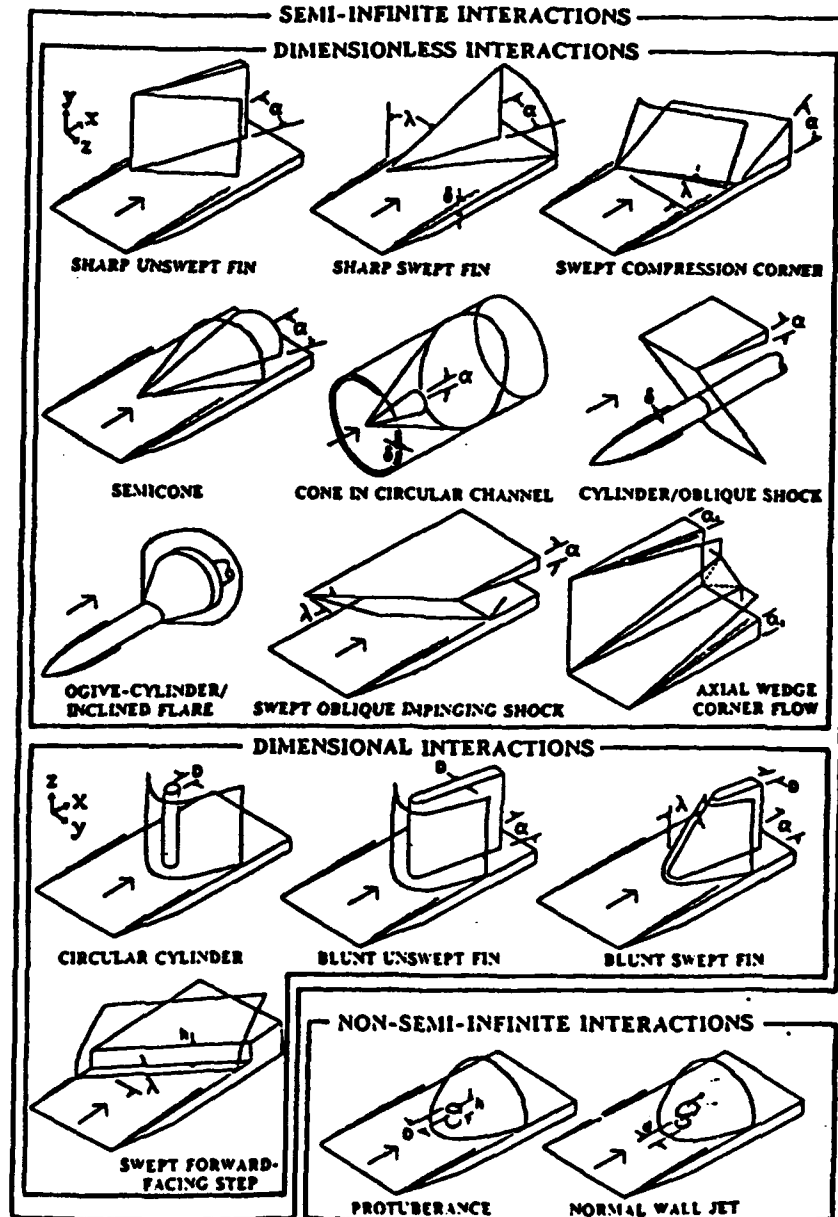
Fig. 1. Interaction Classifications (Ref. 7)

61
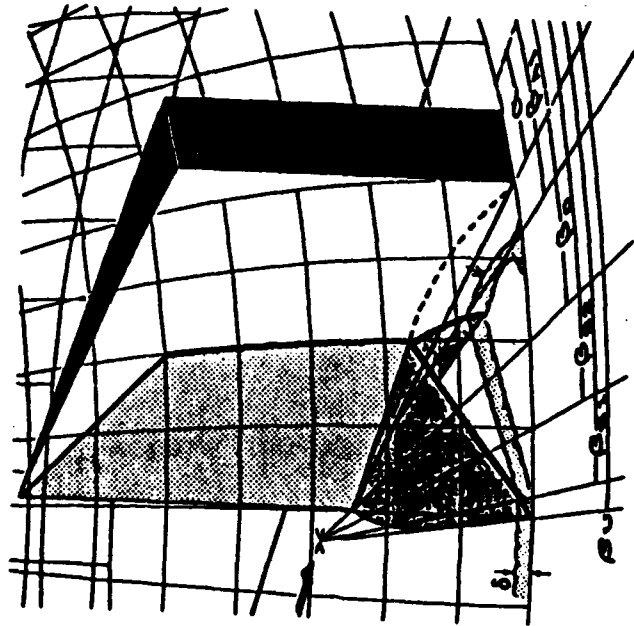
Fig. 3. Interaction Features and Nomenclature (Ref. 8)
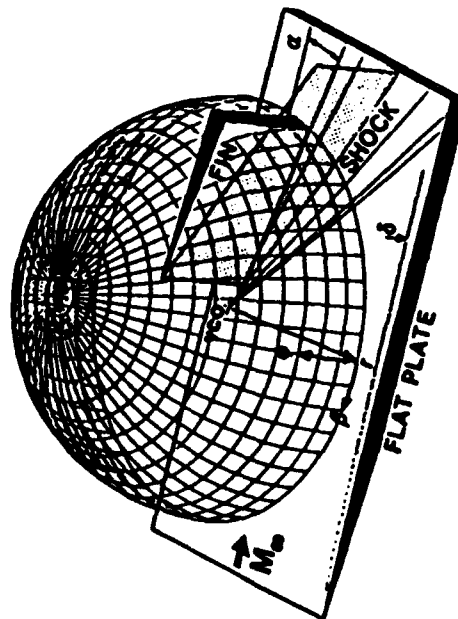
Fig. 2. Spherical/Polar Coordinate System (Ref. 8)

Line of Divergence (attachment)

Surface No. 1

Line of Coalescence (separation)

Surface No. 2

Fin

Not to Scale

Fig. 5. Interaction Stream Surfaces (Ref. 1)

Fig. 4. Surface Flow Features (Ref. 8)

Fig. 7. Conical Collapse of Mean Pressure Distribution (Data of Ref. 12, figure taken from Ref. 5.)

Fig. 6. Planar Laser Scattering Images (Ref. 11)

64
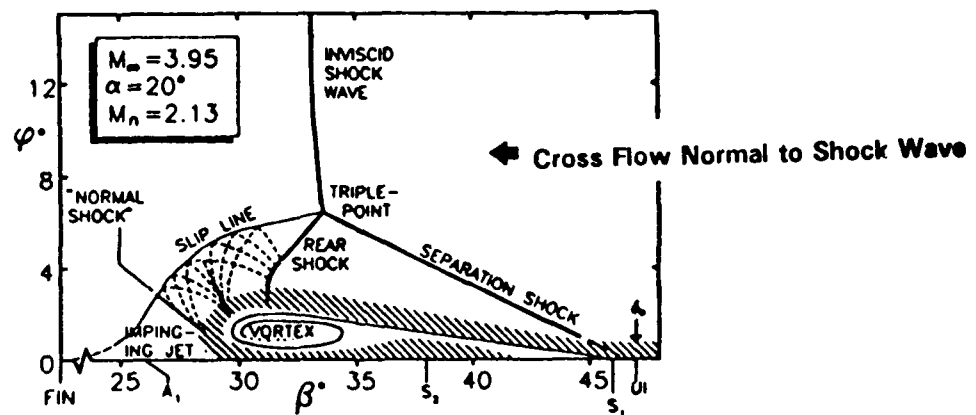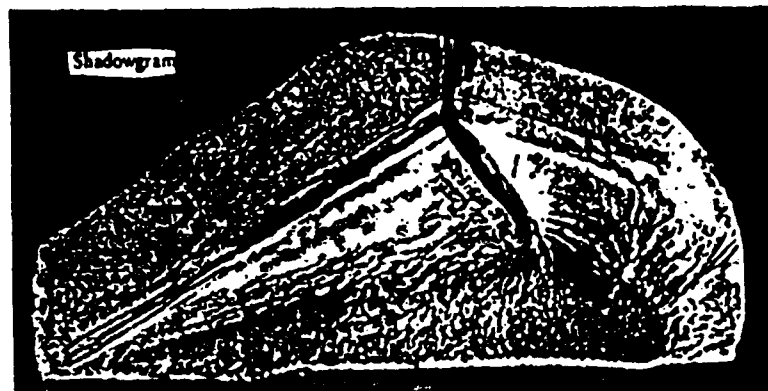
Fig. 8. Shadowgraph, PLS Image and Flowfield Map for
Mach 4, $\alpha = 20$ deg. Interaction (Ref. 11 and 15)
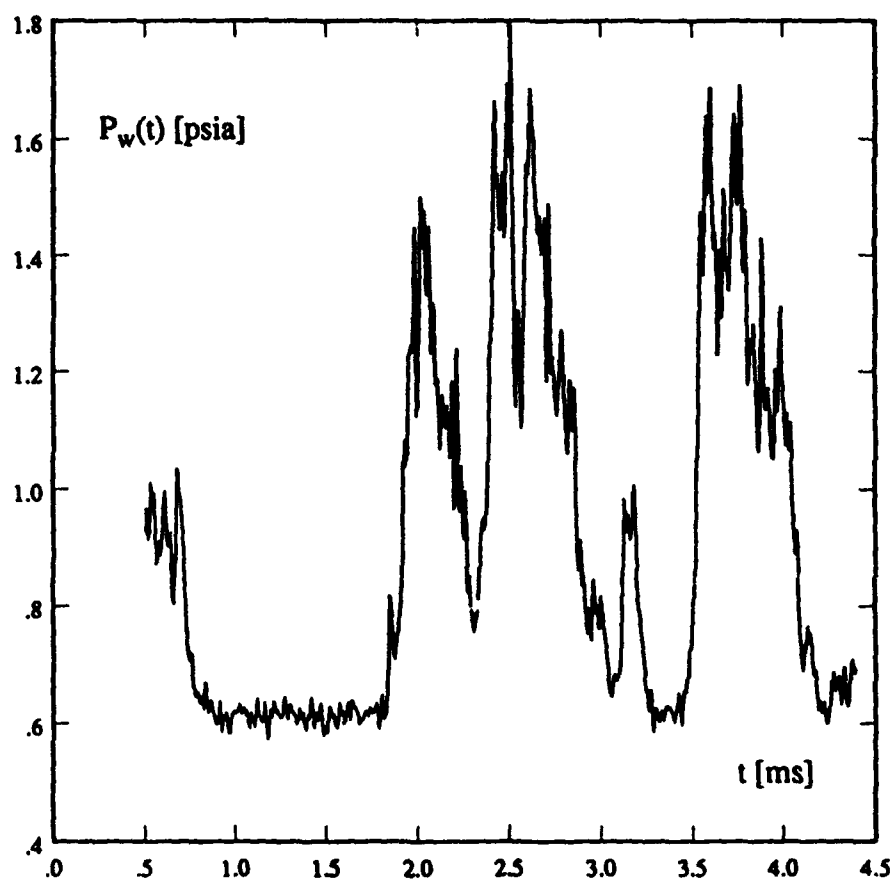
Fig. 9a. Wall Pressure Signals in the Intermittent Region (Ref. 19)

66
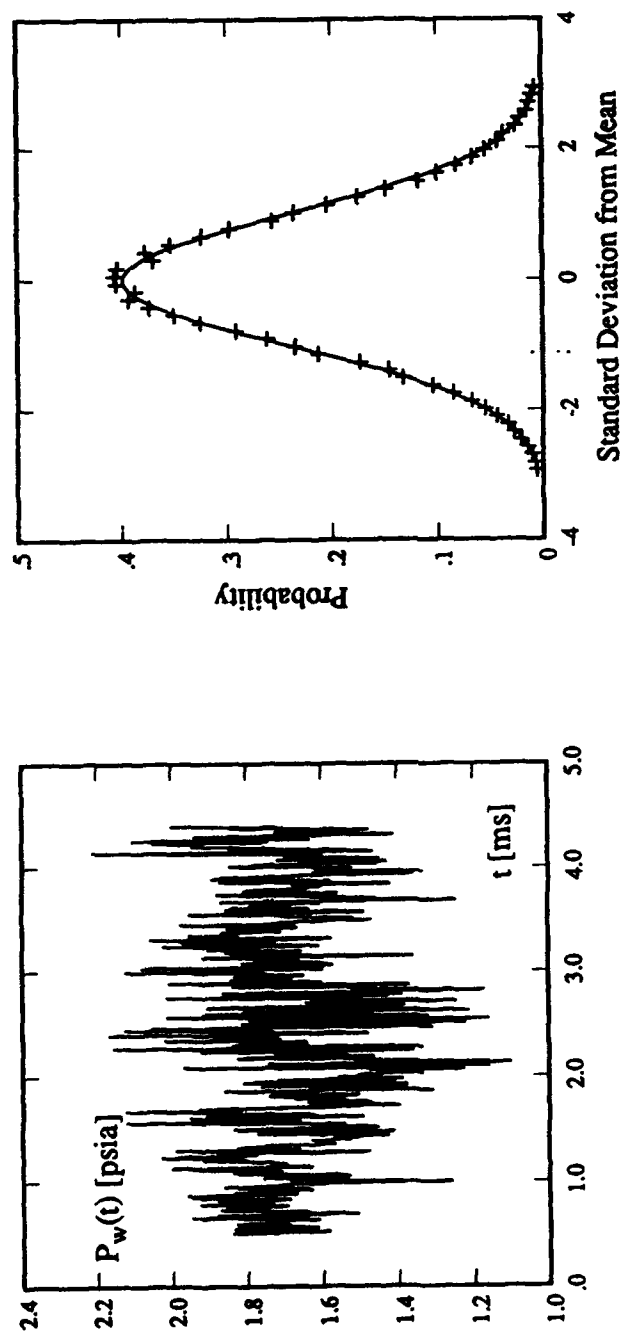
Fig. 9b. Wall Pressure Signal and Corresponding PDD in the Separated Region (Ref. 19)

67
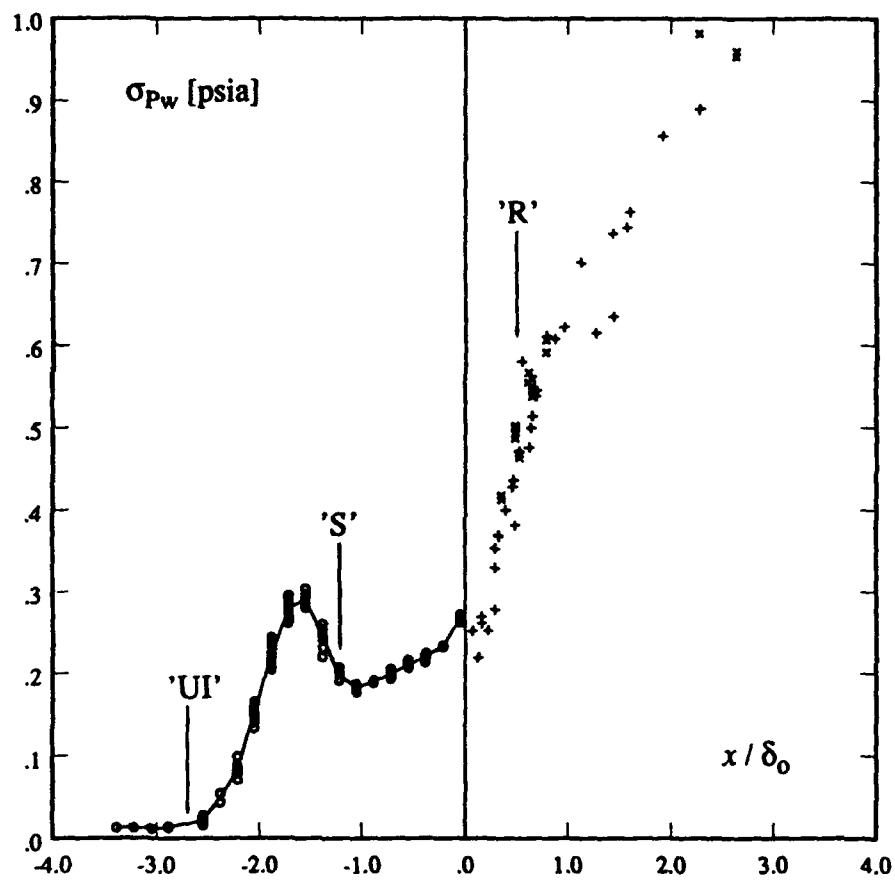
Fig. 10. Distribution of Standard Deviation of Wall Pressure (Ref. 19)
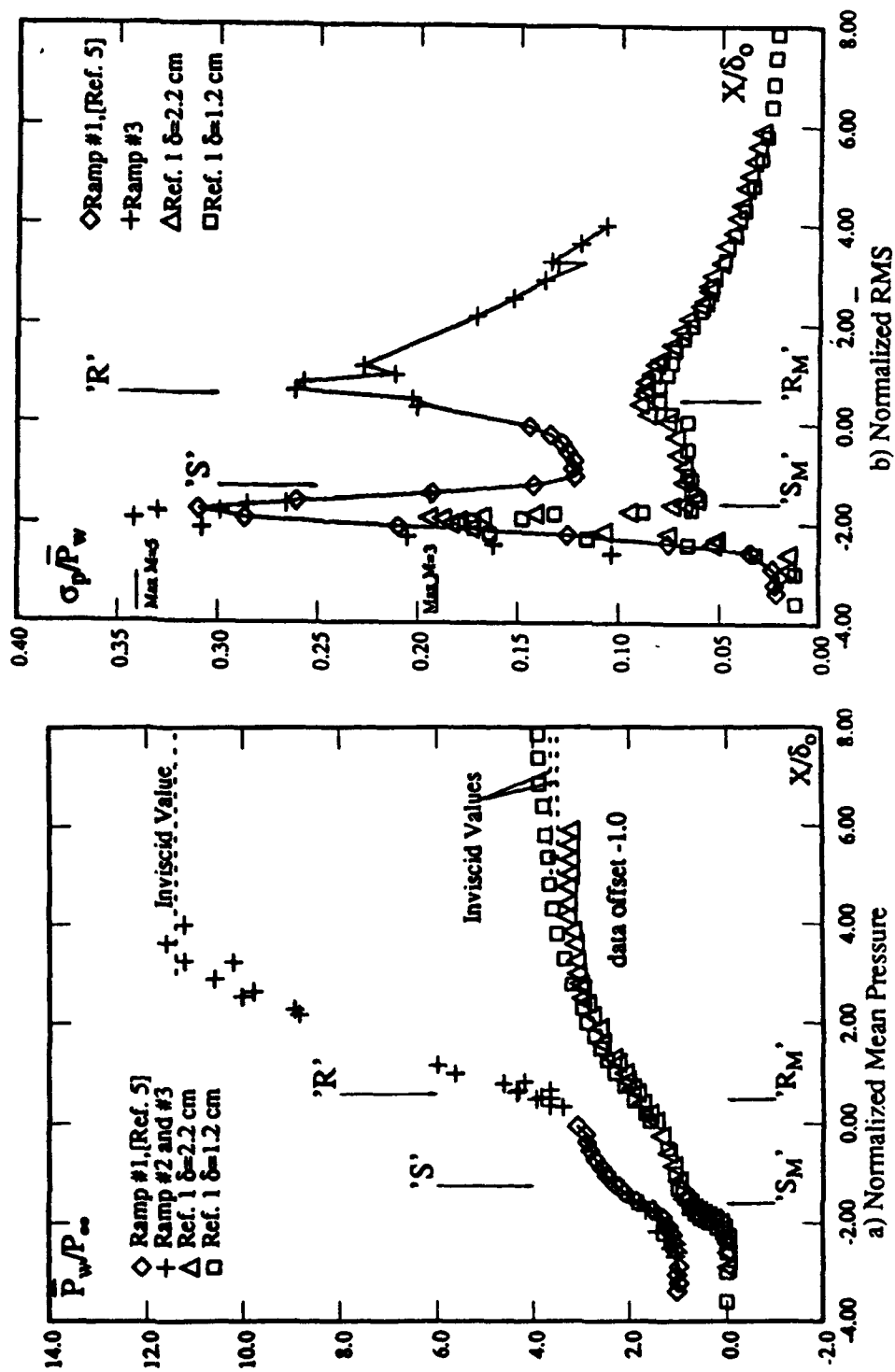
Fig. 11. Unswept Compression Ramp Data (Ref. 18)
Note: References in legend correspond to those in Ref. 18

69
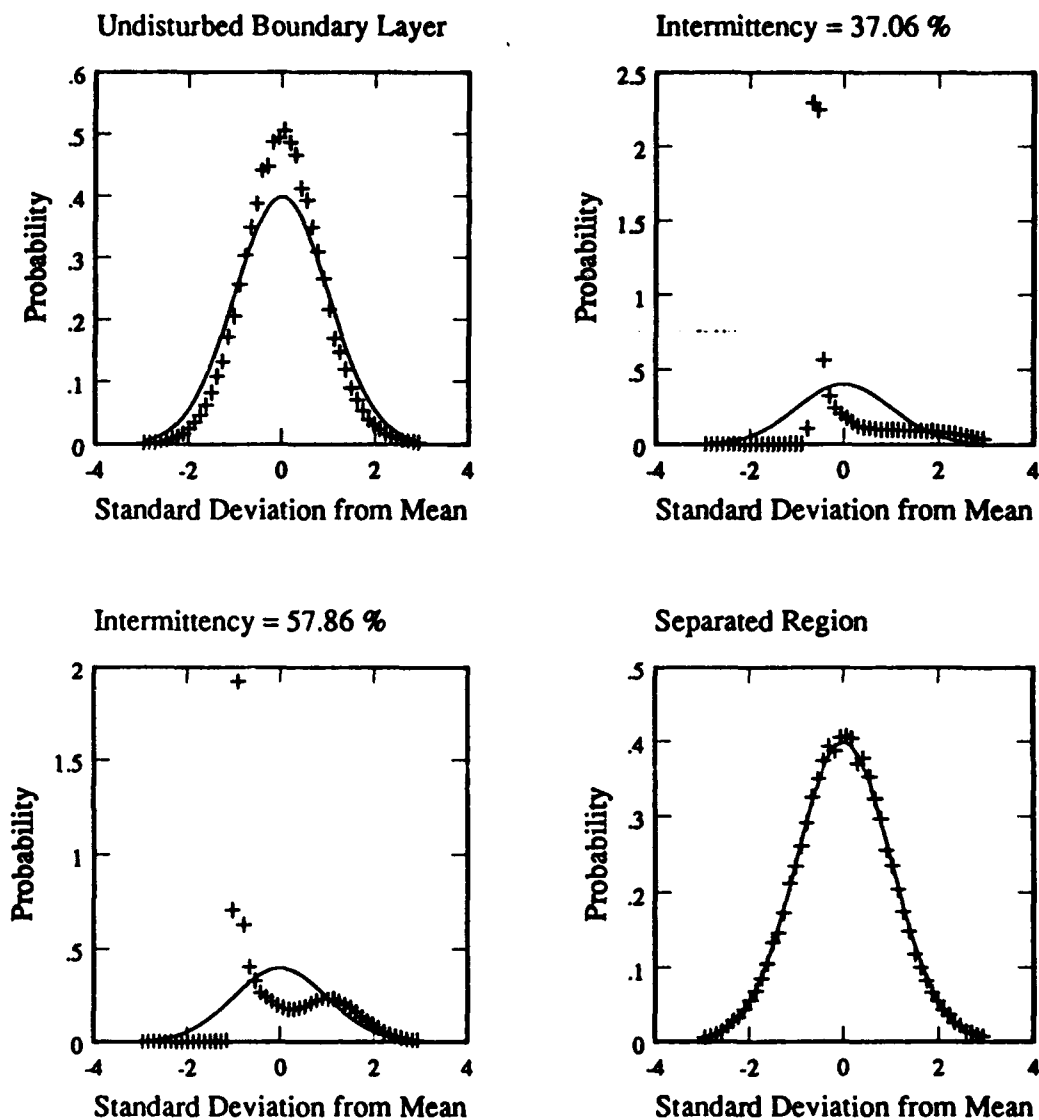
Fig. 12. Probability Density Distributions for Unswept
Compression Ramp Interactions (Data of Ref. 19)

70
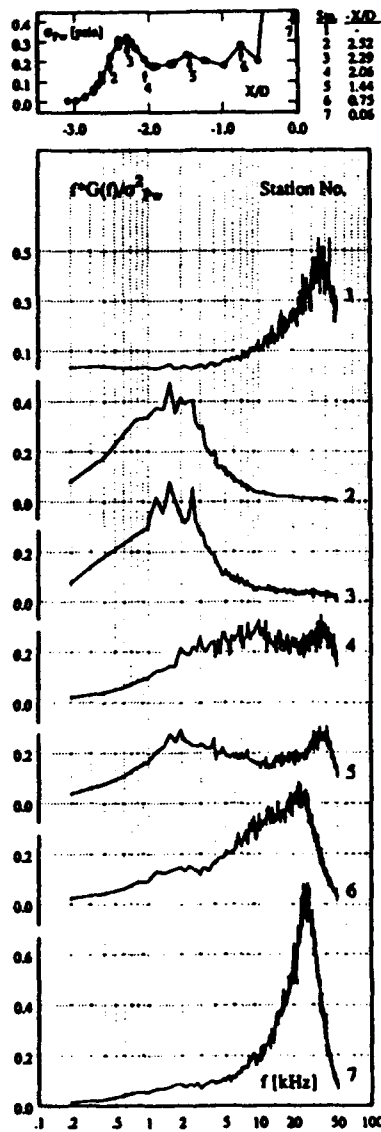
Fig. 13. RMS distribution and PSDs in Mach 5 Cylinder Induced Interaction (from Dolling, D.S., and Brusniak, L., "Correlation of Separation Shock Motion in a Cylinder-Induced Interaction with Pressure Fluctuations Under the Separated Region," AIAA paper 91-0650, AIAA 29th Aerospace Sciences Meeting, Reno, Nevada, January 1991.)

71
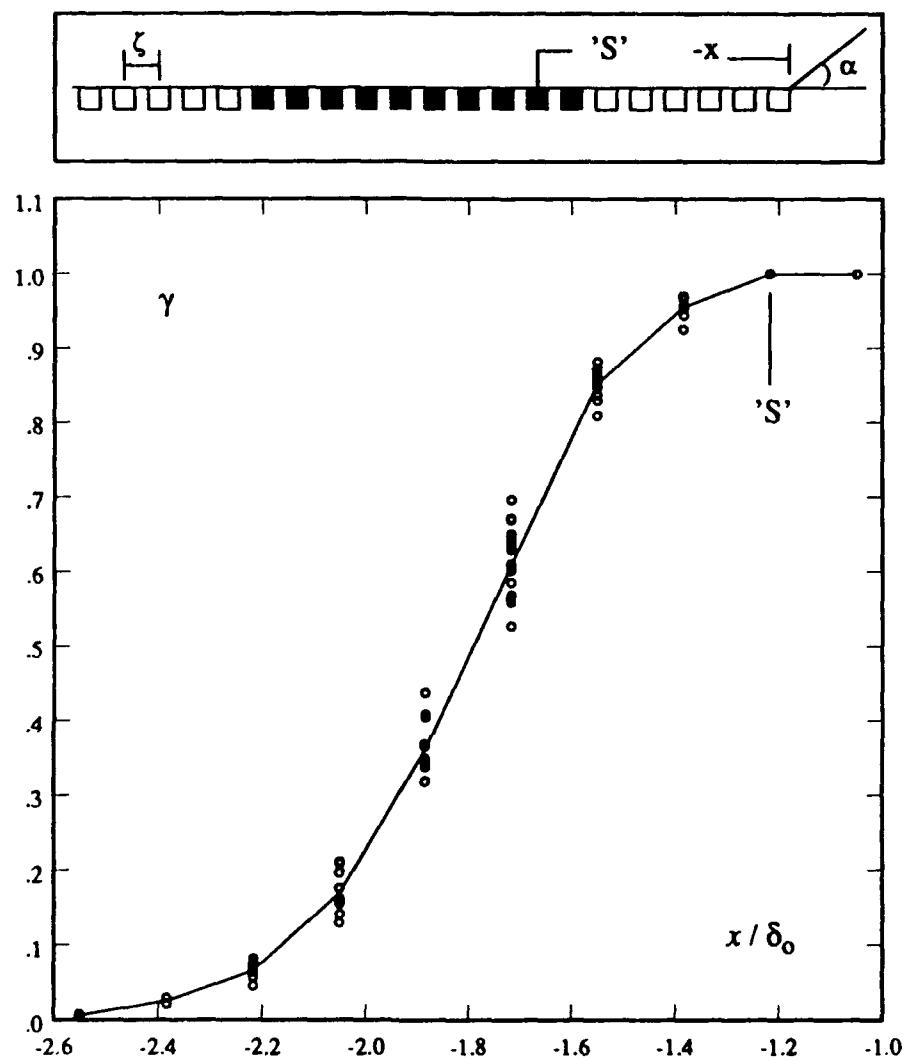
Fig. 14. Intermittency Distribution (Ref. 19)
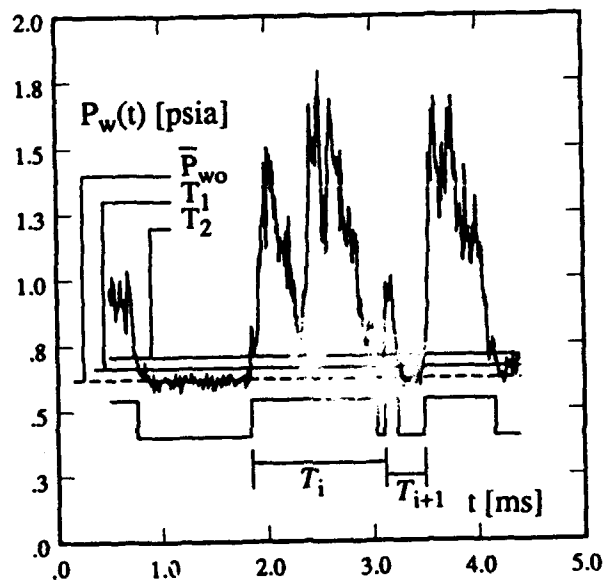
Fig. 15. Illustration of Shock Period, T_i (Ref. 19)

73
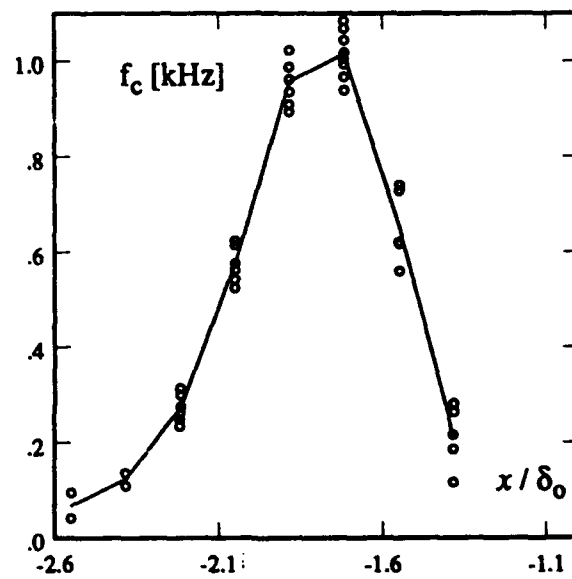
Fig. 16. Zero-Crossing Frequency Distribution (Ref. 19)
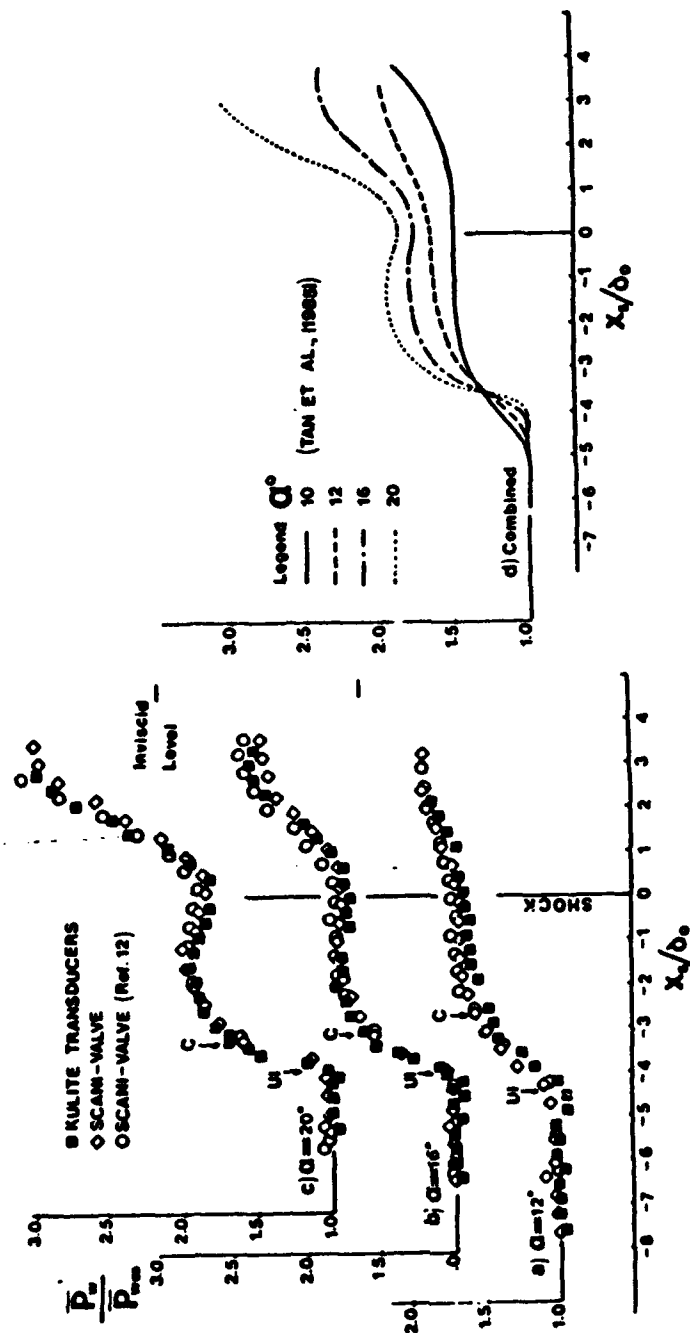
Fig. 17. Mean Pressure Distributions for Sharp Fin Interactions (Ref. 2)

75
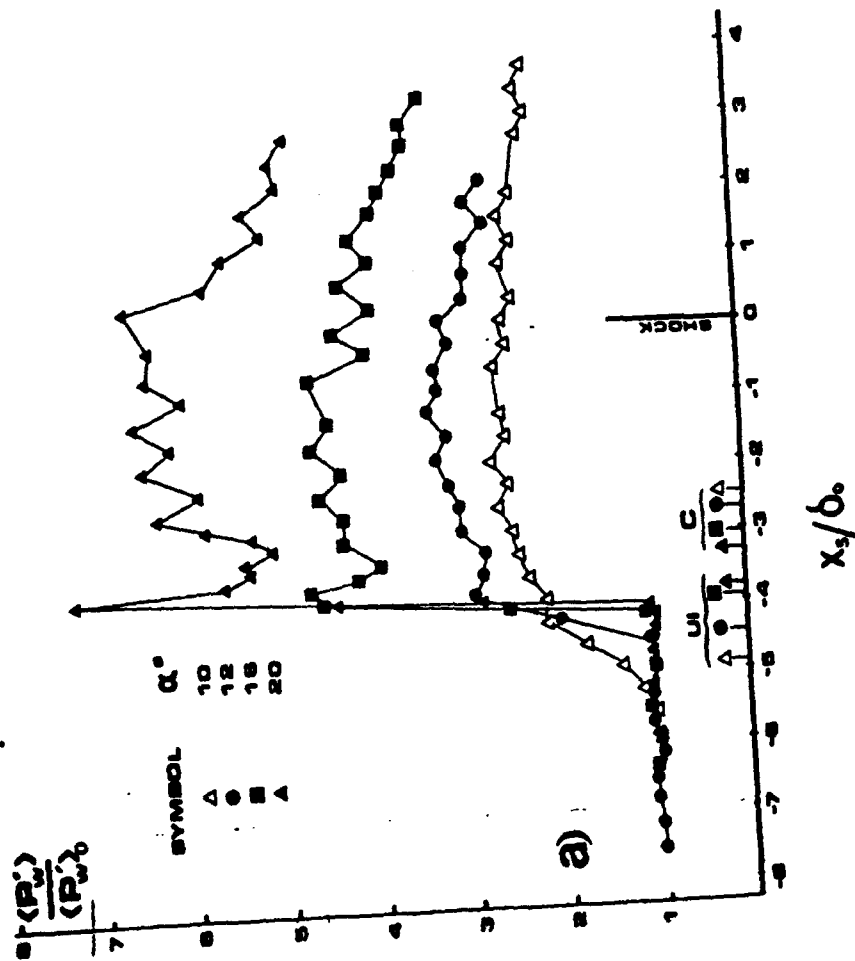
Fig. 18a. RMS Distributions Normalized by Undisturbed Value (Ref. 2)

76
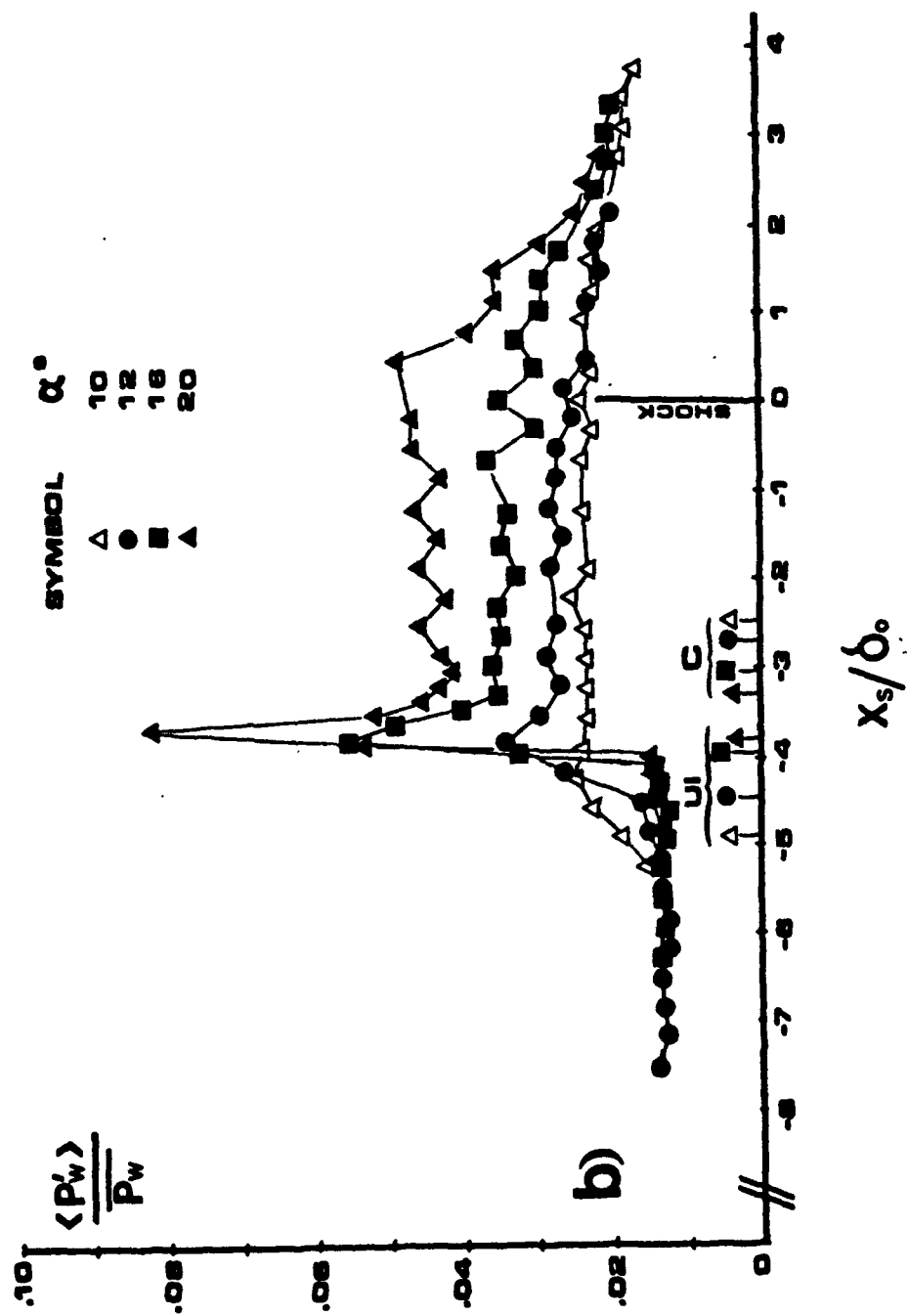
Fig. 18b. RMS Distributions Normalized by Local Mean Wall Pressure (Ref. 2)
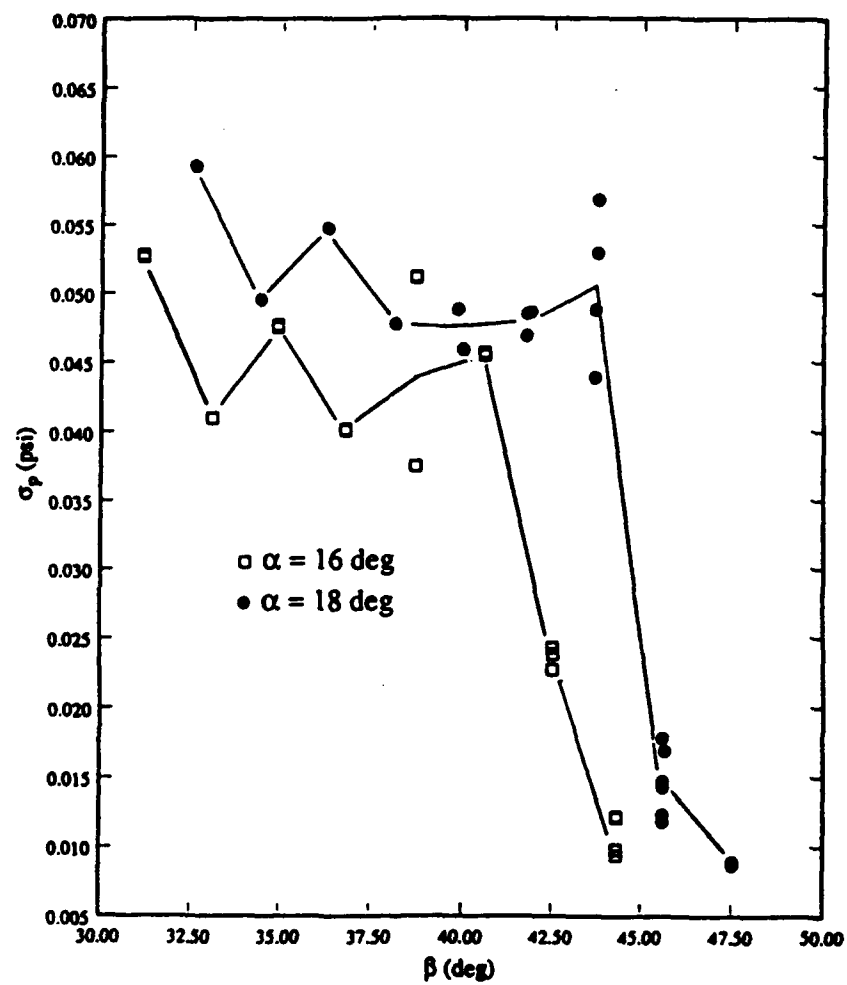
Fig. 19. RMS distributions for Mach 5 Sharp Fin Interaction (Ref. 5)
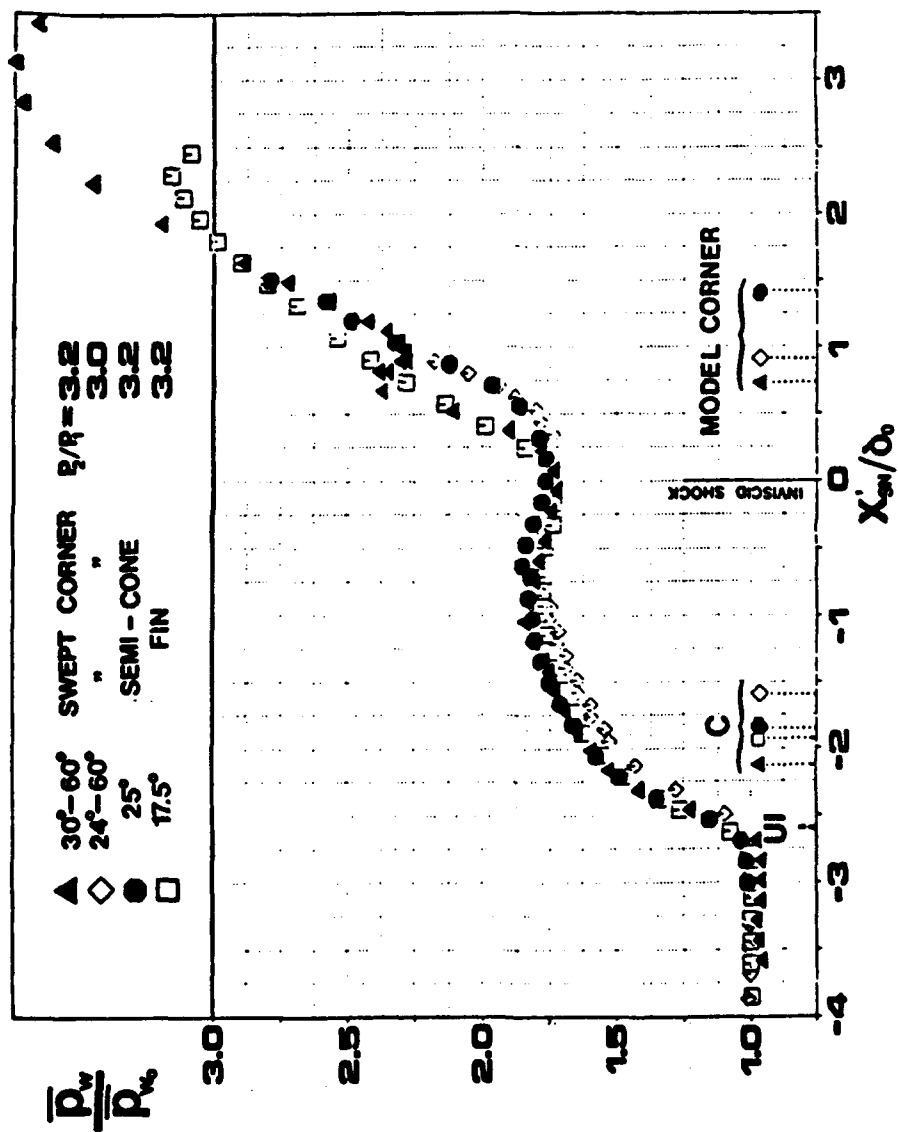
Fig. 20. Mean Pressure Distributions for Various Shock Generator Geometries (Ref. 2)
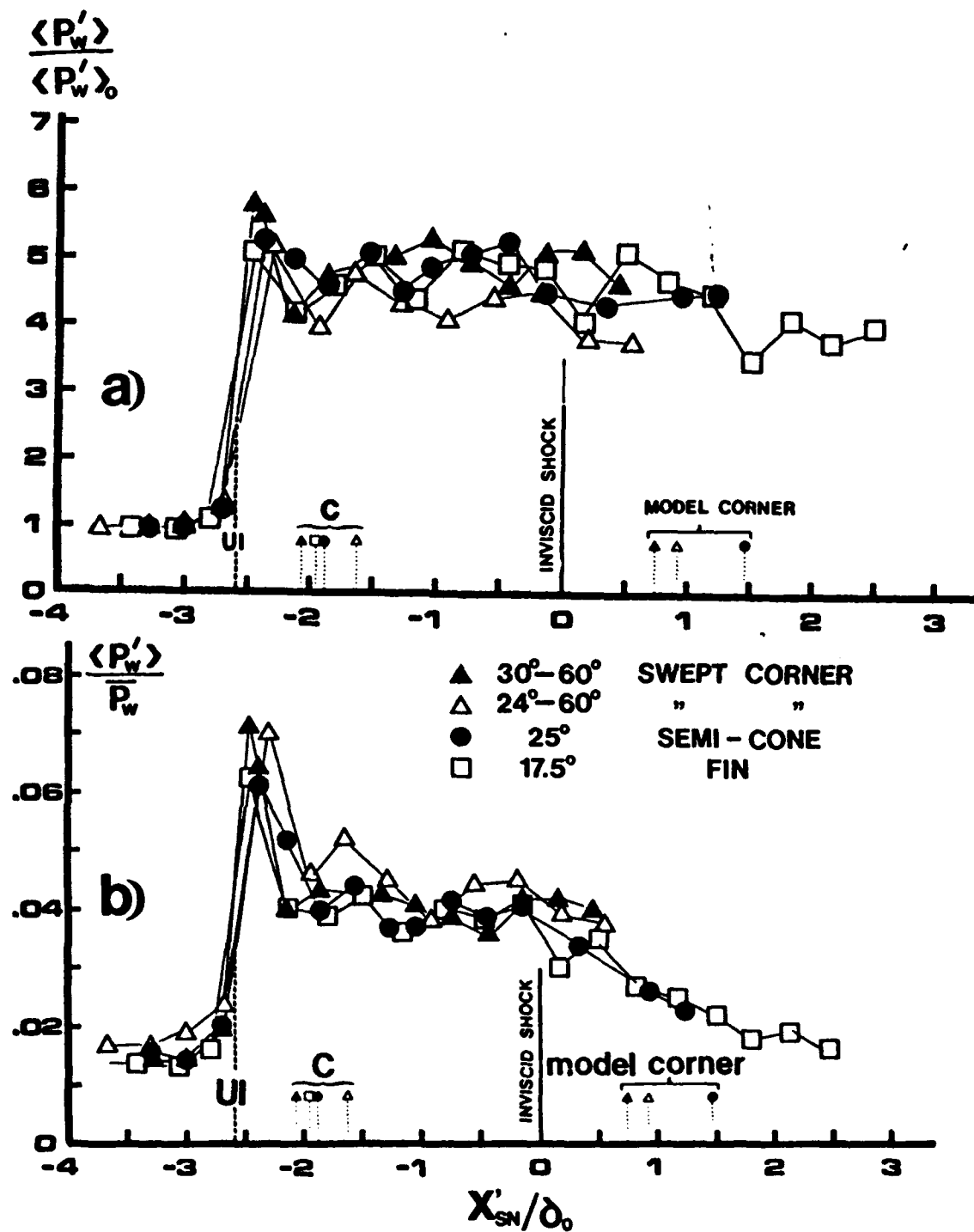
Fig. 21. RMS distributions for Various Geometries (Ref. 2)

80
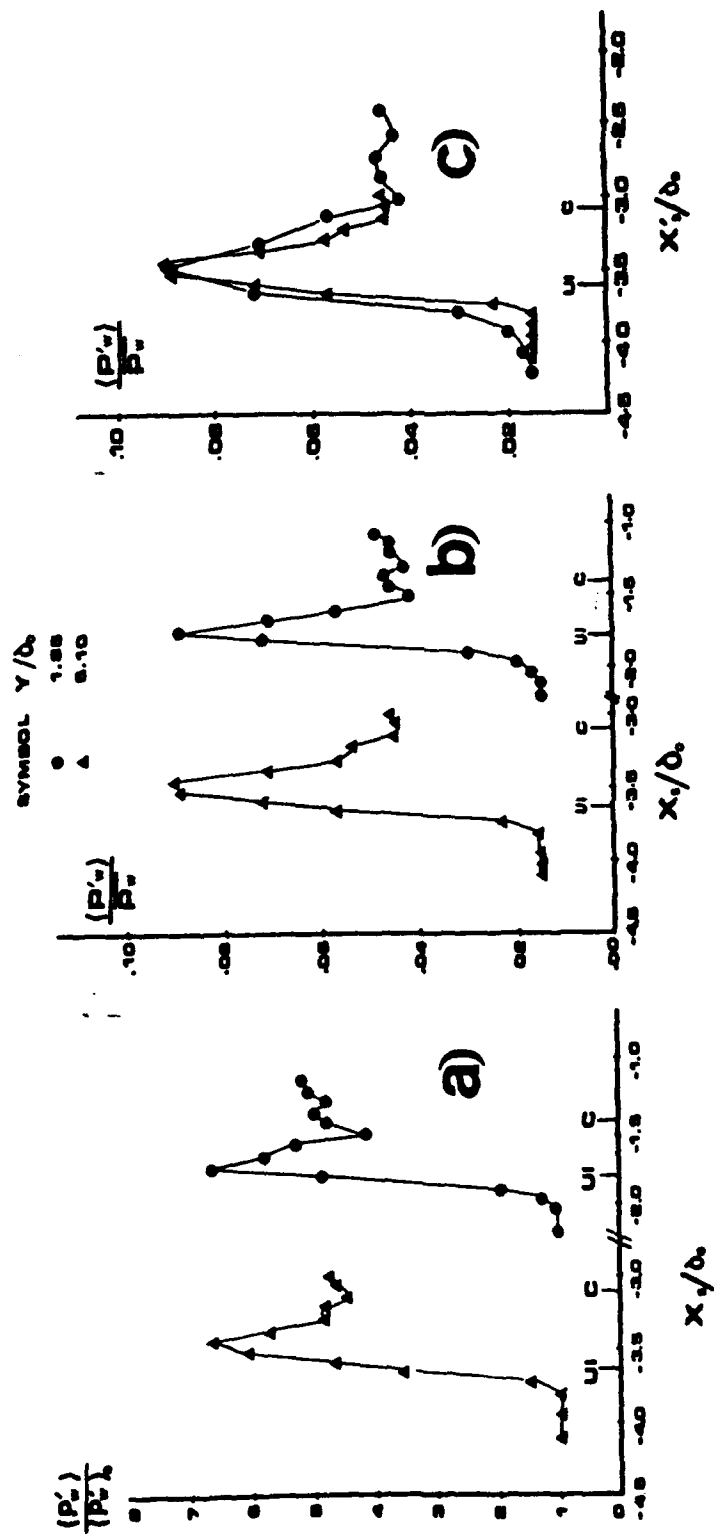
Fig. 22. RMS Distributions at Various Spanwise Distances (Ref. 2)
a) Normalized by Freestream Value
b) Normalized by Mean Pressure
c) Normalized by Mean Pressure and Scaled to Same Interaction Length

81
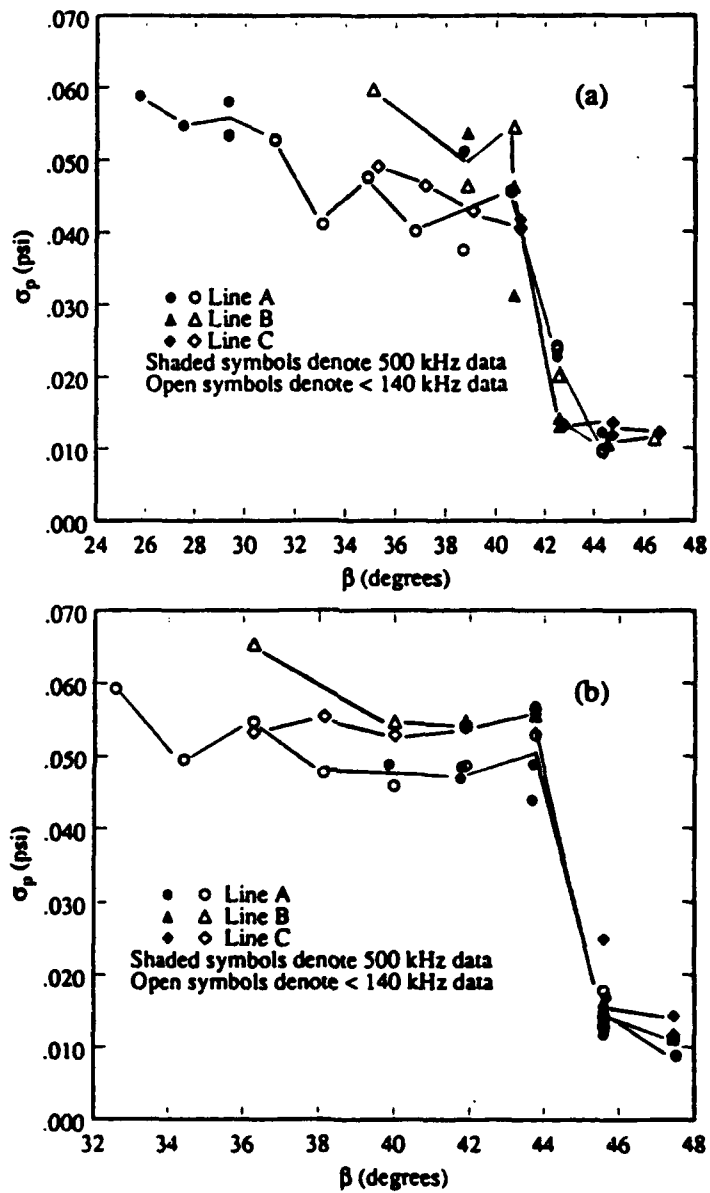
Fig. 23. RMS distributions in Conical Coordinates (Ref. 5)
a) α = 16 deg. b) α = 18 deg.

82
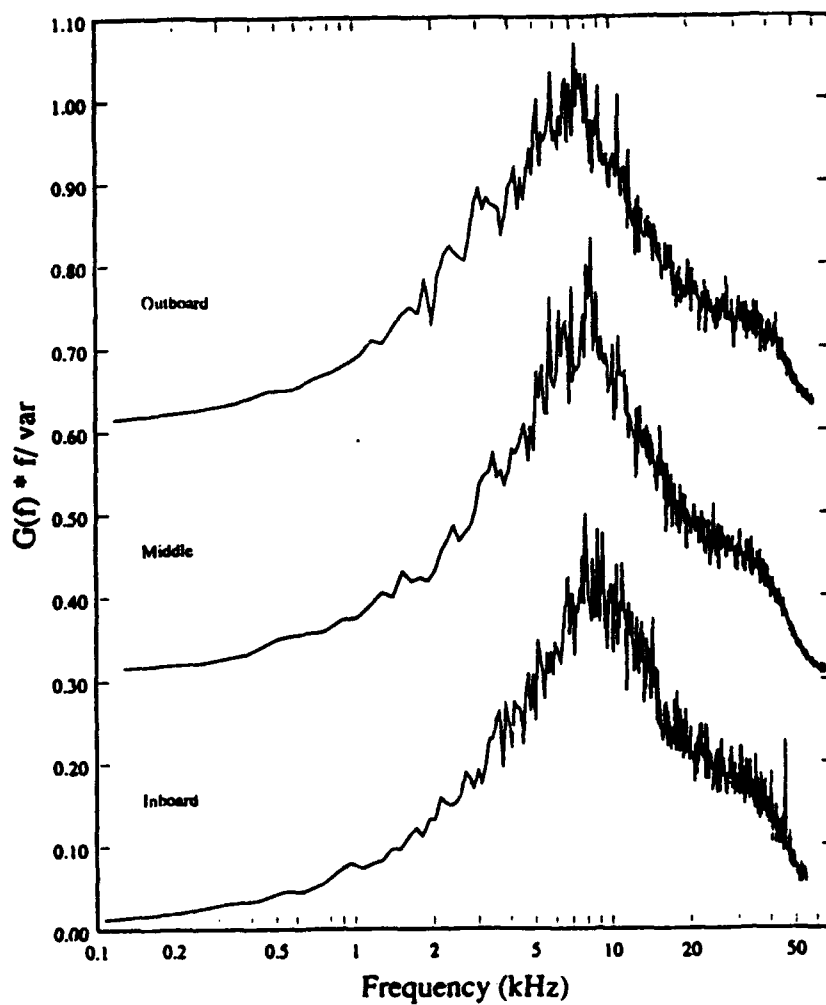
Fig. 24. PSDs along a ray in the Compression Region (Ref. 5)
Note: Middle and Outboard Curves are Shifted Upward 0.3
and 0.6 units, respectively.

83
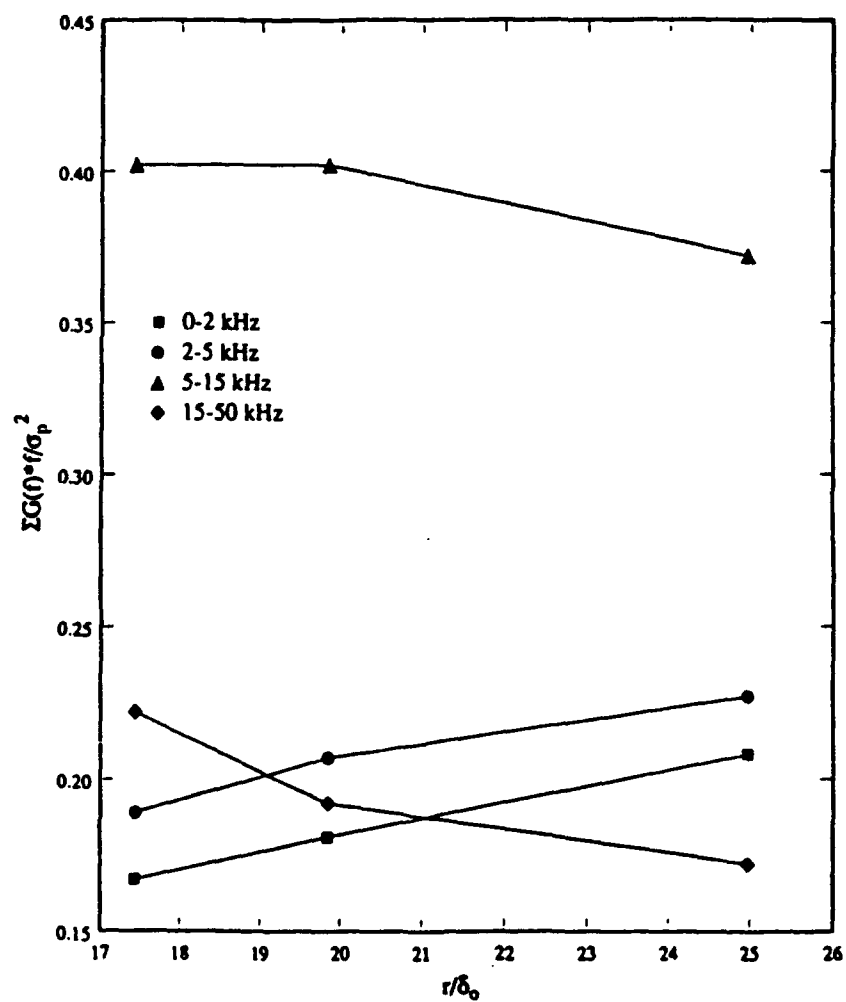
Fig. 25. Fraction of Variance in each Frequency Band for data of Fig. 24 (Ref. 5)
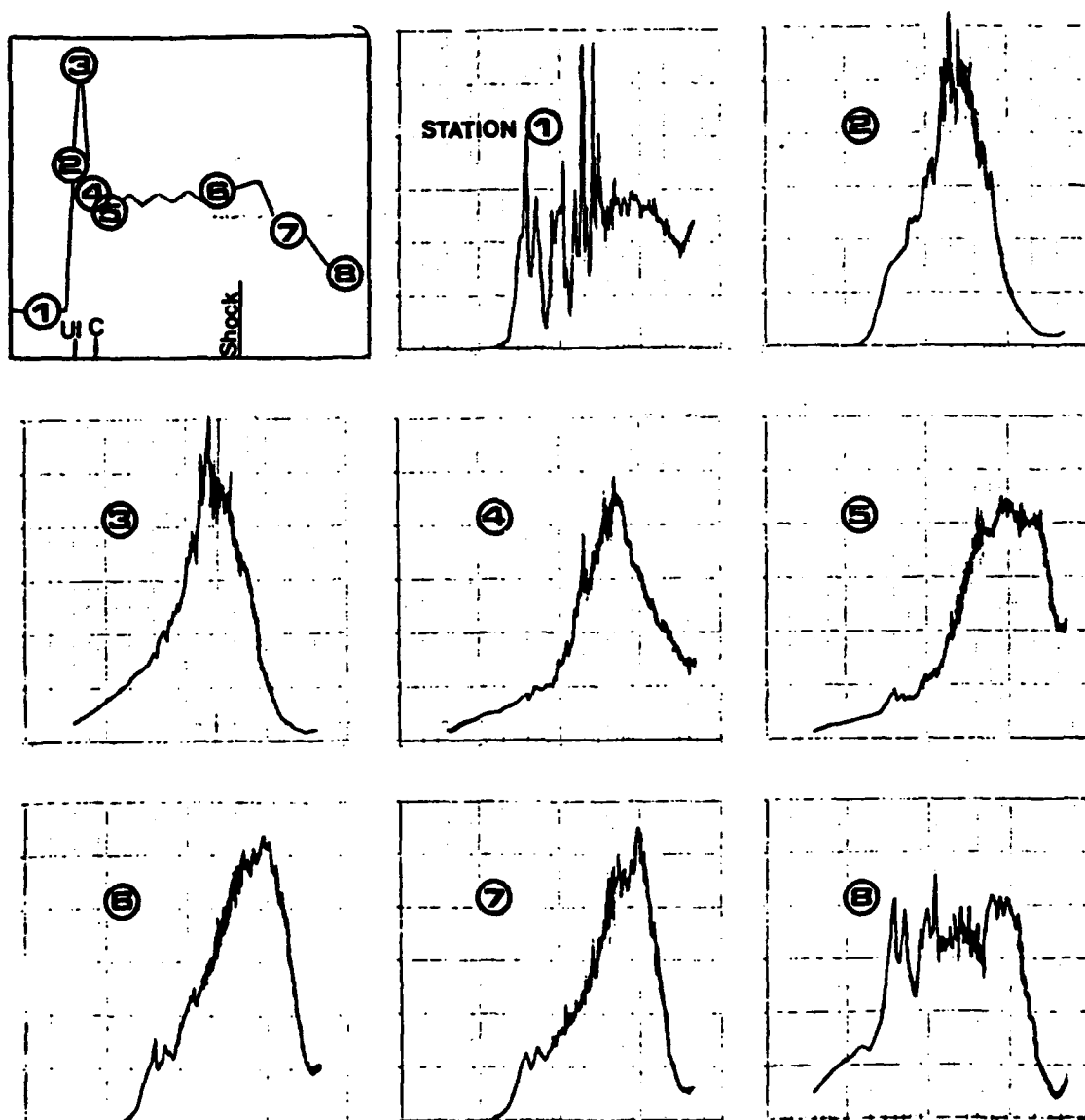
Fig. 26. Power Spectra for 20 degree Sharp Fin Interaction (Ref. 2)
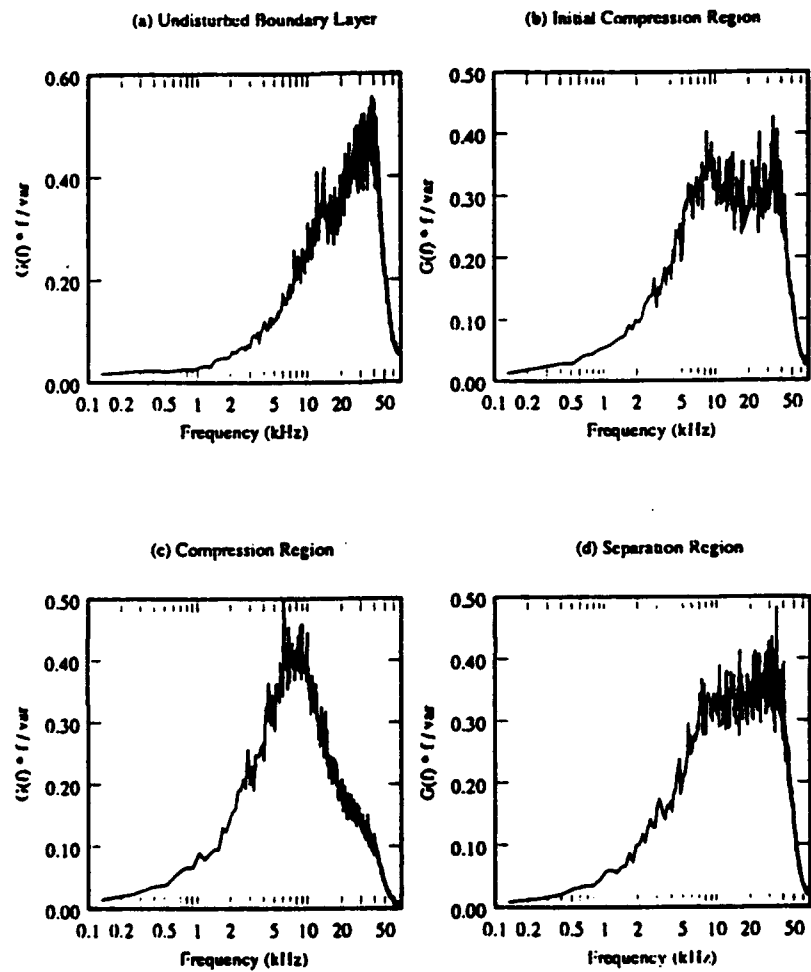
Fig. 27. Power Spectra for 18 degree Sharp Fin Interaction (Ref. 5)
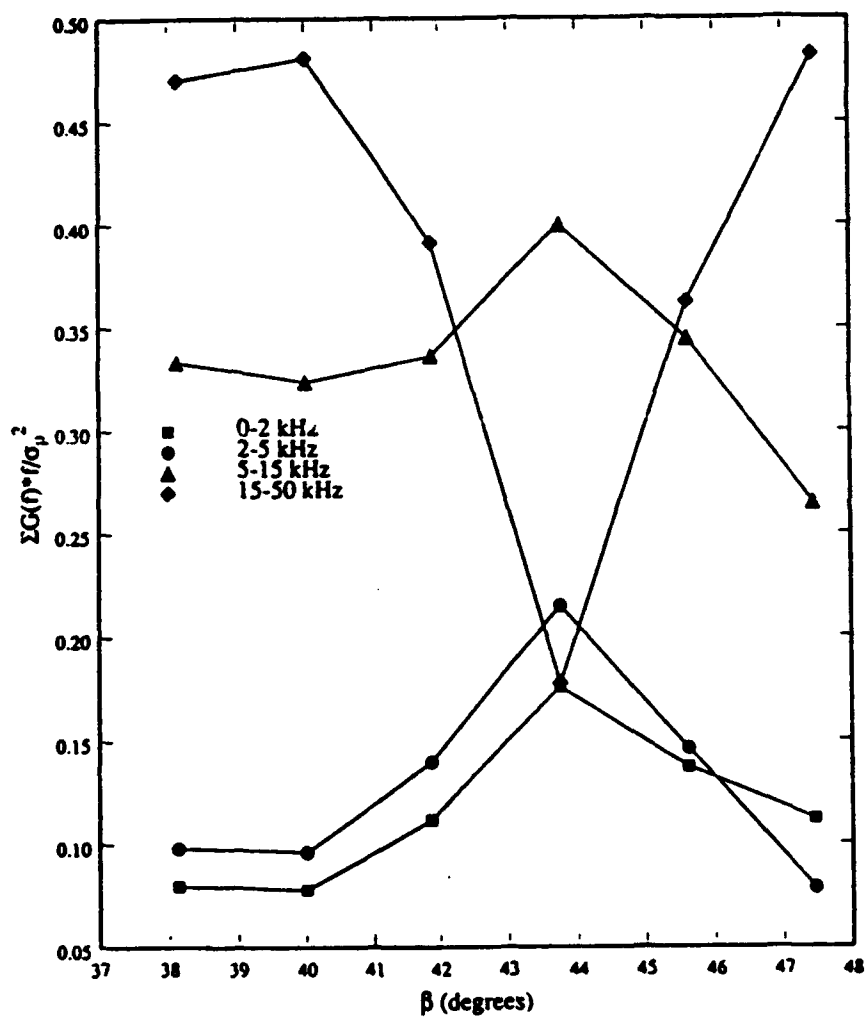
Fig. 28. Fraction of Variance in Various Frequency Bands for data of Fig. 27 (Ref. 5)
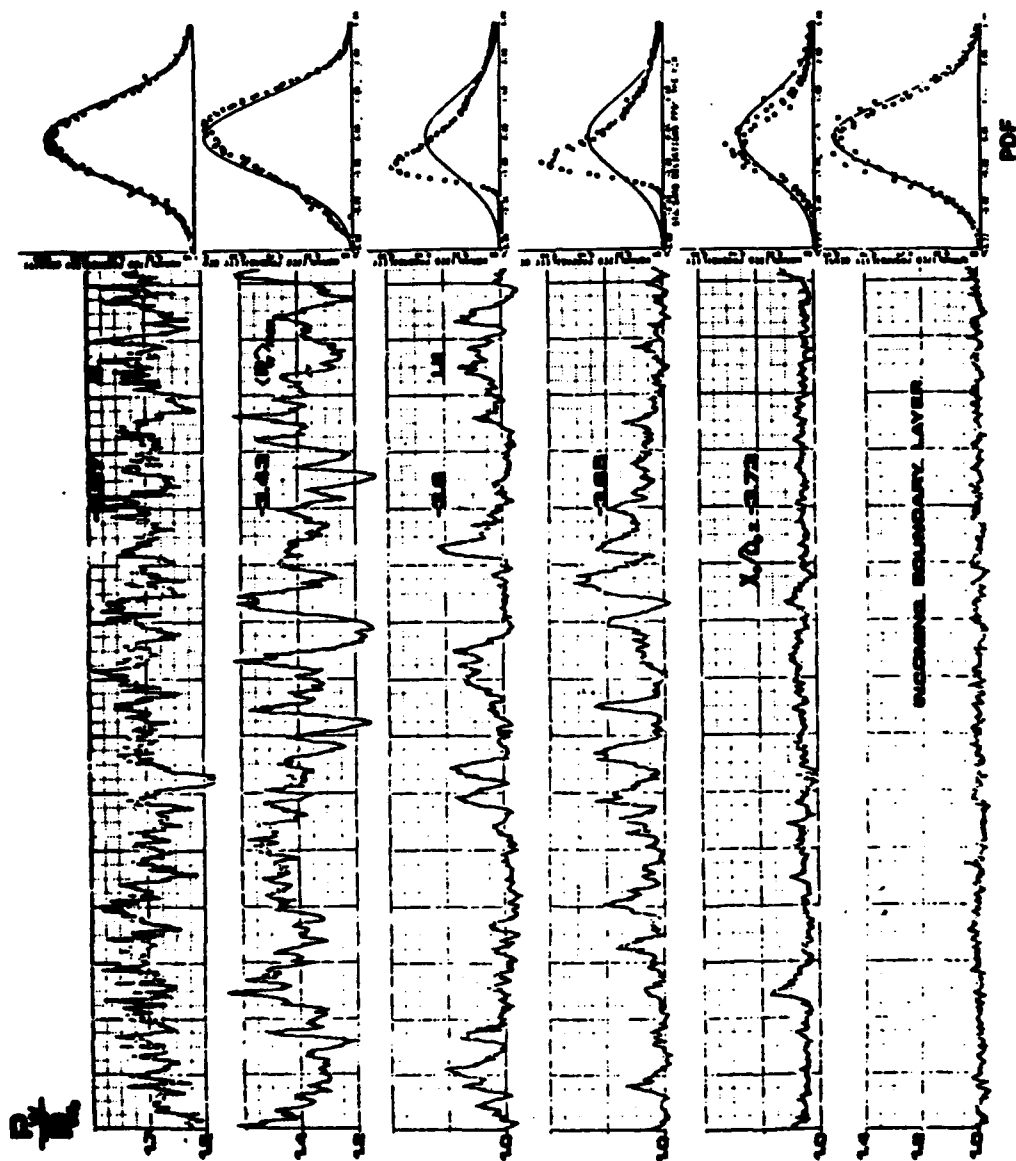
Fig. 29. Time-Histories and PDDs in Sharp Fin Interaction (Ref. 2)
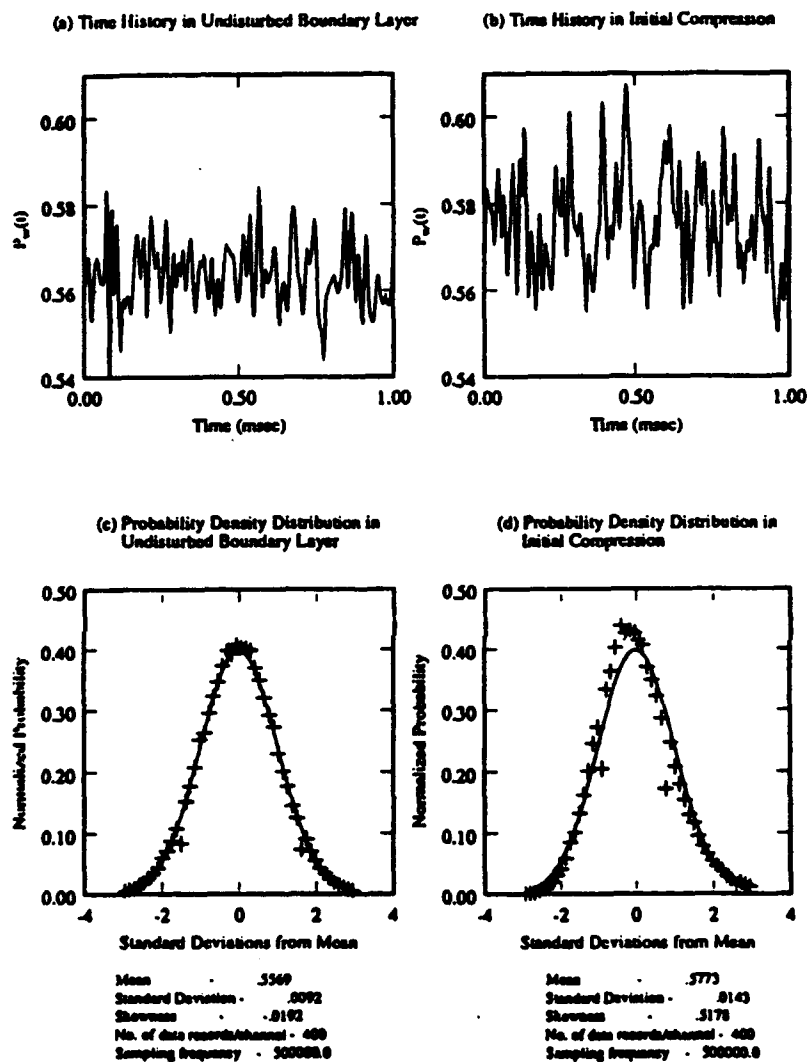
Fig. 30. Time-Histories and Corresponding PDDs for Mach 5 Sharp Fin Interaction (Ref. 5)
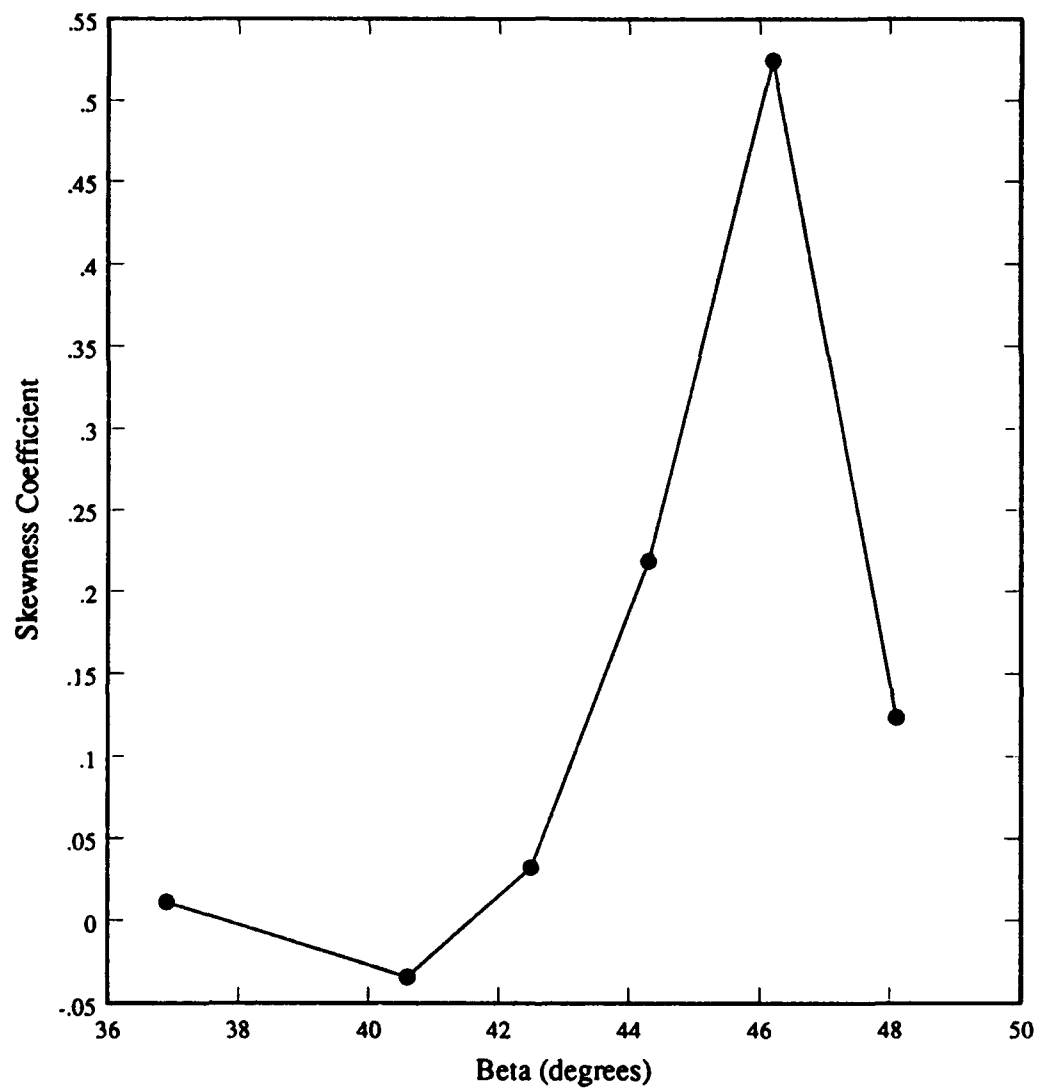
Fig. 31. Skewness Distribution for Mach 5, 18 deg.
Sharp Fin Interaction
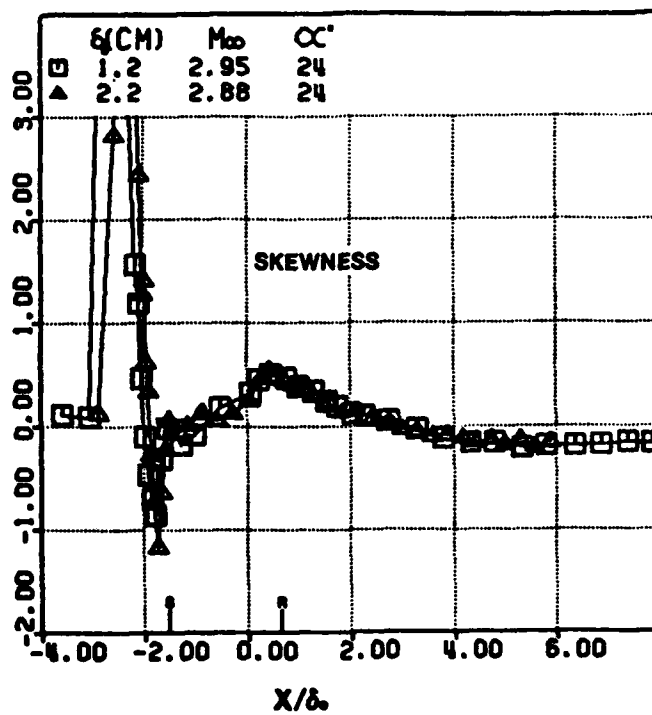
Fig. 32. Skewness Coefficient Distribution for Mach 3 Compression Ramp Interaction.
Figure is taken from Ref. 17 (originally from Ref. 36 of Ref. 17)
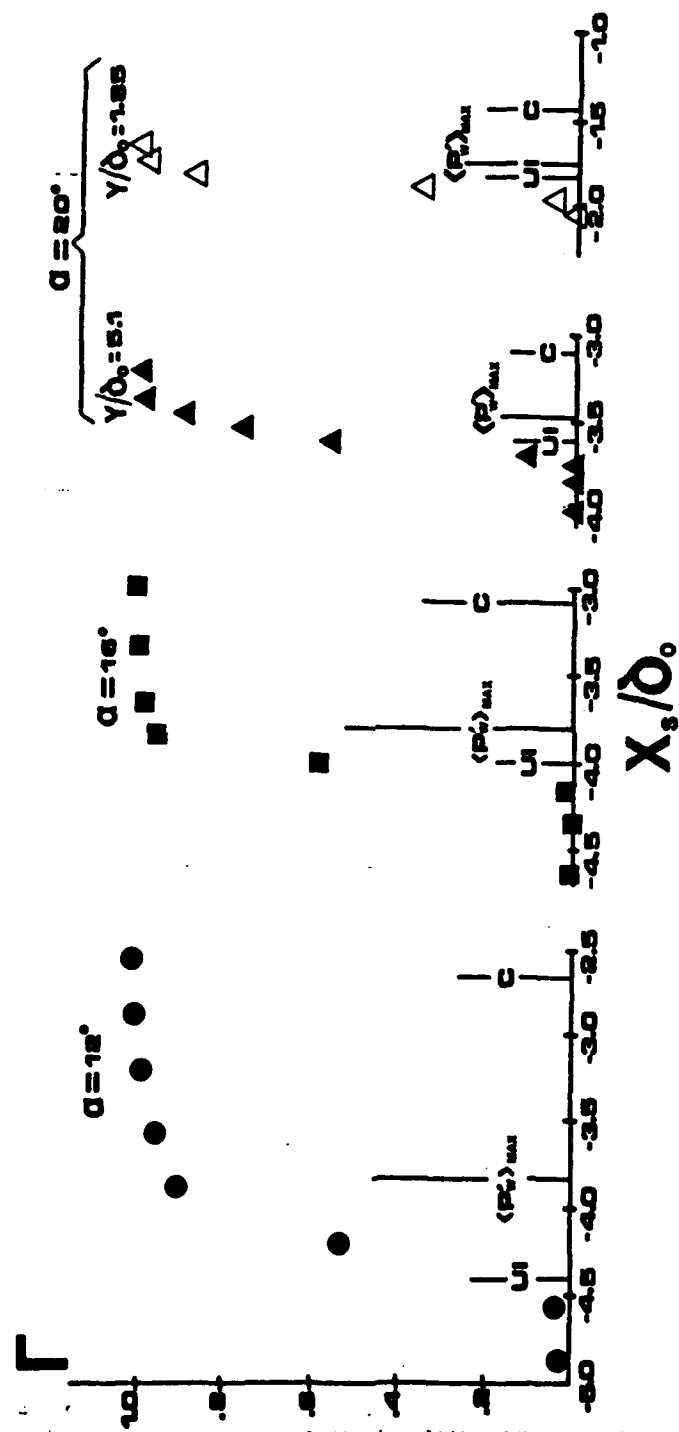
Fig. 33. Intermittency Distributions for Sharp Fin Interactions (Ref. 2)
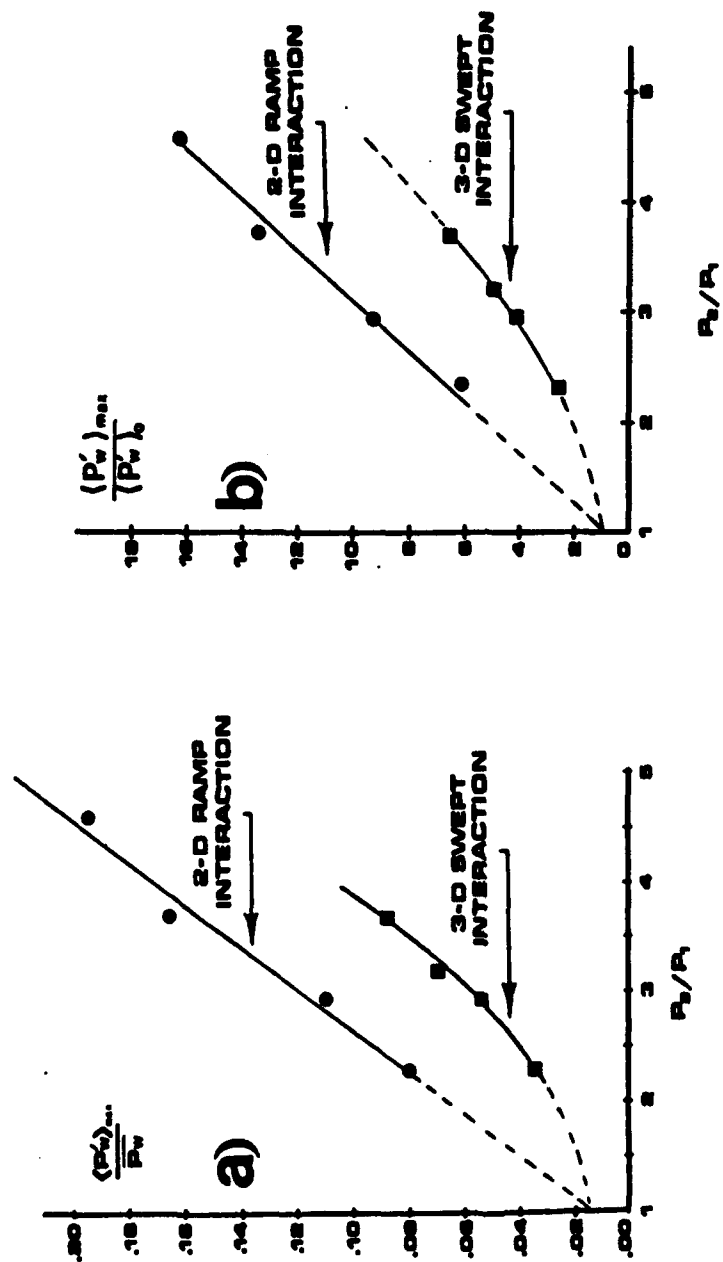
Fig. 34. Normalized RMS Vs. Inviscid Pressure Rise for Swept and Unswept Interactions (Ref. 2)
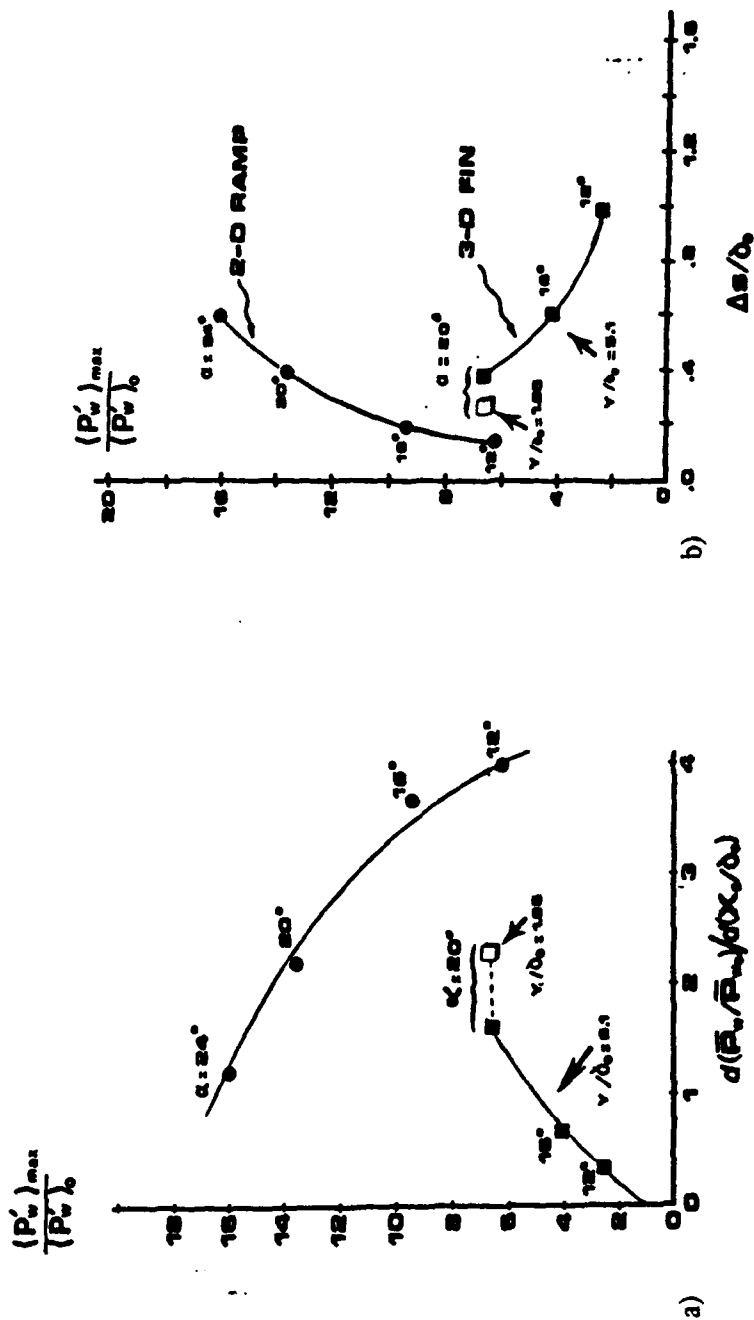
Fig. 35.   Normalized RMS Vs.   a) Initial Pressure Gradient
b) Spatial Extent of Intermittency (Ref. 2)

94

$$\Delta P = \frac{\Delta S}{\delta_o} \cdot \frac{d\left(\overline{P}_w / \overline{P}_{wo}\right)}{d\left(X_e / \delta_o\right)}$$
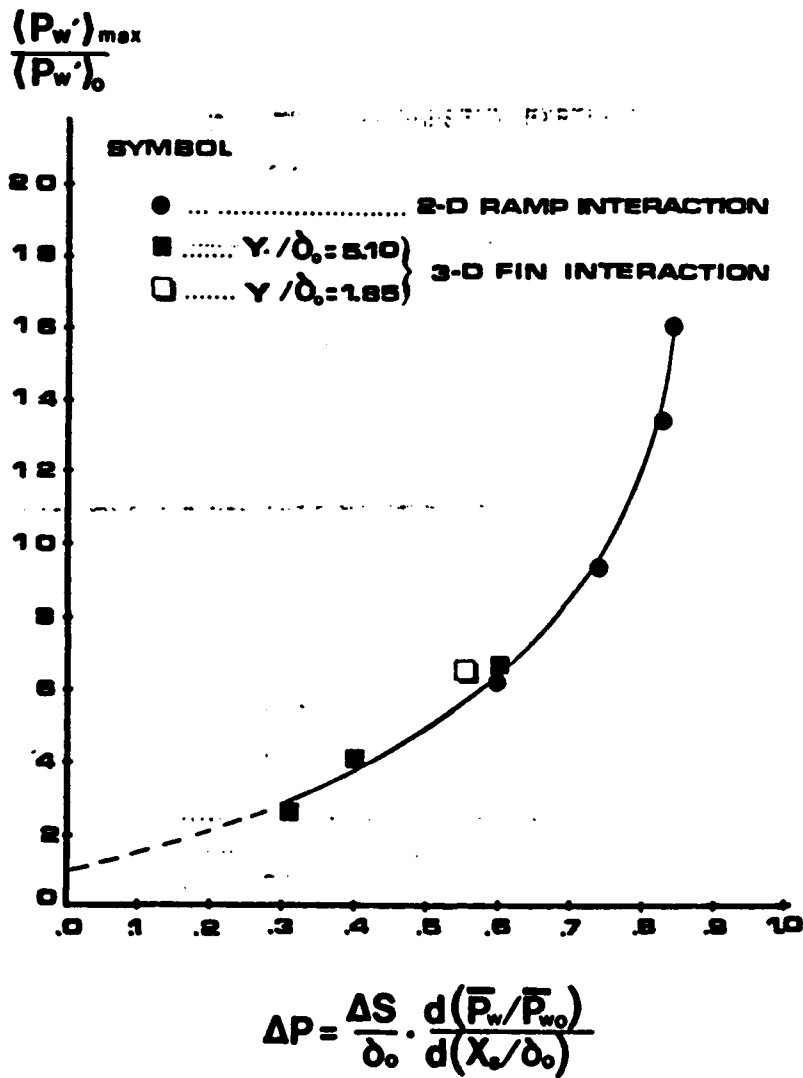
Fig. 36. RMS as a function of the Parameter ΔP (Ref. 2)
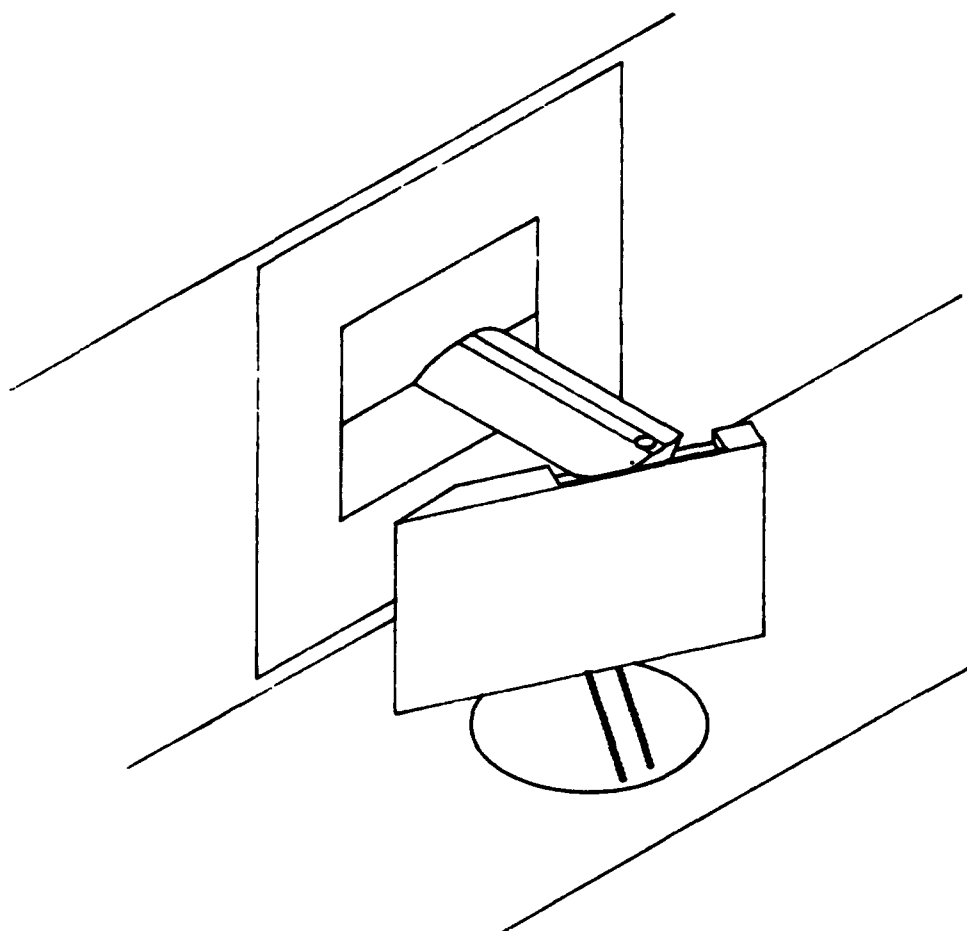
Figure 37. Schematic of Test Section with Fin Installed

Door Plates

Arm

Tunnel Door

Pin

Collar

Block

left-hand threads

right-hand threads

Bolt
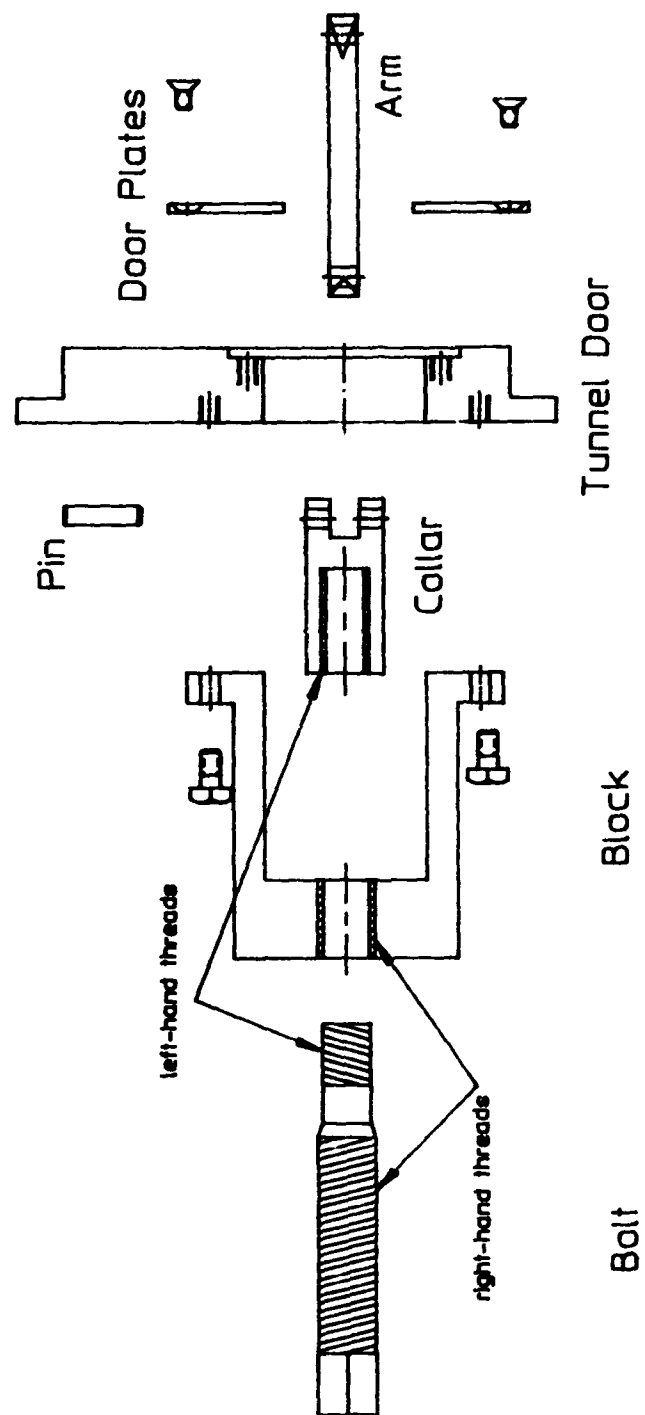
Figure 38a. Exploded Angle of Attack Mechanism

97
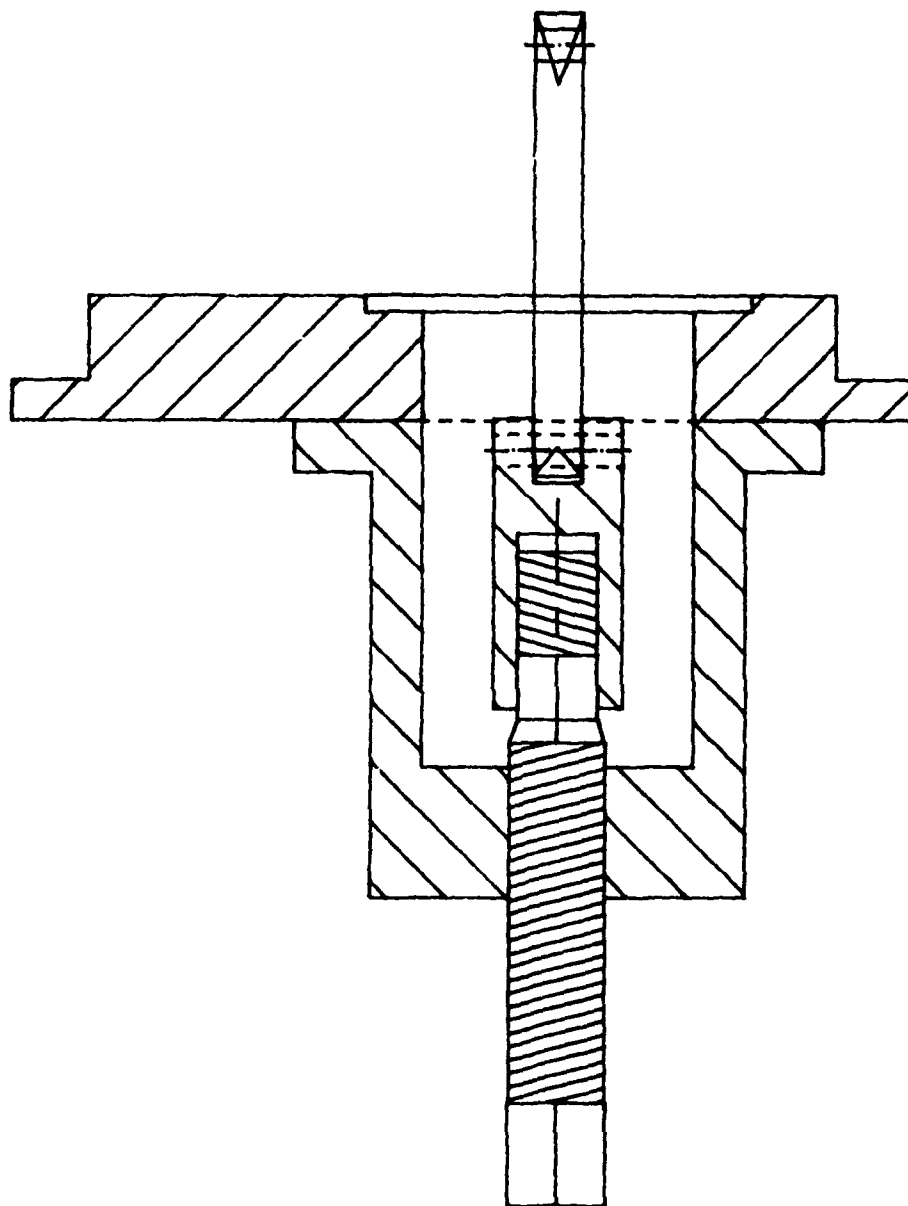
Figure 38b. Assembled Angle of Attack Mechanism

ledge

slots for pin and arm
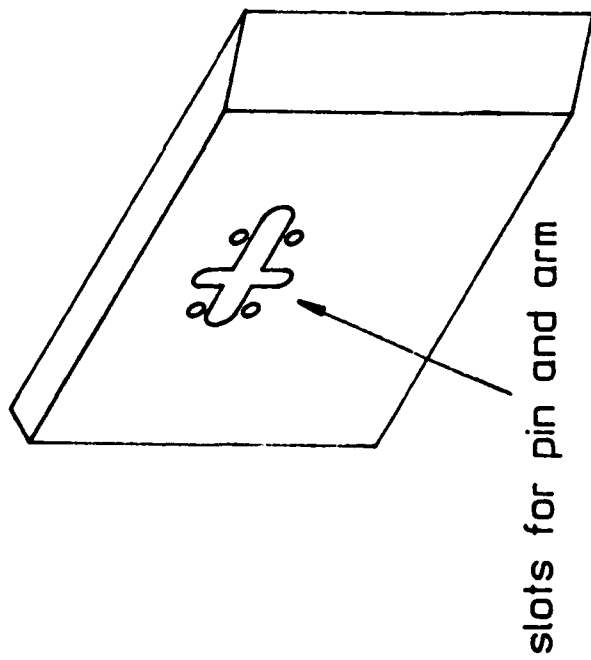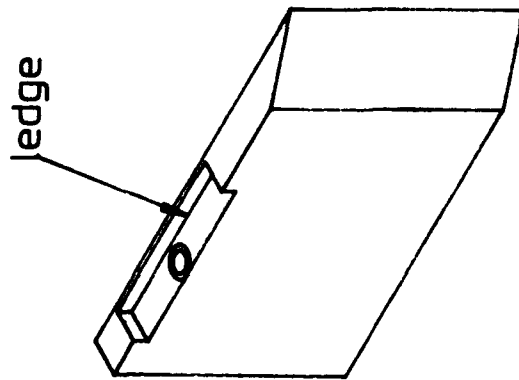
large fin used during first phase   small fin used during second phase

Figure 39. Sharp Fins Used for Experiment

Freestream Direction

Rotatable Plug

Fin

Inviscid Shock
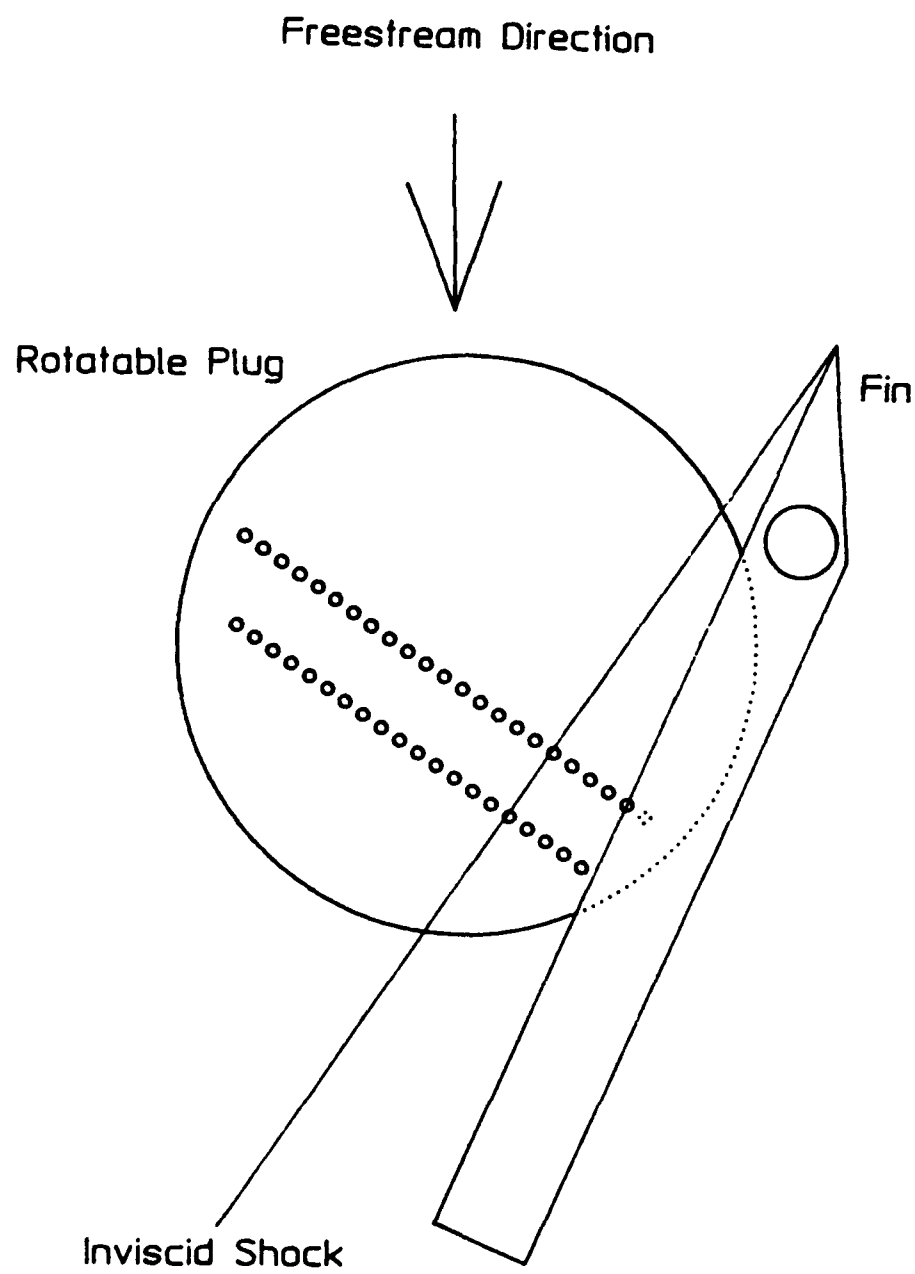
Figure 40. Orientation of Rotatable Plug with Respect to the Fin

Freestream Direction

Row B
0.2 in. from center

Row C
0.6 in. from center
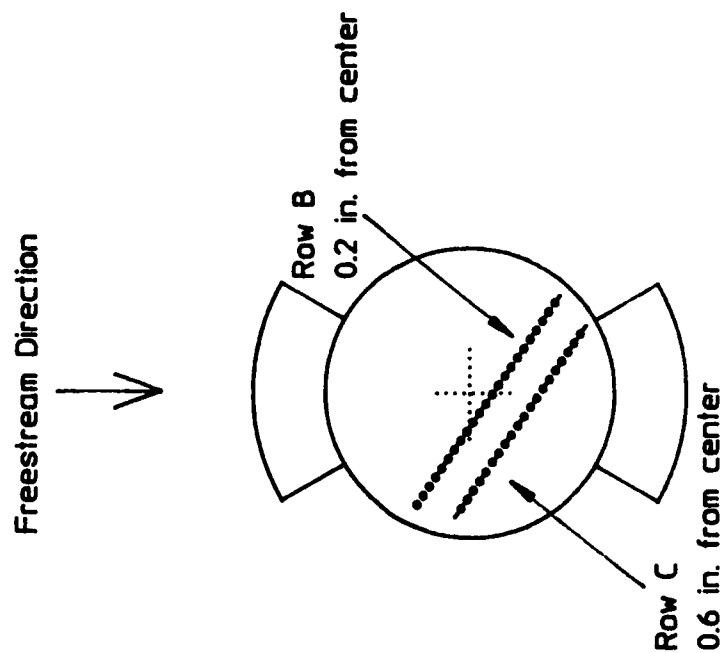
Figure 42. Transducer Port Locations
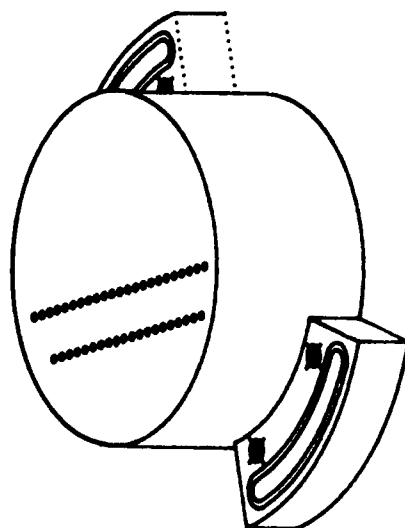
Figure 41. Isometric View of Plug

101

Upstream Influence Line

Separation Line

Reference Line
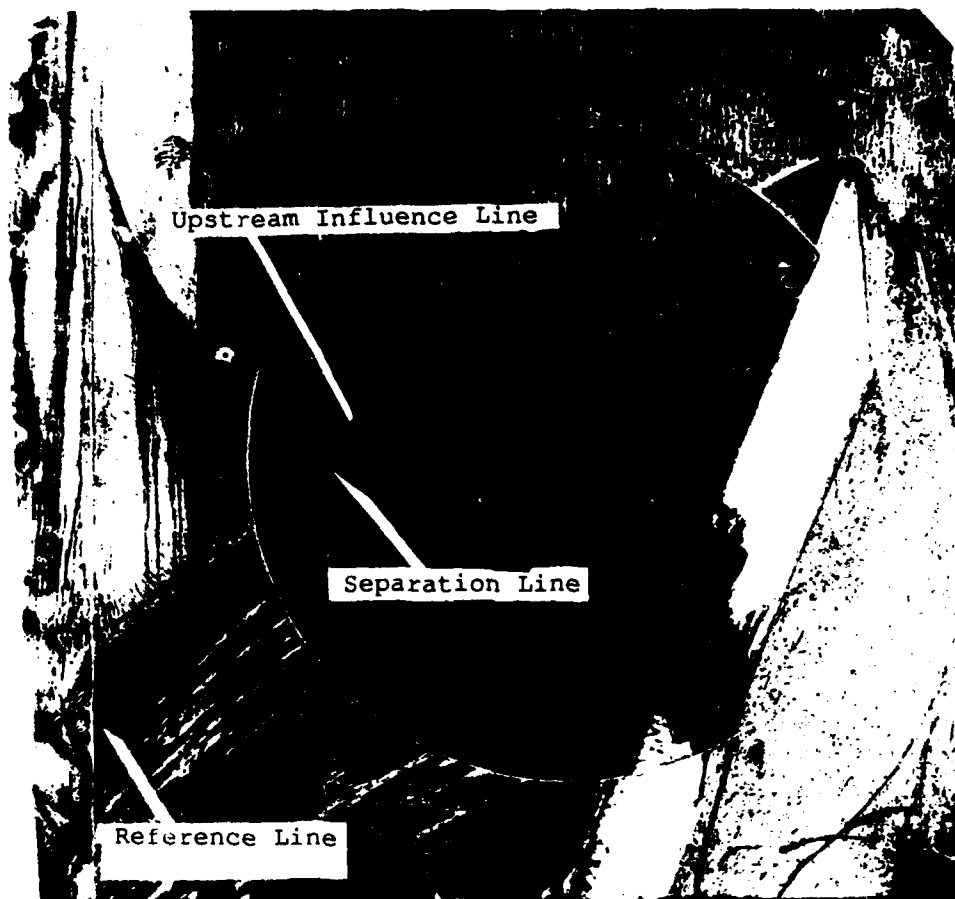
Fig. 43. Typical Surface Flow Visualization Pattern
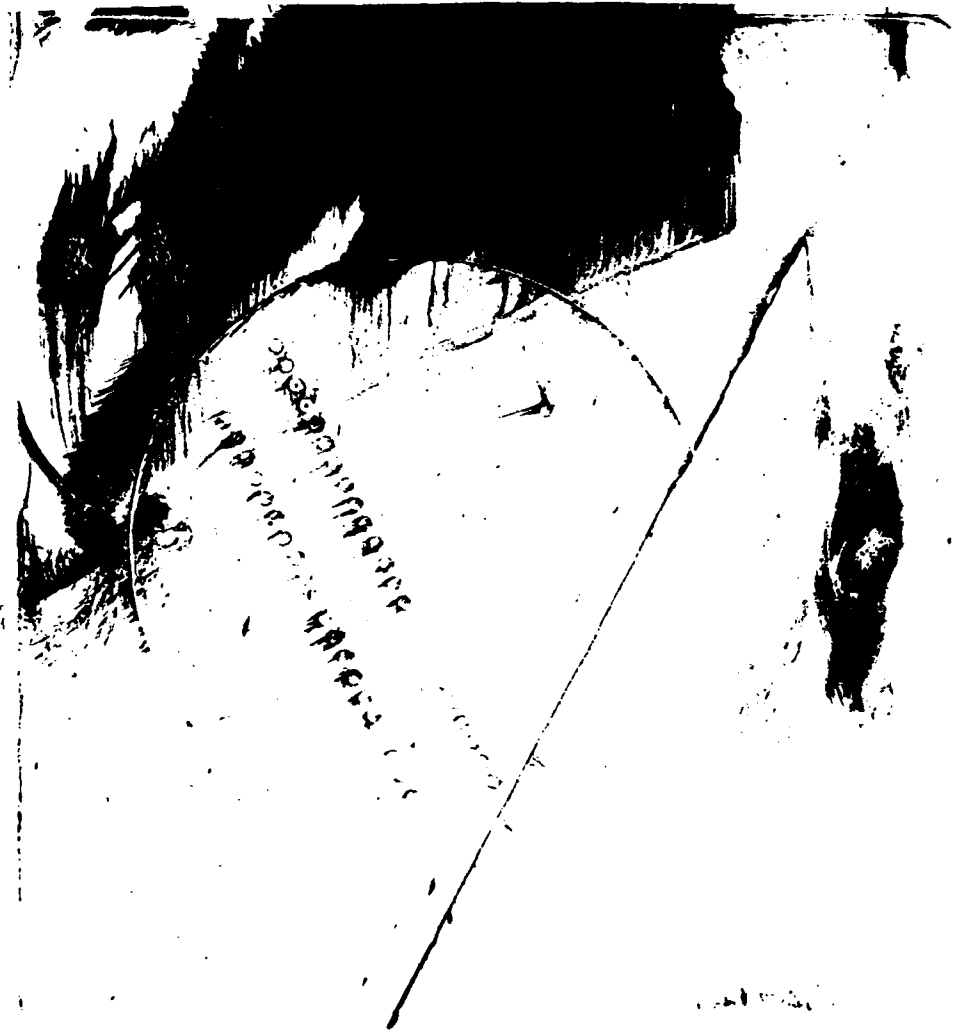
Fig. 44. Surface Flow Visualization Pattern for 28 deg. Interaction
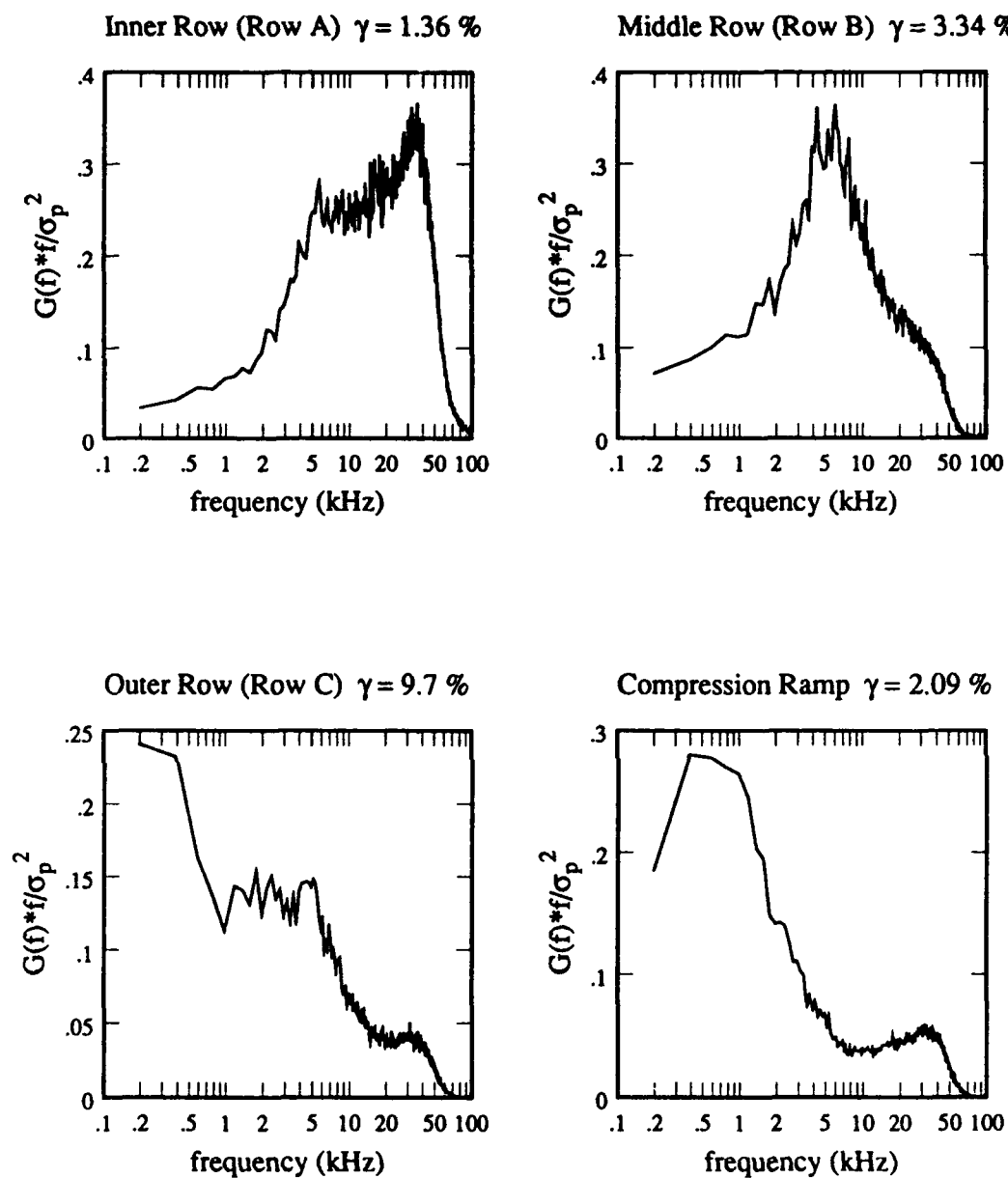
Fig. 45. PSDs for 28 deg. Interactions

104

Fig. 46. Surface Flow Visualization Pattern for 26 deg. Interaction
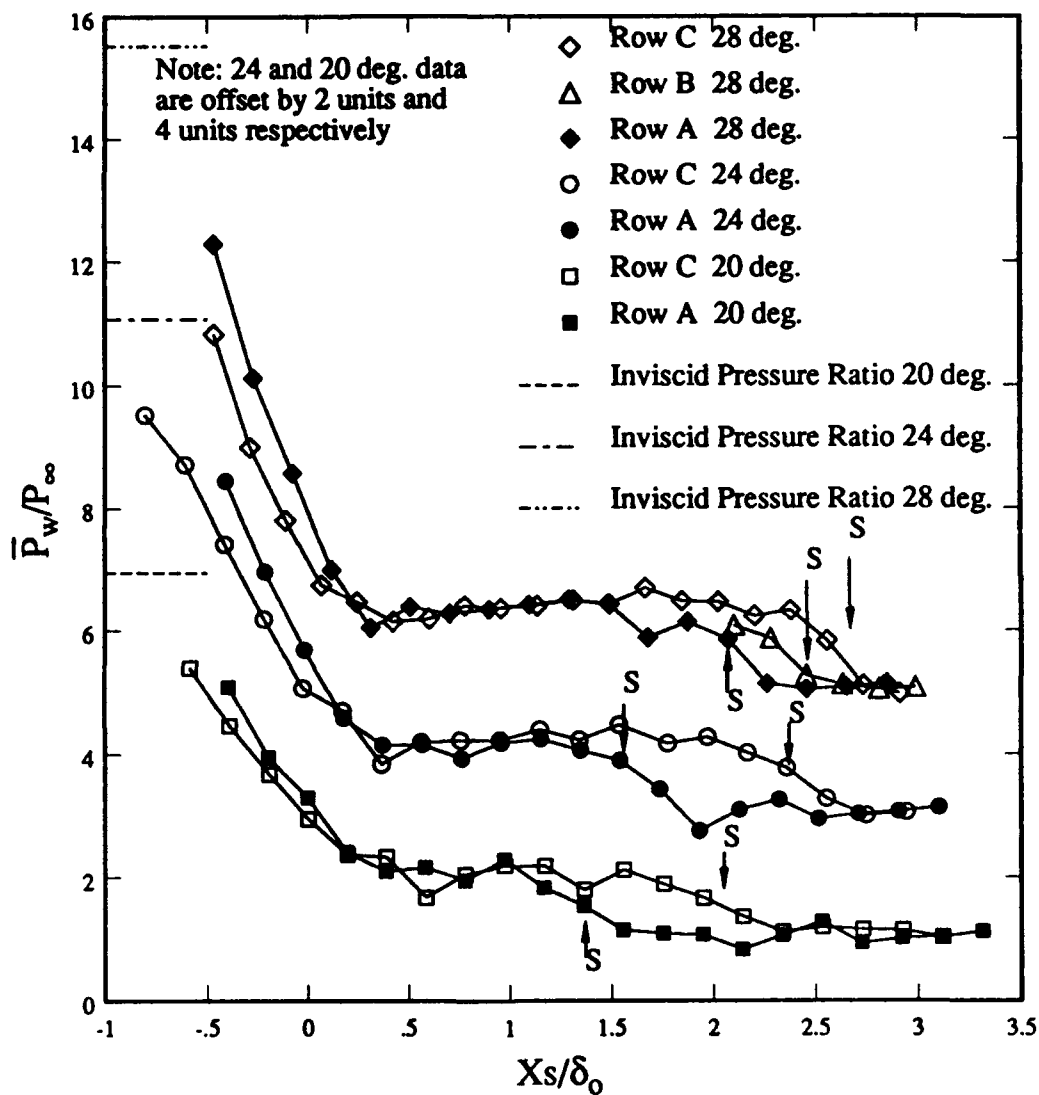
Fig. 47. Sharp Fin Interaction Mean Surface Pressure Distributions:
Normal to the Inviscid Shock Location

106
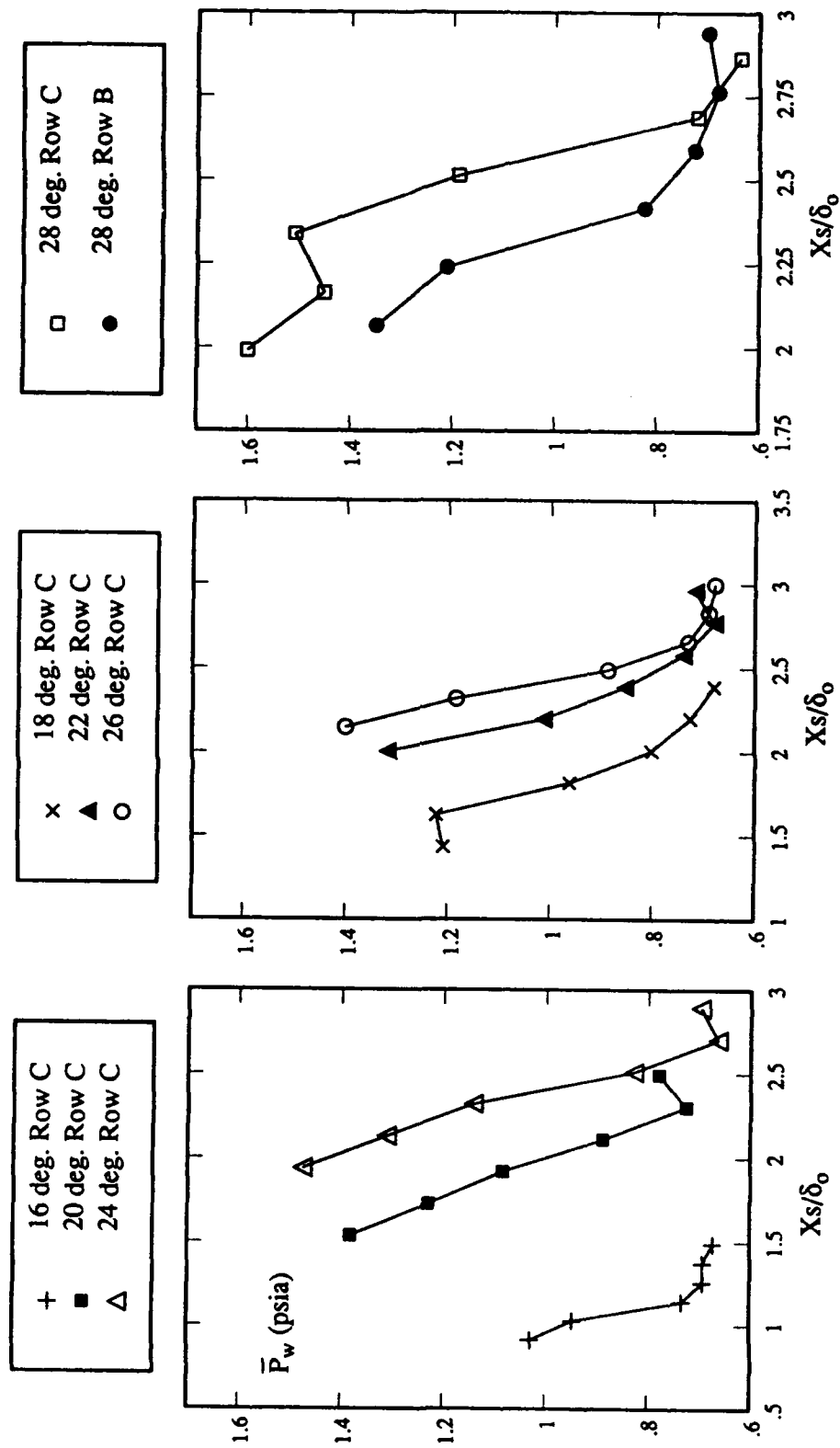
Figure 48. Mean Pressure In the Upstream Region of the Interaction
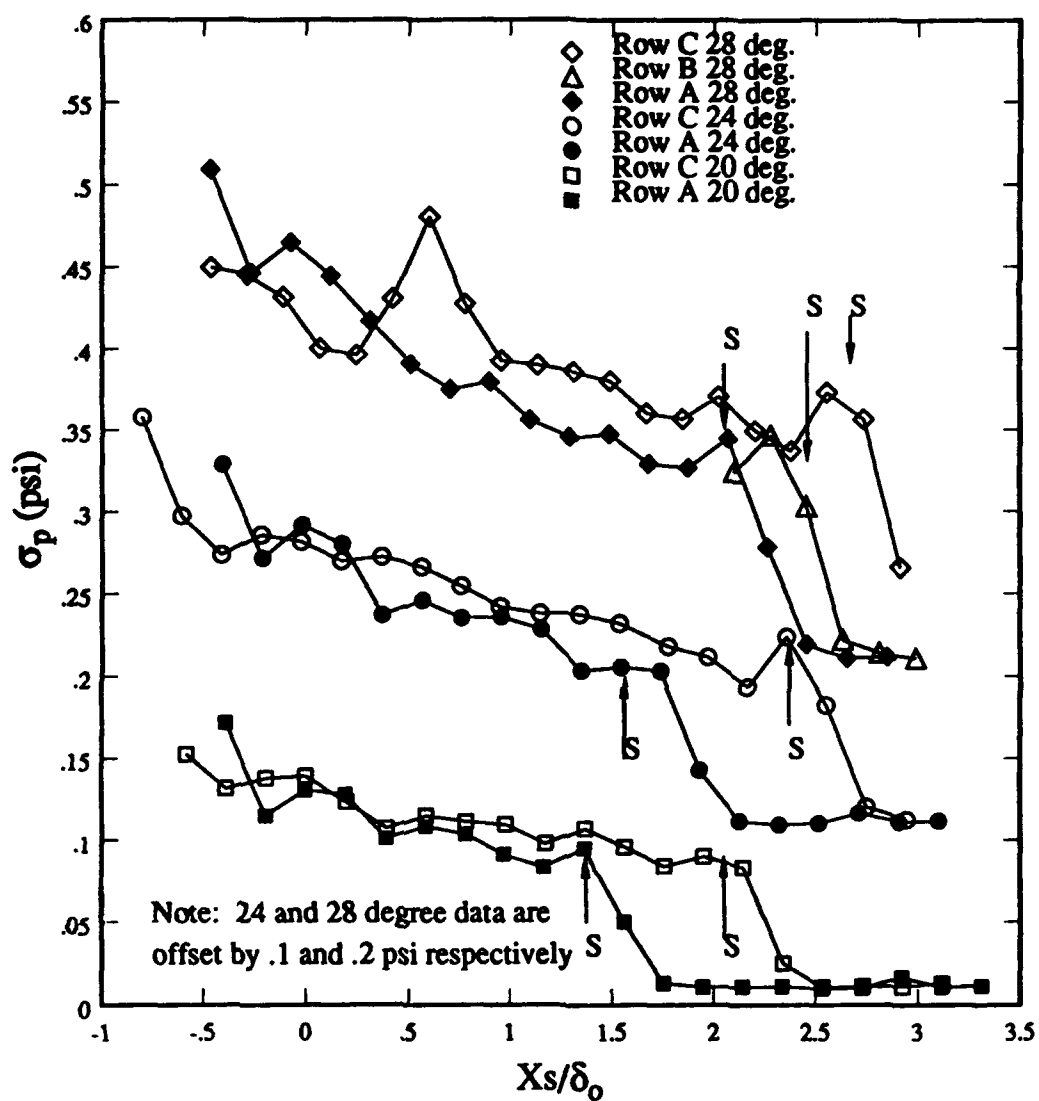
Fig. 49. Sharp Fin Interaction RMS Distributions:
Normal to the Inviscid Shock Location

108
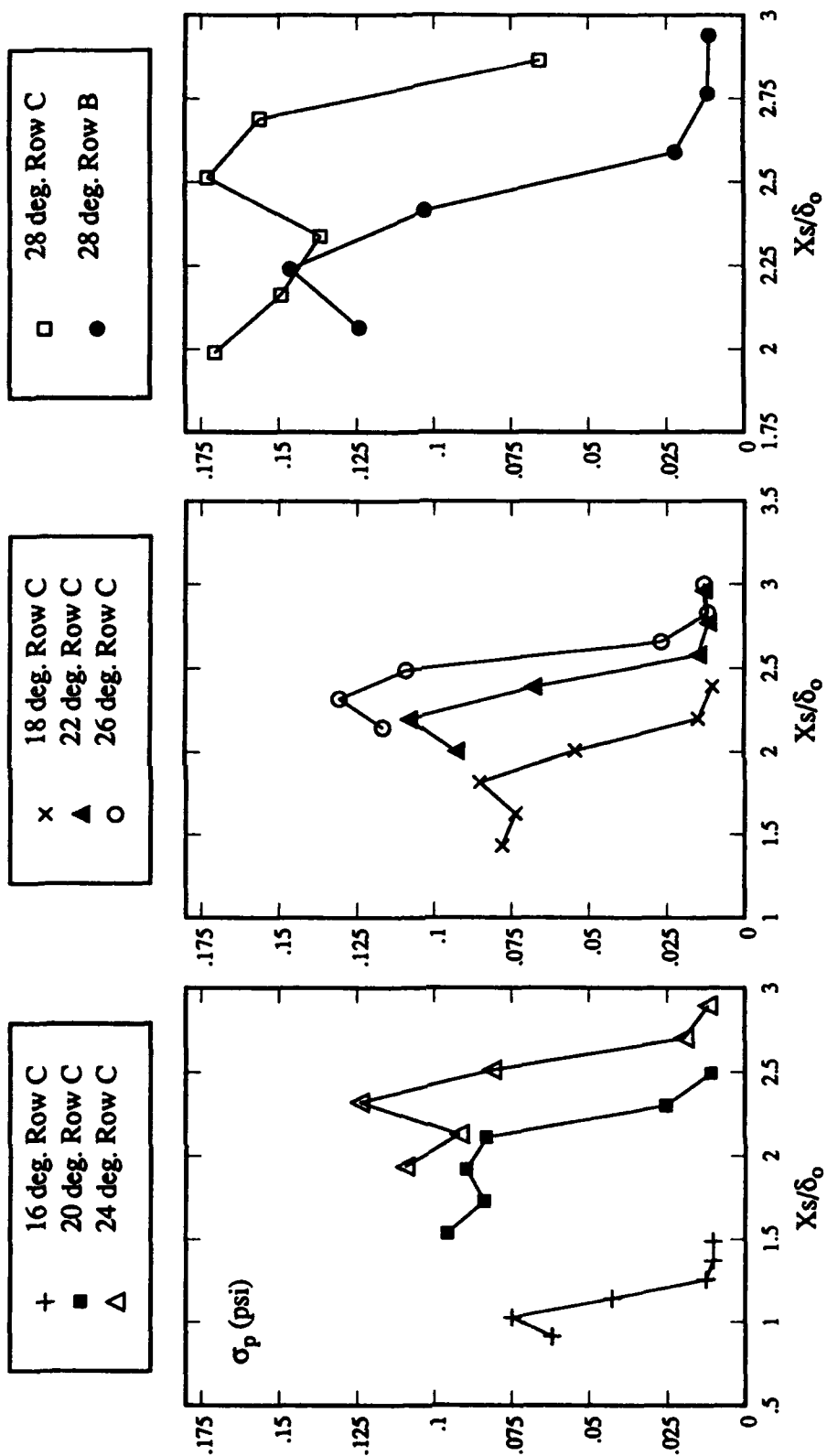
Figure 50. Standard Deviation In the Upstream Region of the Interaction
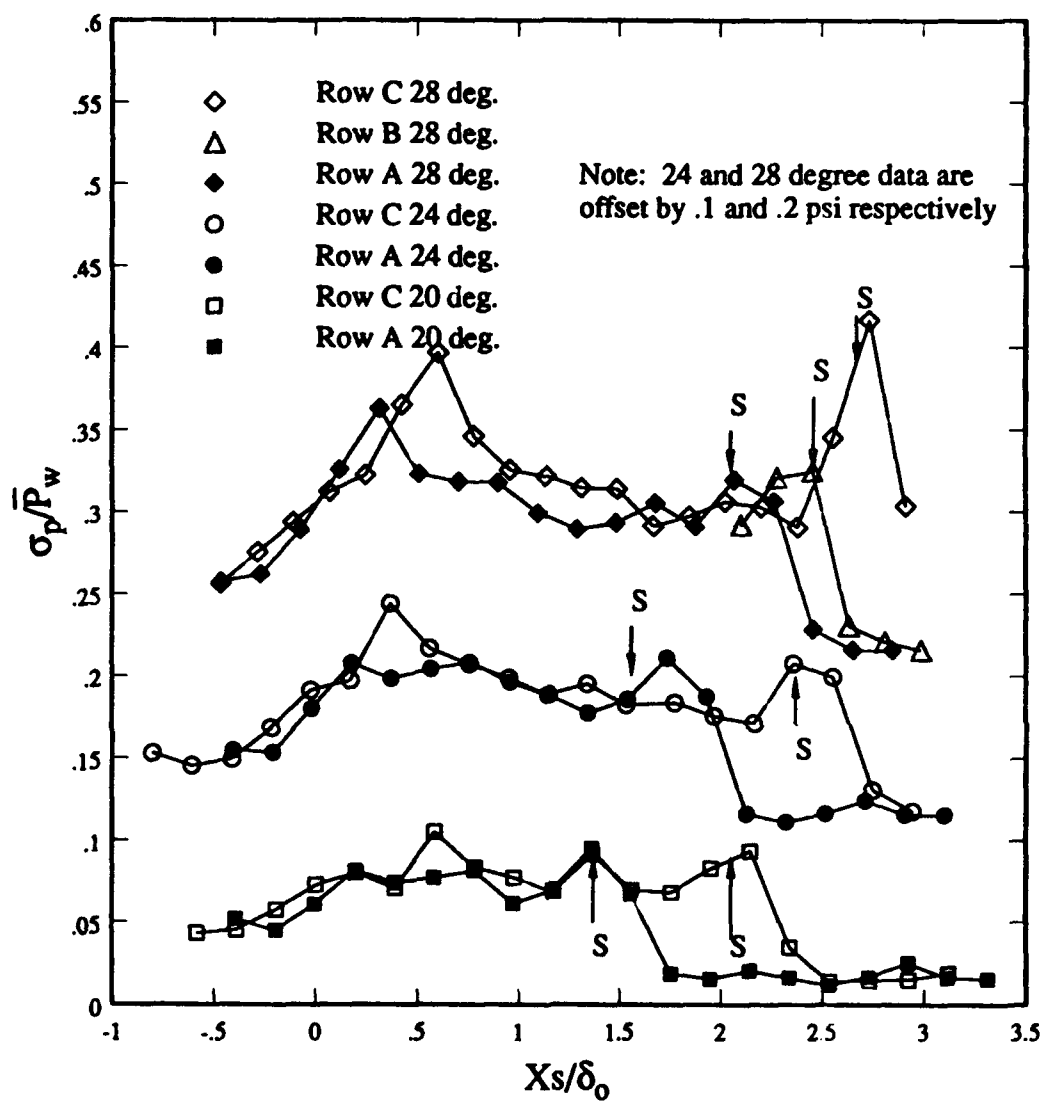
Fig. 51. Normalized RMS Distributions:
Normal to the Inviscid Shock Location
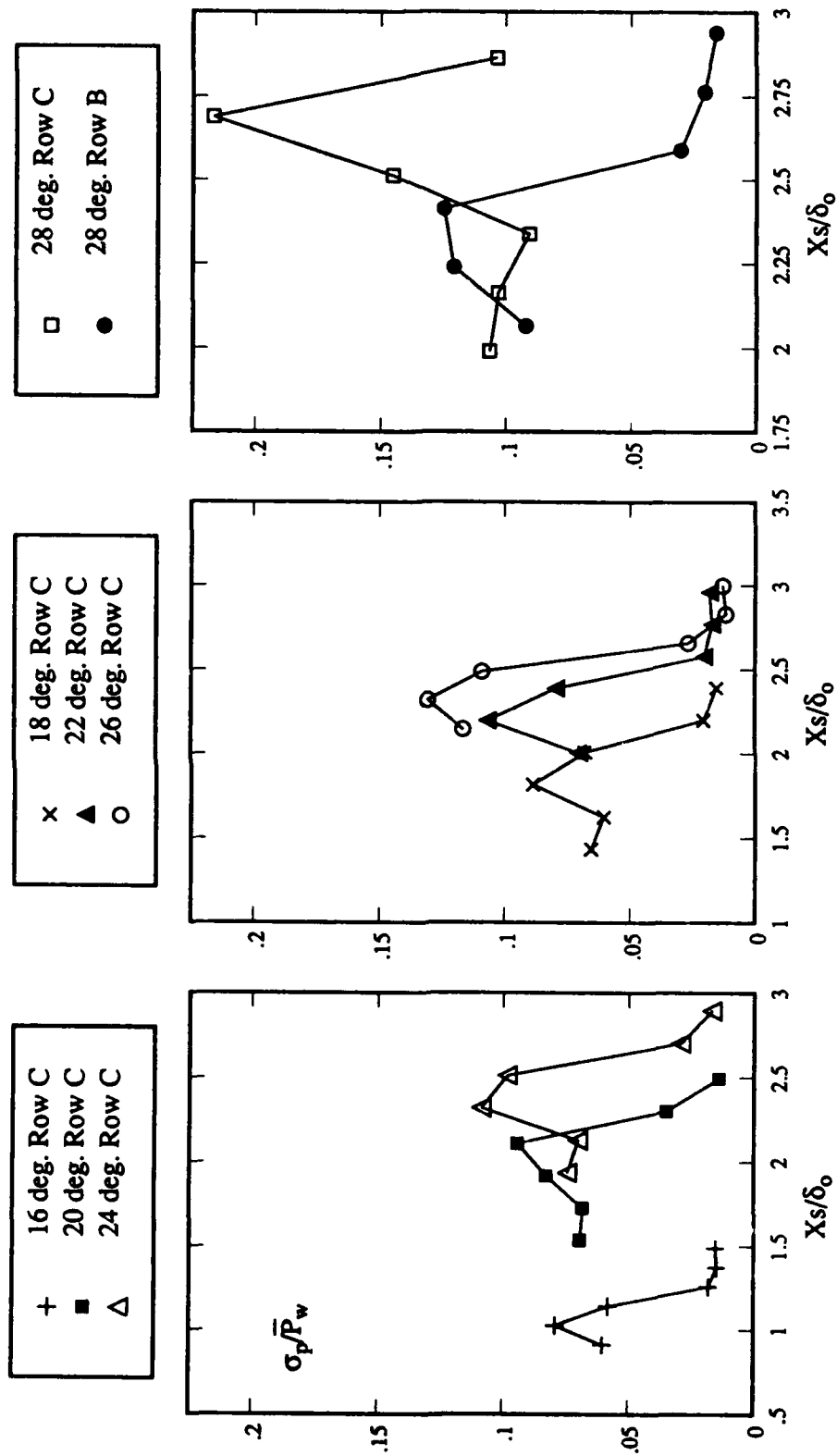
Figure 52. Normalized Standard Deviation In the Upstream Region of the Interaction
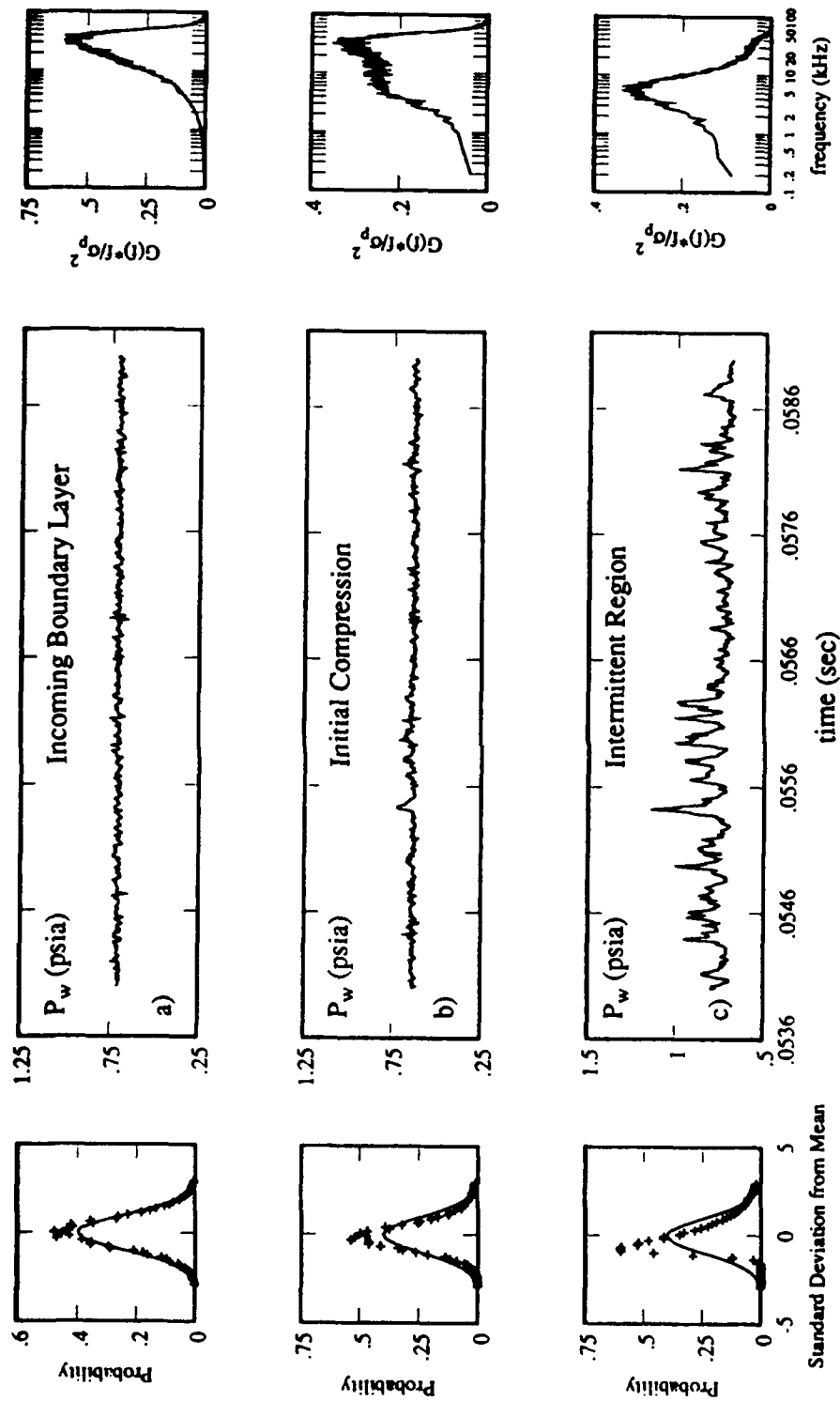
Fig. 53. PDDs, Time-Histories, and PSDs for α = 24 deg. Interaction

112

Fig. 53. continued

113
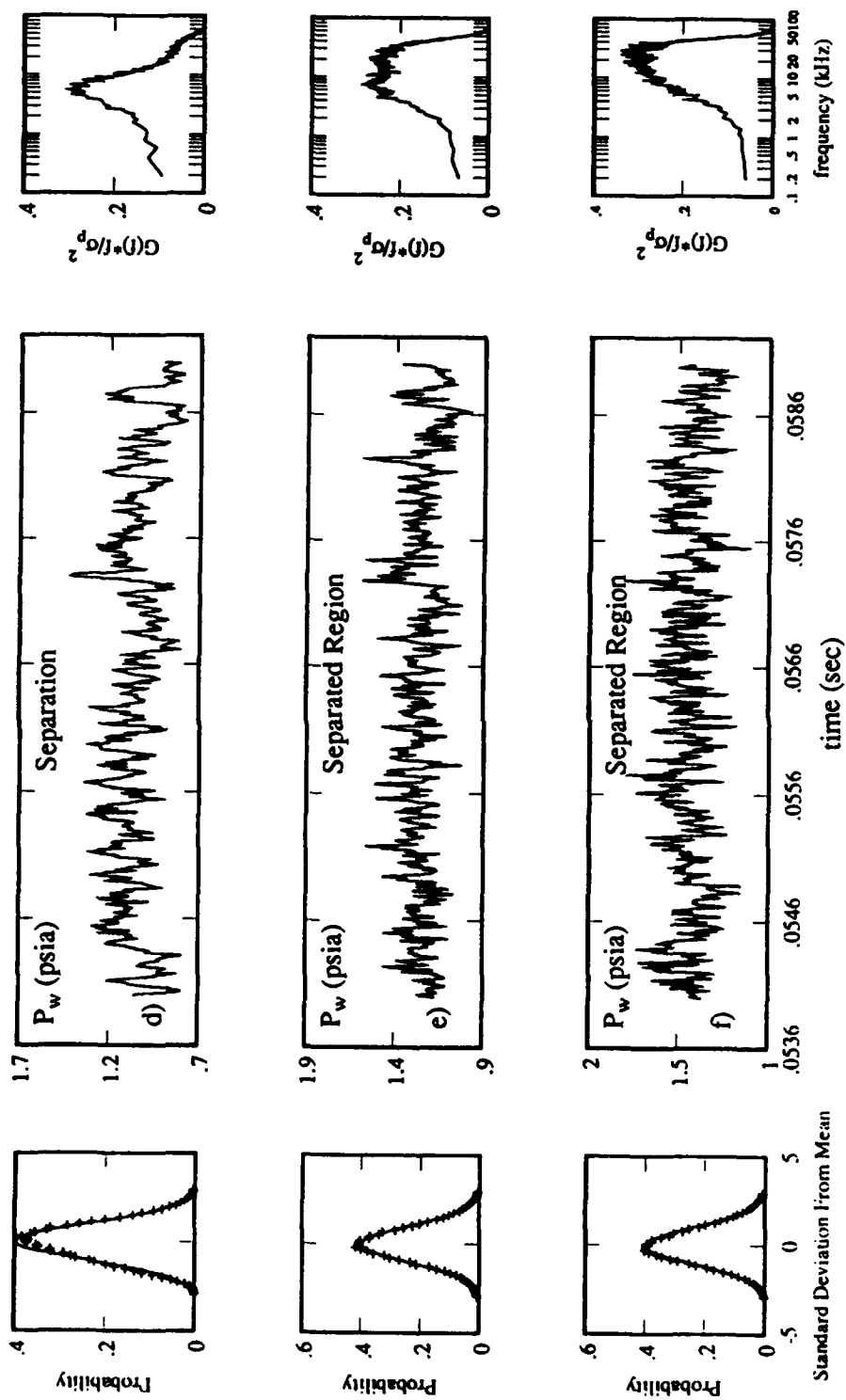
Fig. 54. Surface Flow Visualization Pattern for 24 deg. Interaction

114
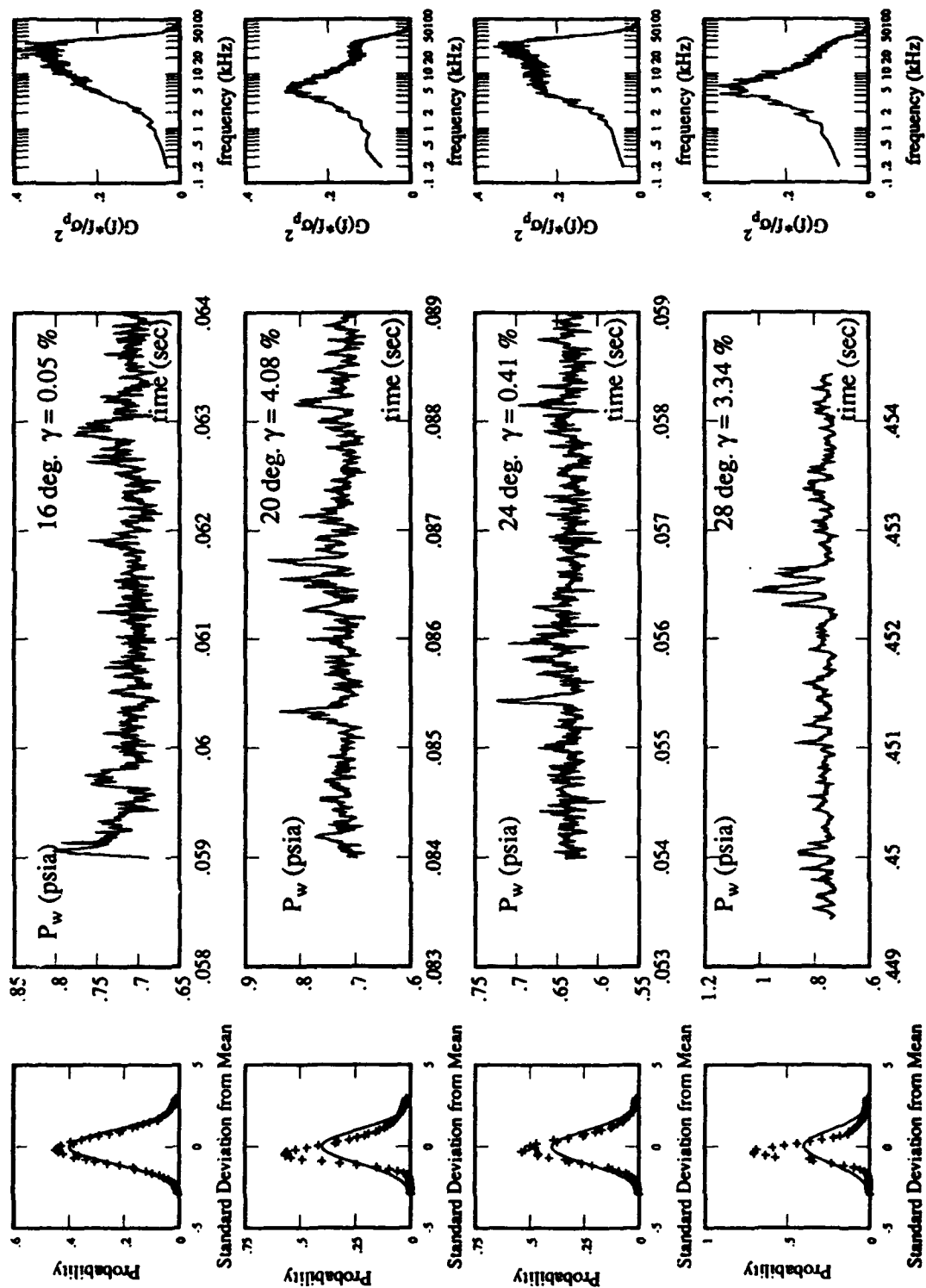
Figure 55. PDDs, Time-Histories, and PSDs for First Intermittent Channel

115
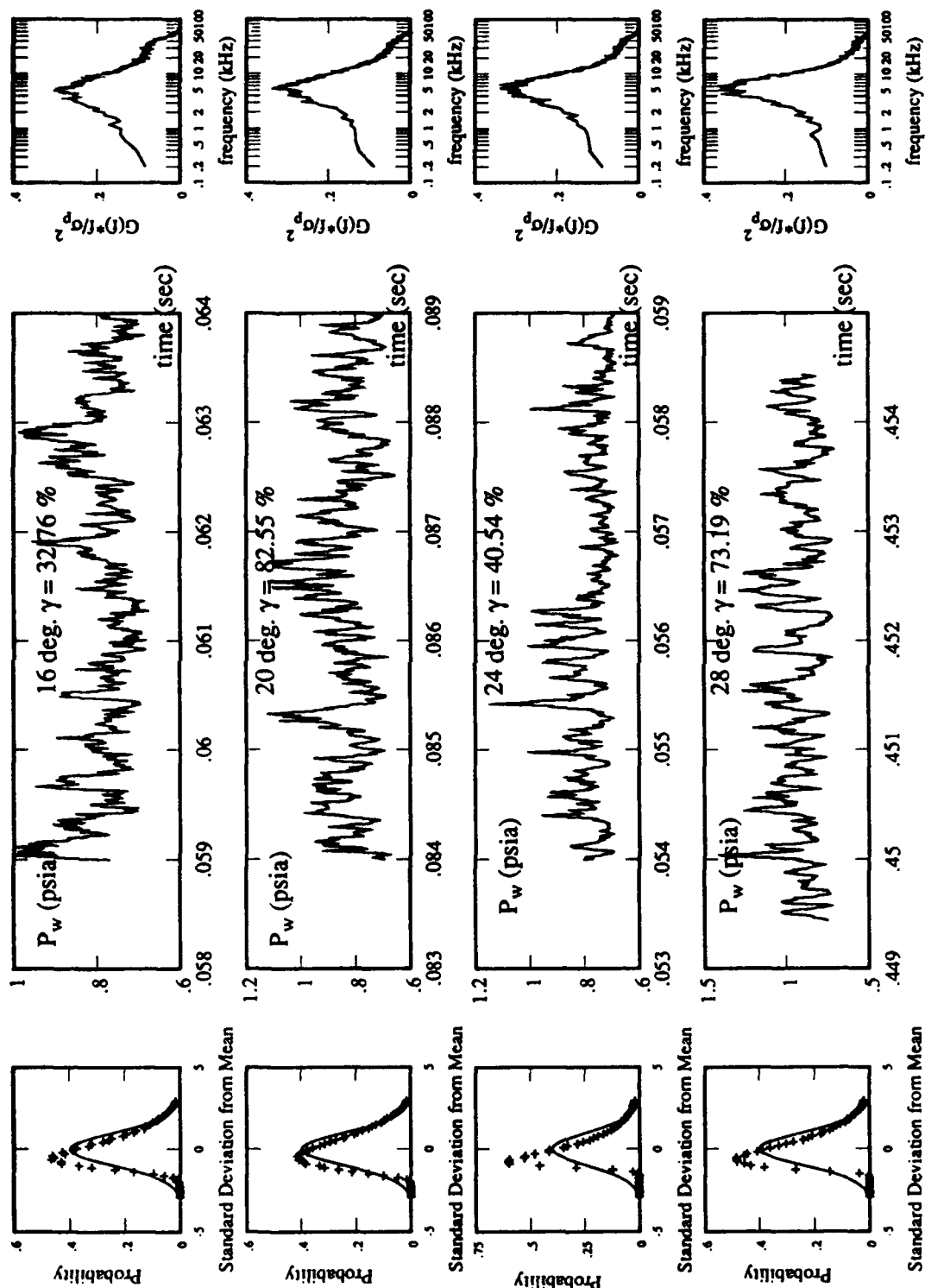
Figure 56. PDDs, Time-Histories, and PSD's for Second Intermittent Channel

116
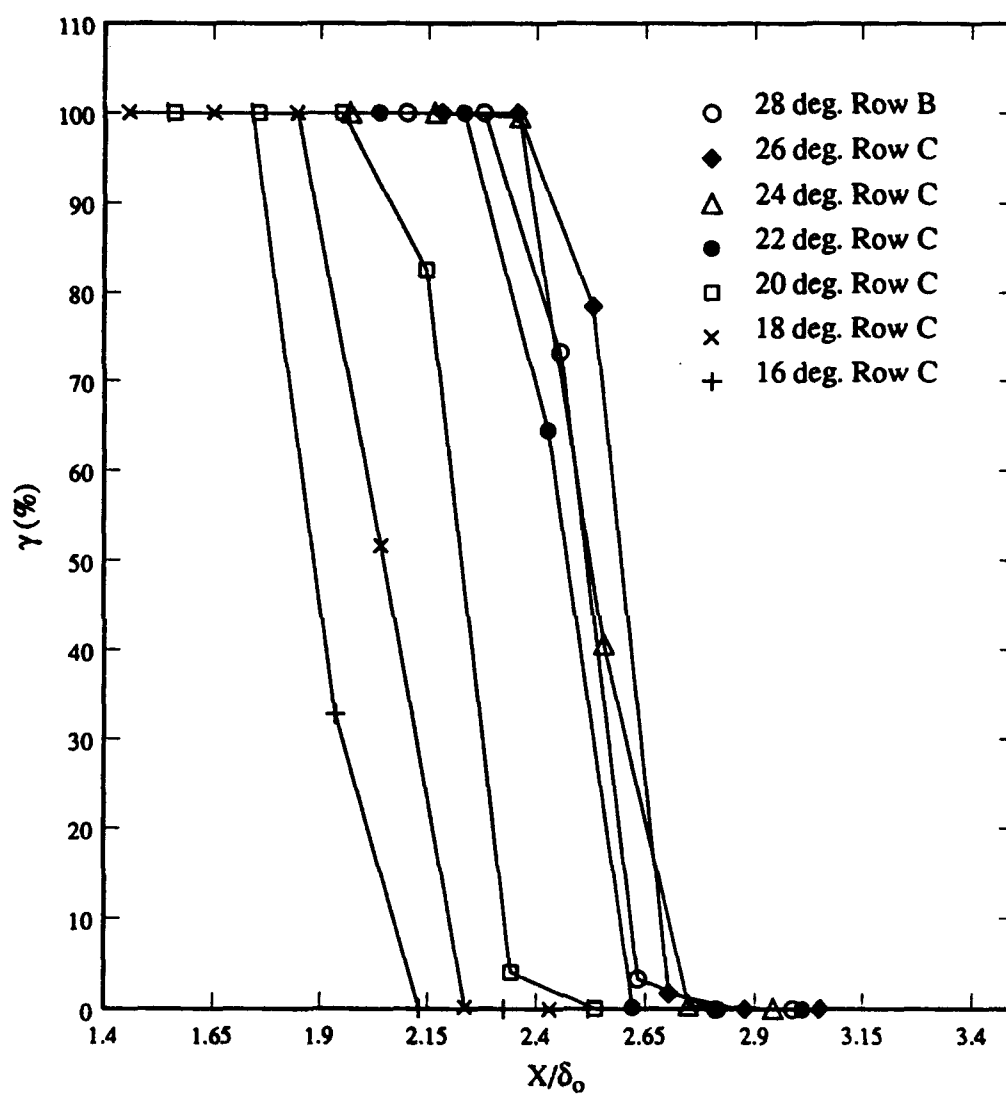
Fig. 57. Intermittency Distributions

117
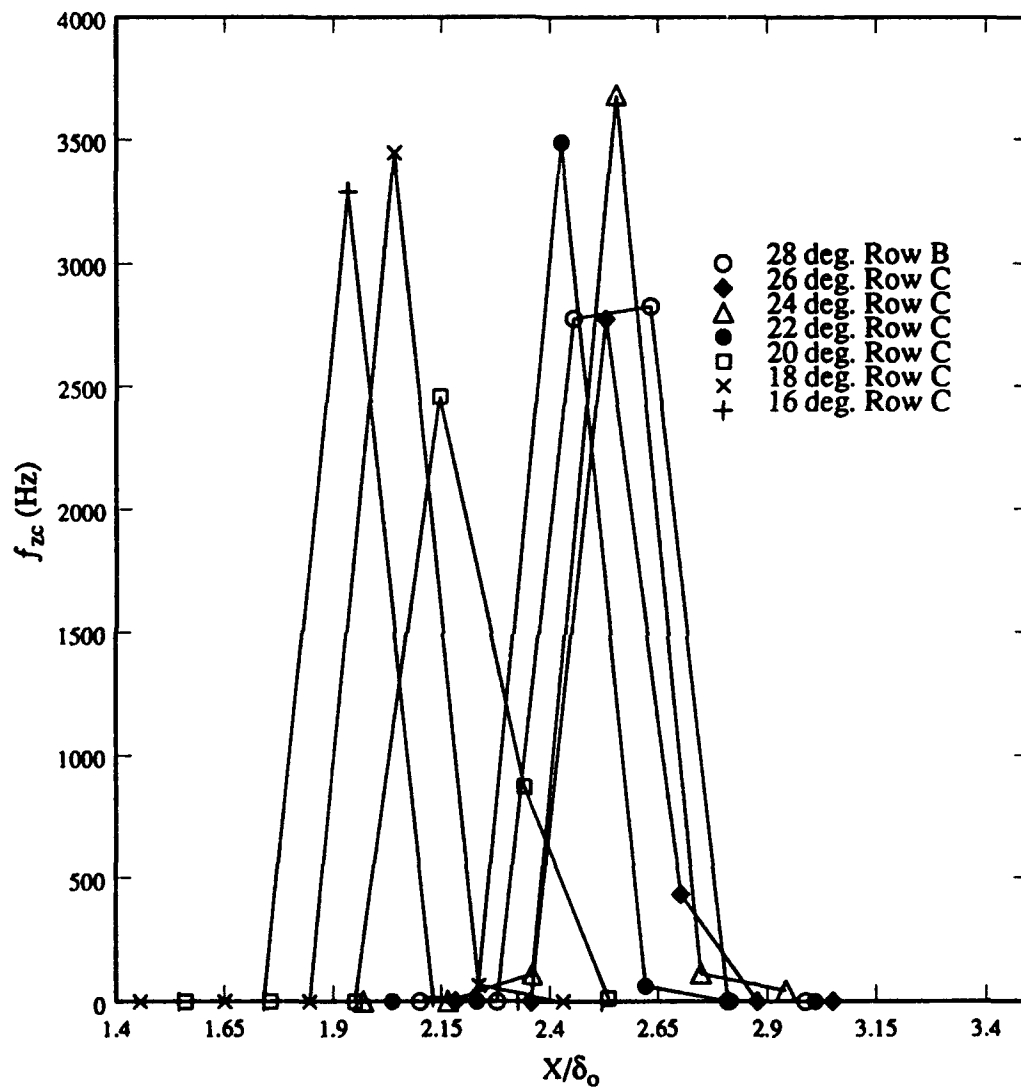
Fig. 58. Zero Crossing Frequency Distributions

118
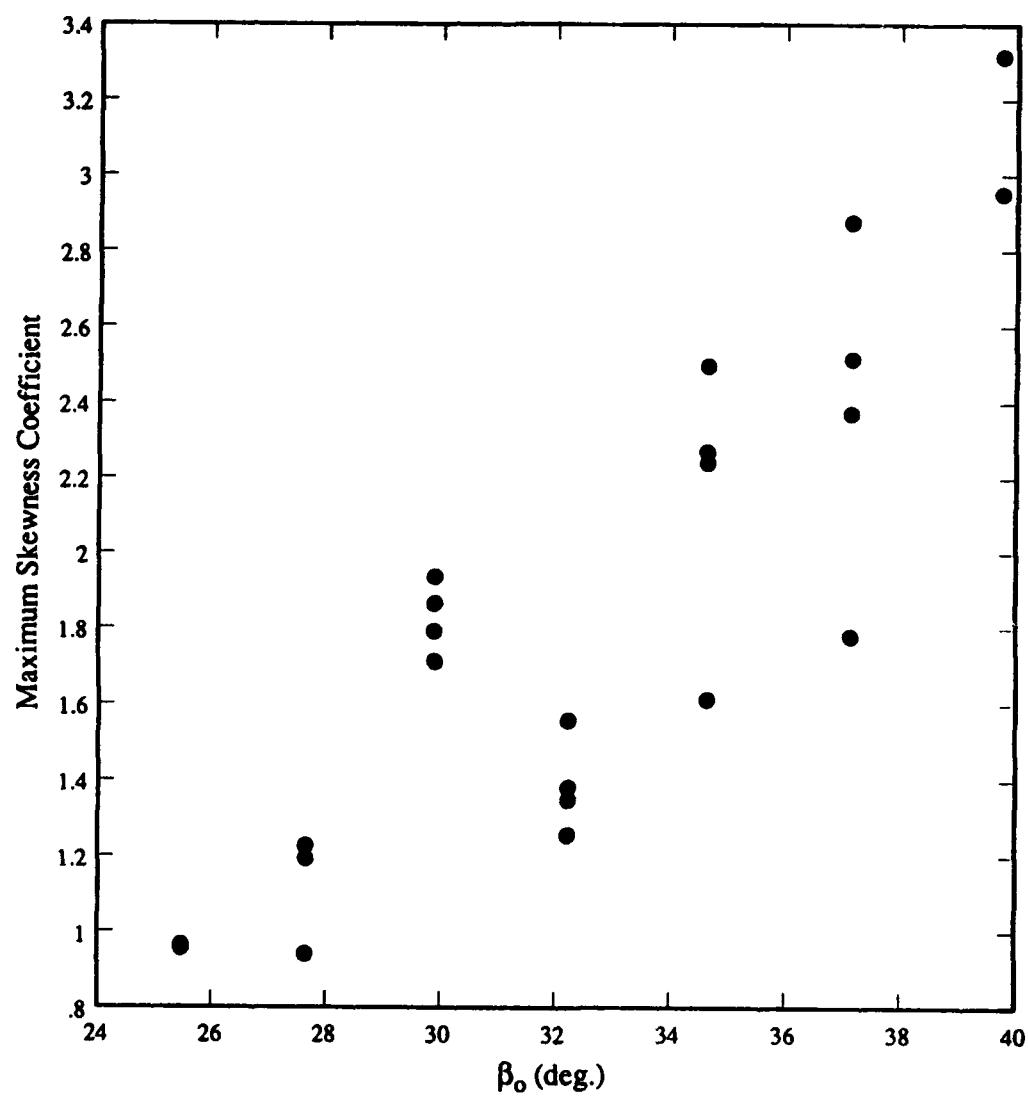
Fig. 59. Maximum Skewness Coefficient Vs. Inviscid Shock Angle
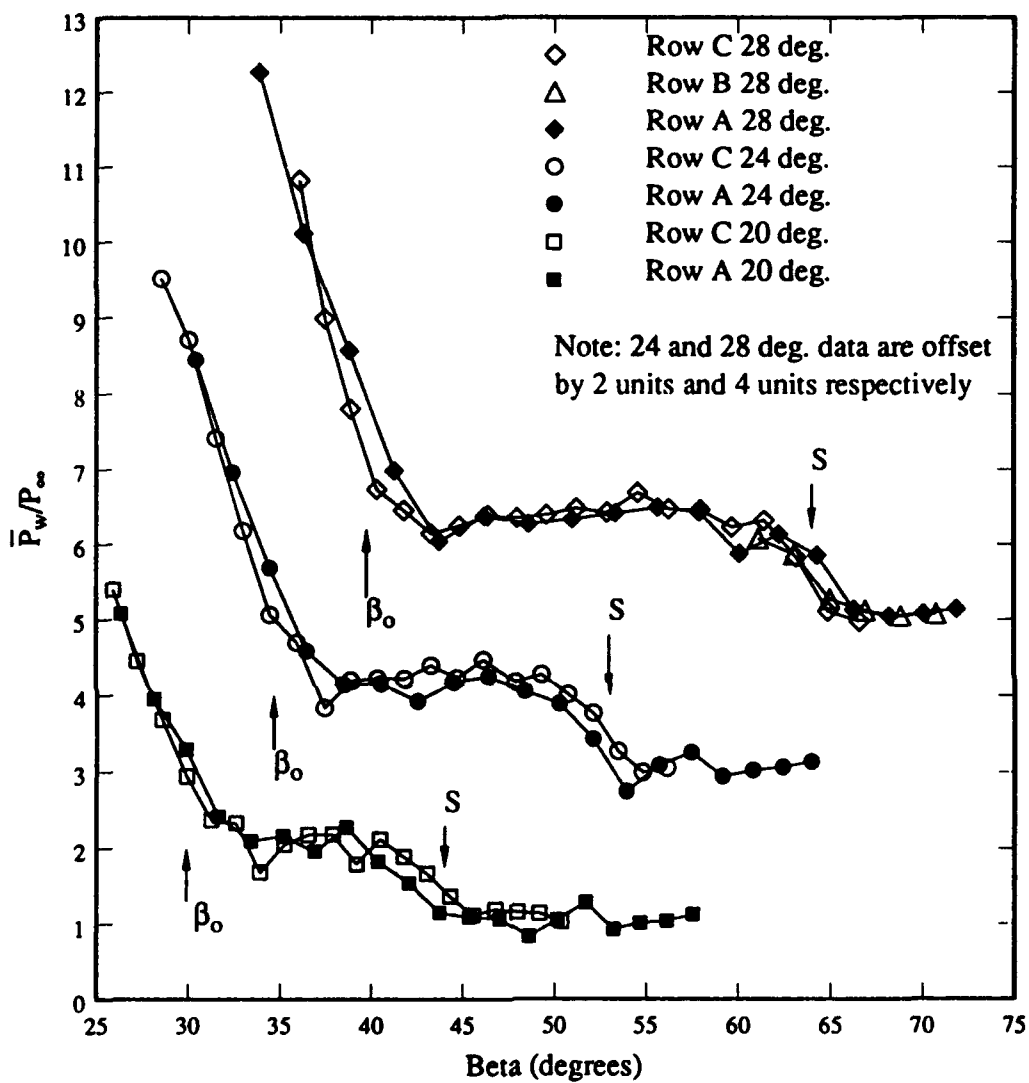
Fig. 60. Mean Surface Pressure Distributions:
VCO determined from Surface Flow Visualization

120
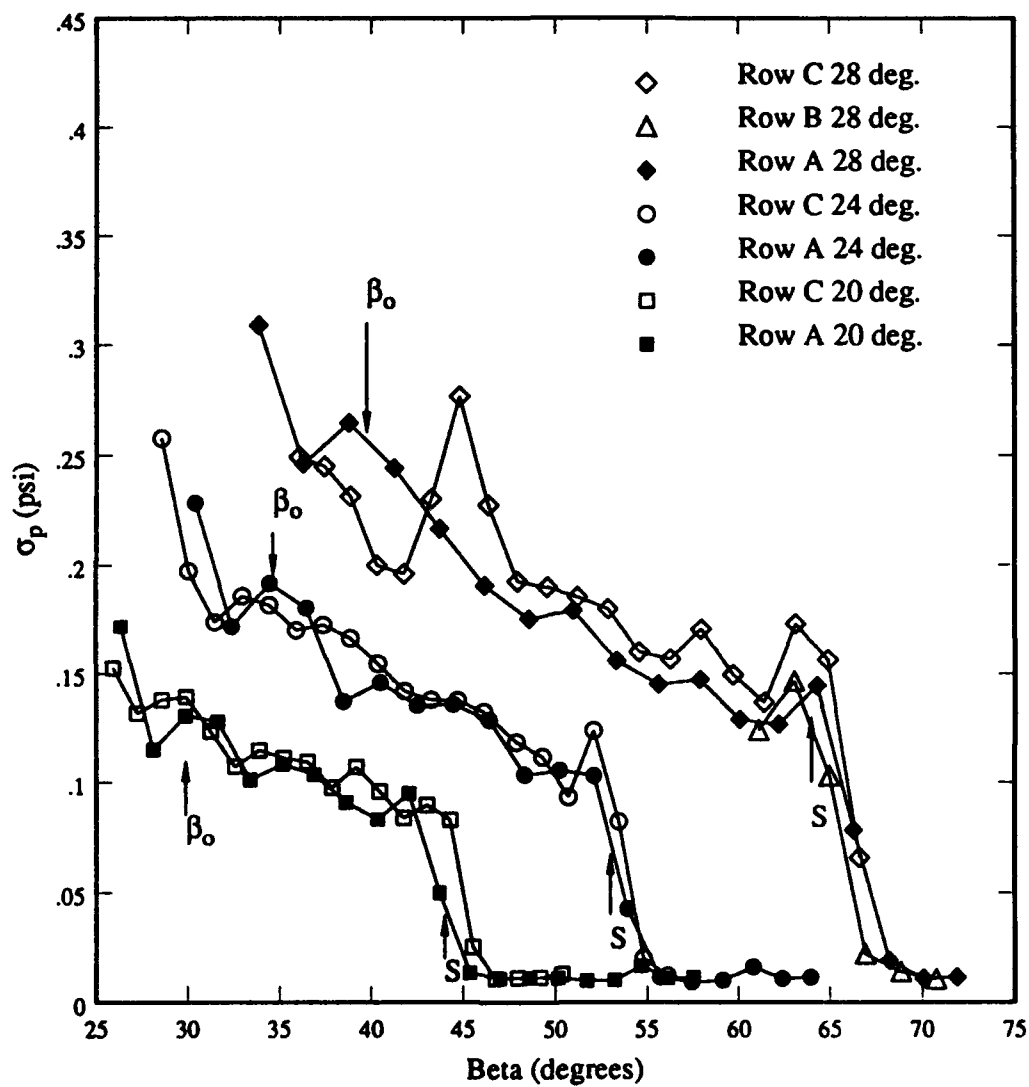
Fig. 61. RMS Distributions:
VCO Determined from Surface flow Visualization

121
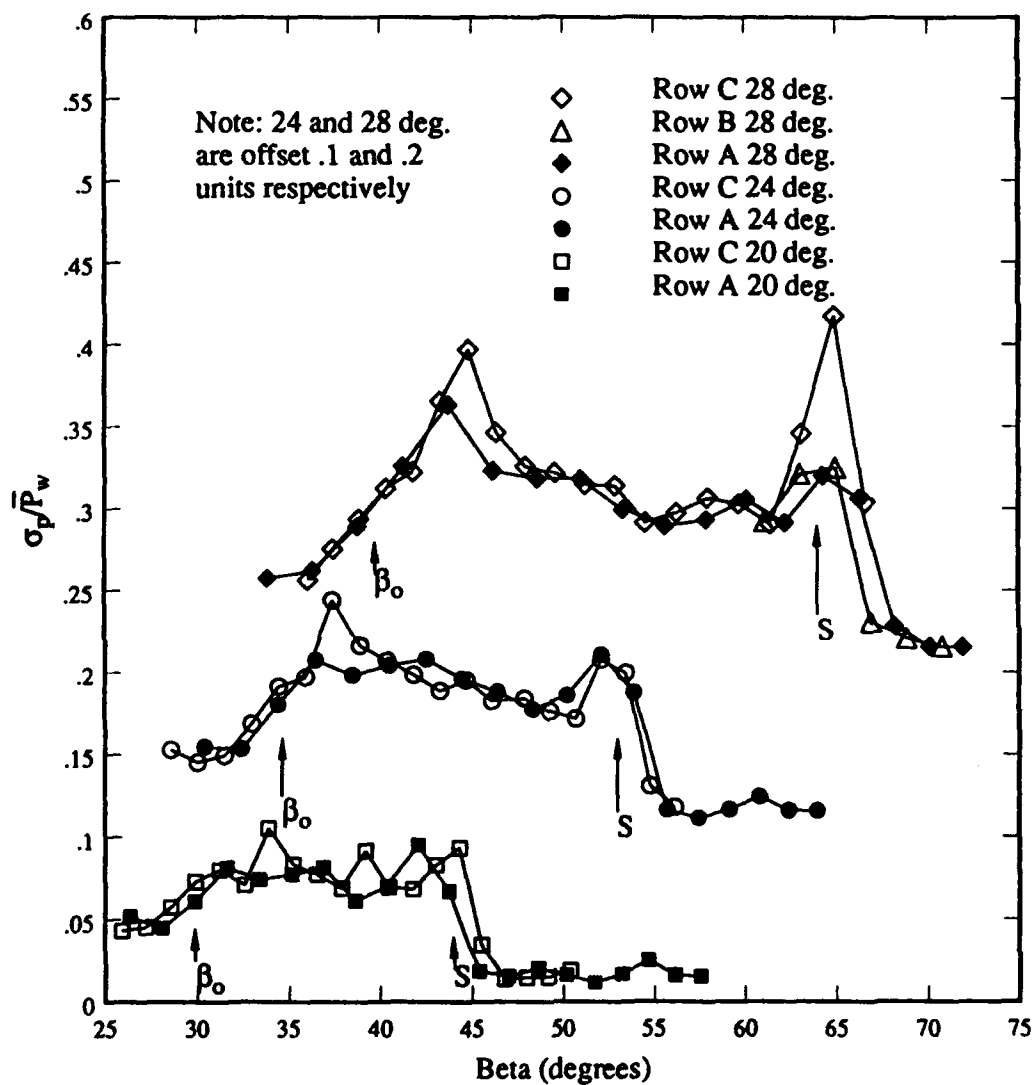
Fig. 62. RMS Distribution Normalized by Local Mean Wall Pressure:
VCO Determined from Surface flow Visualization

122
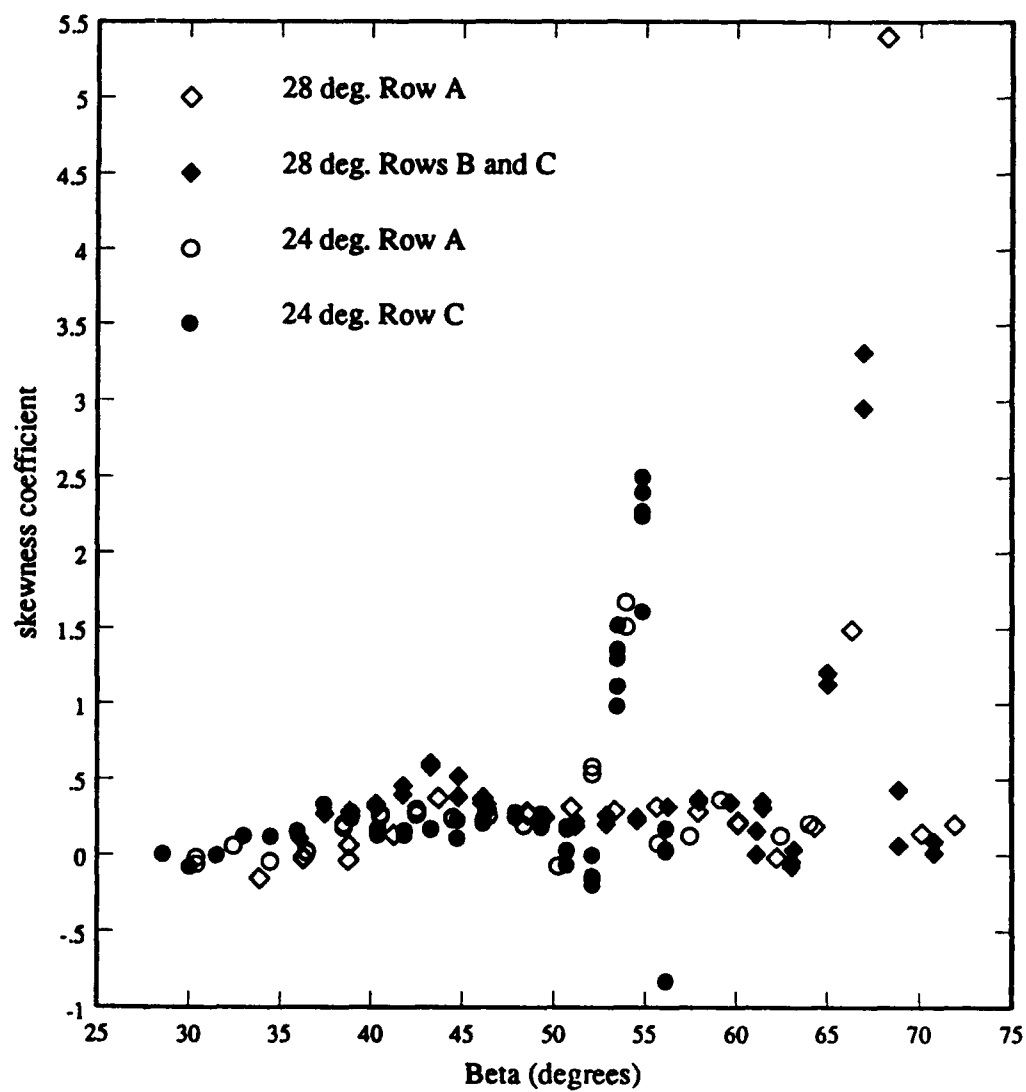
Fig. 63. Skewness Coefficient in Conical Coordinates

123
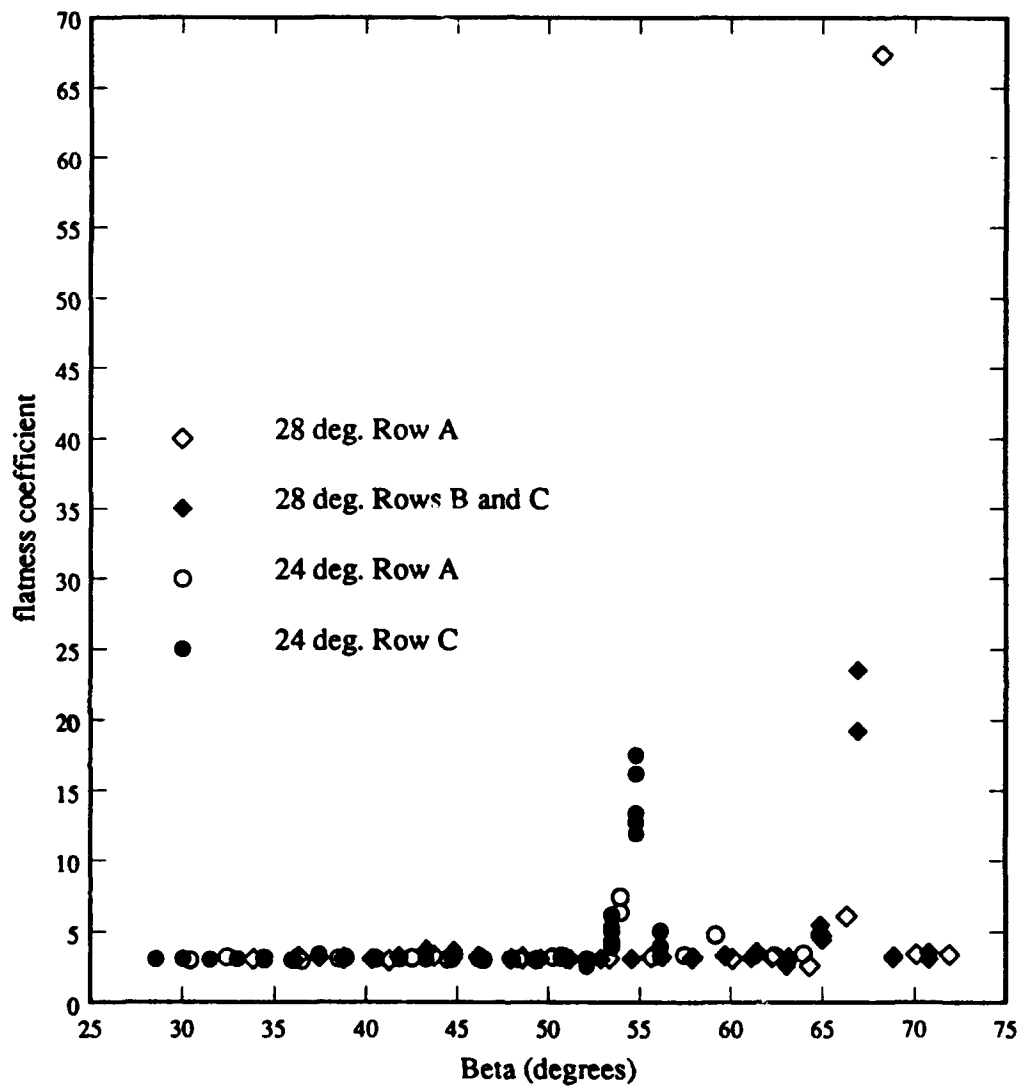
Fig. 64. Flatness Coefficient in Conical Coordinates

124
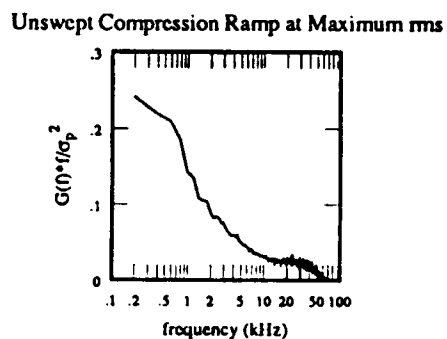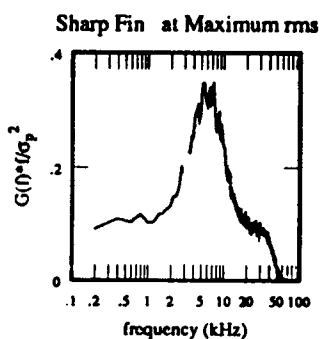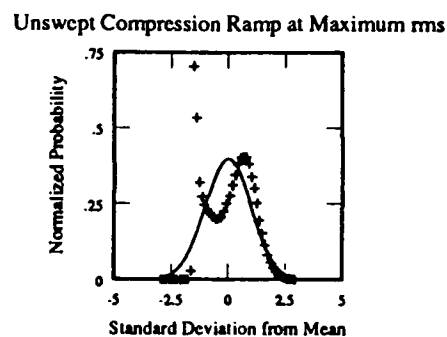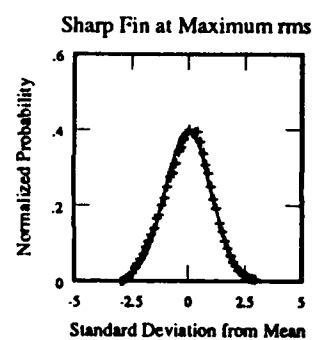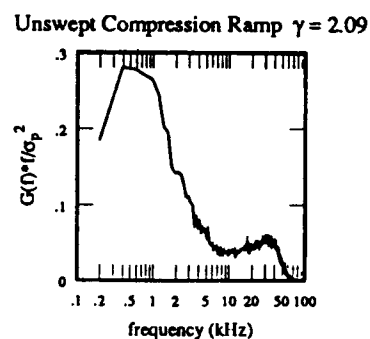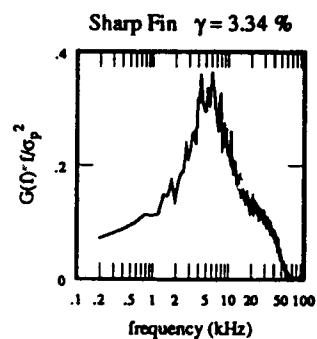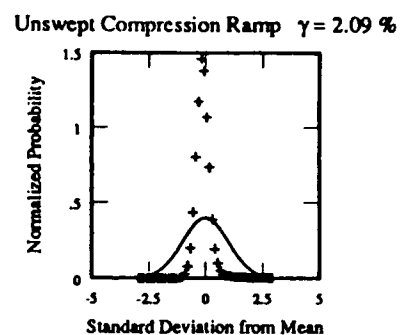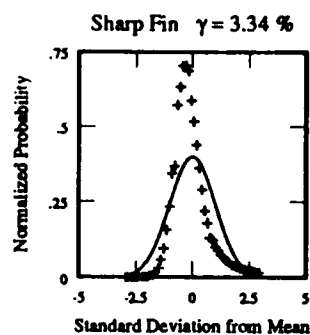
Fig. 65. Sharp Fin and Unswept Compression Ramp Data

125
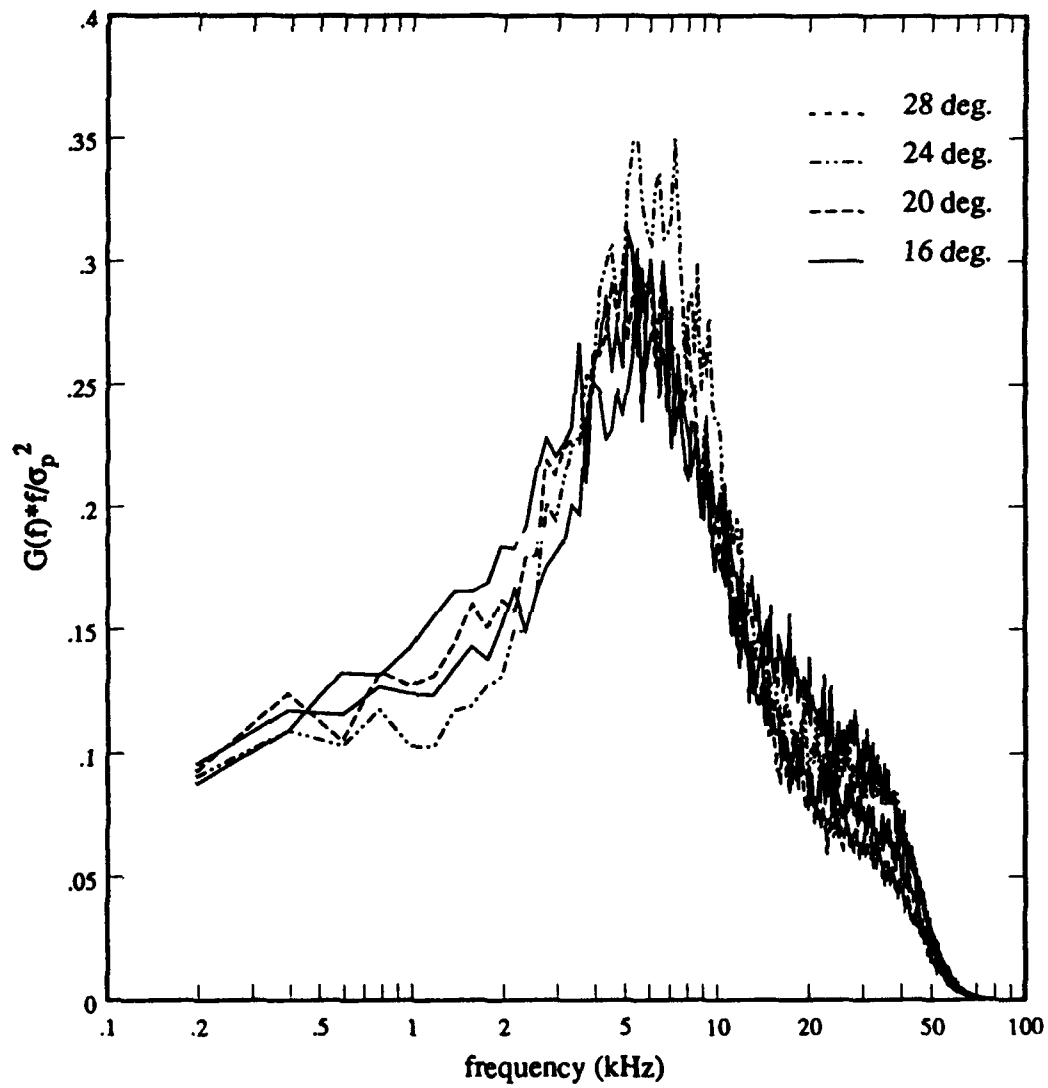
Fig. 66. PSDs at Maximum RMS
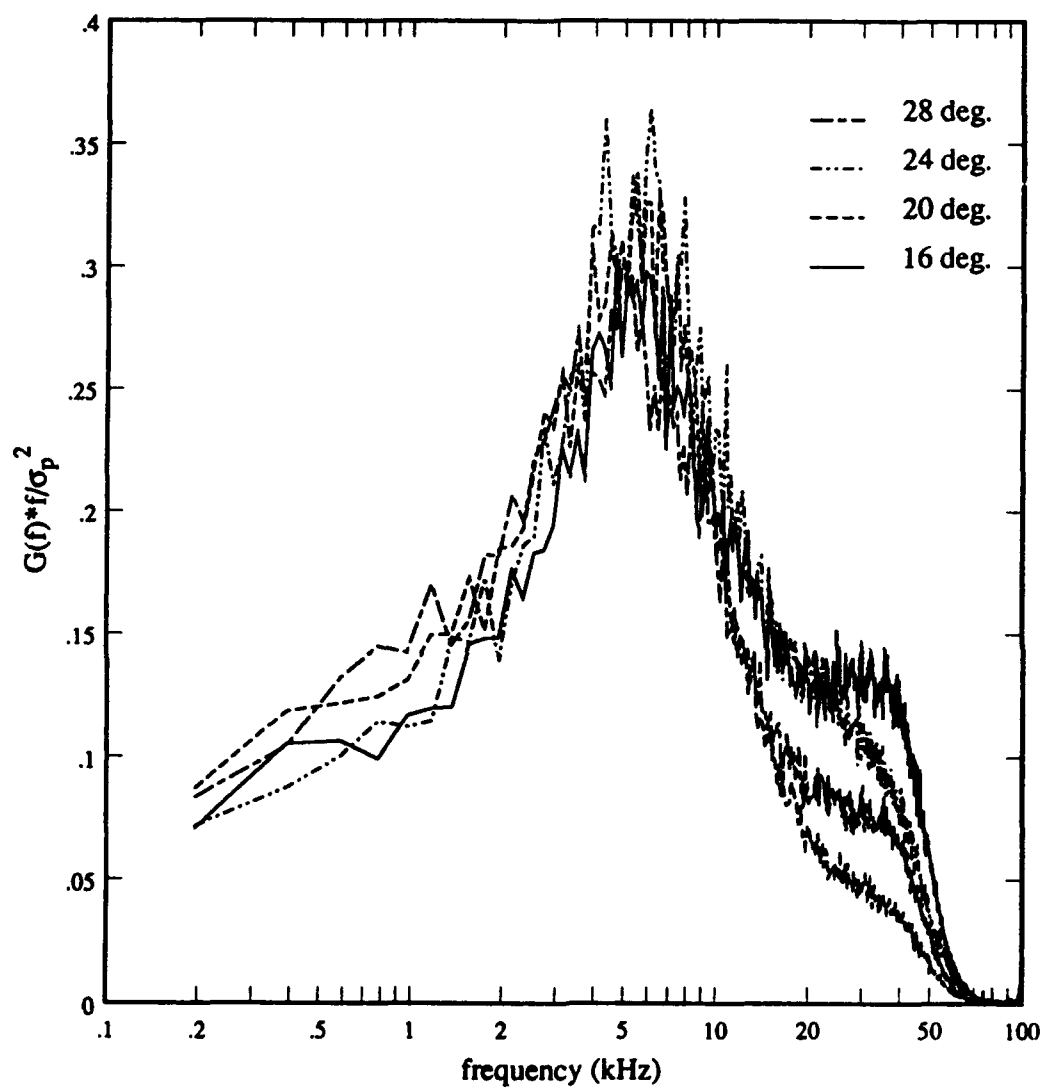
Fig. 67. PSDs at Maximum Skewness Coefficient

127
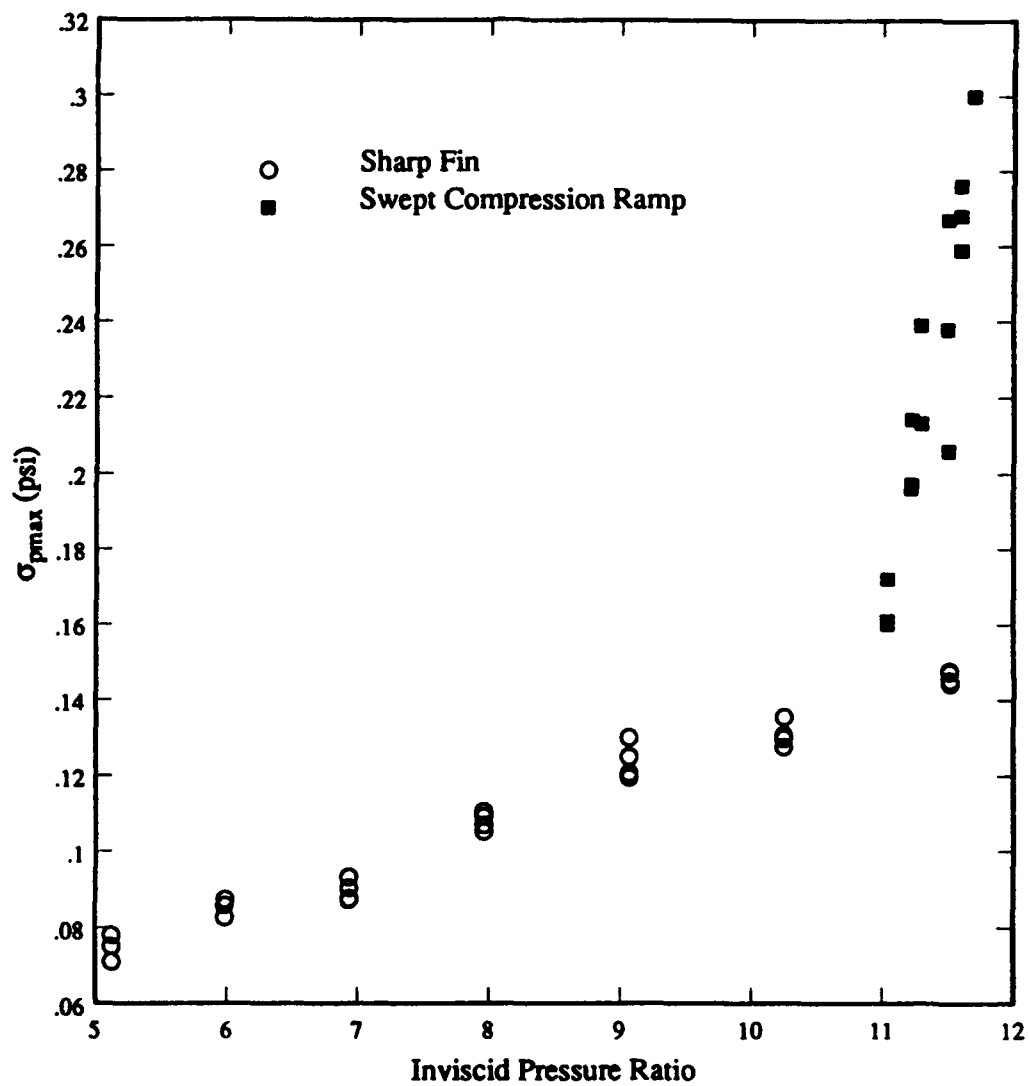
Fig. 68. Maximum RMS Vs. Inviscid Pressure Ratio

128
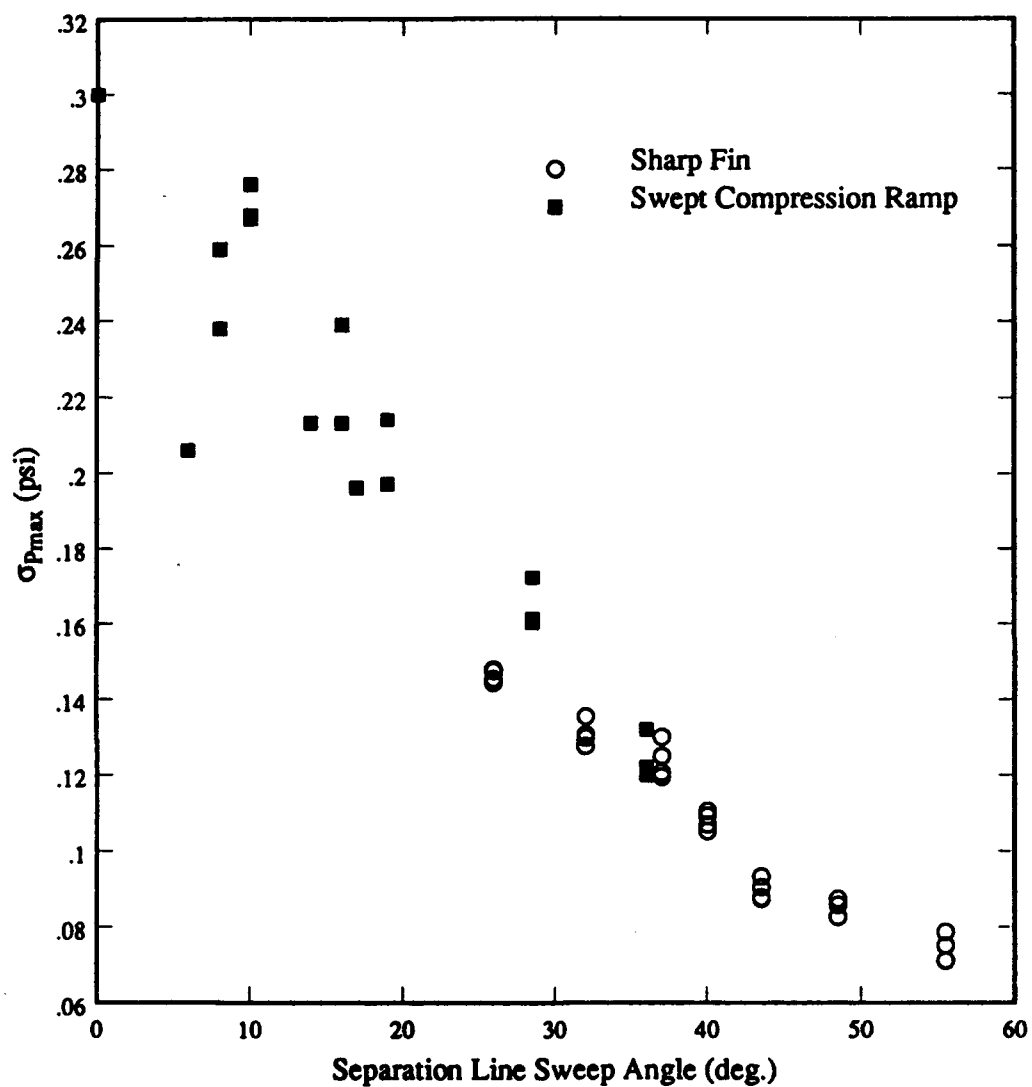
Fig. 69. Maximum RMS Vs. Separation Line Sweep Angle
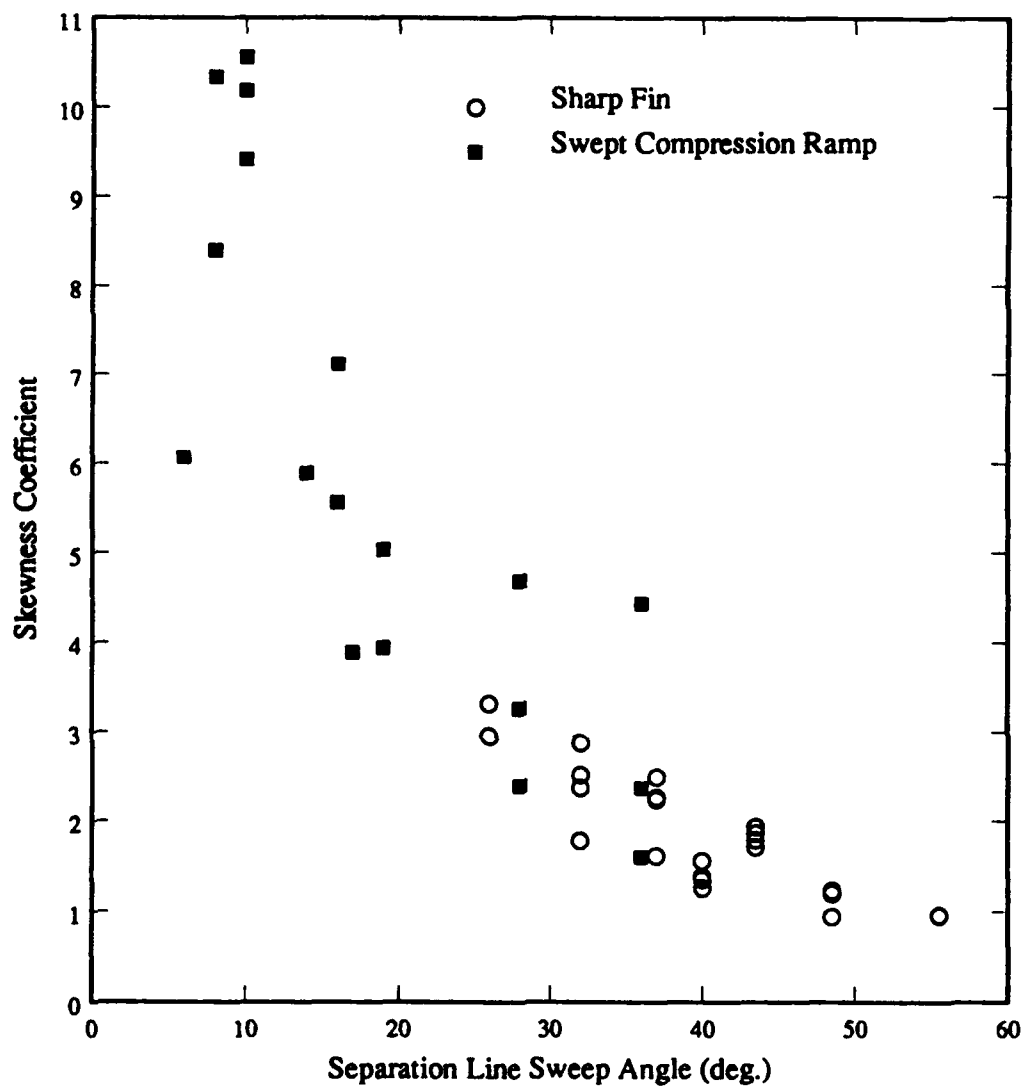
Fig. 70. Maximum Skewness Coefficient Vs. Separation Line Sweep Angle

130
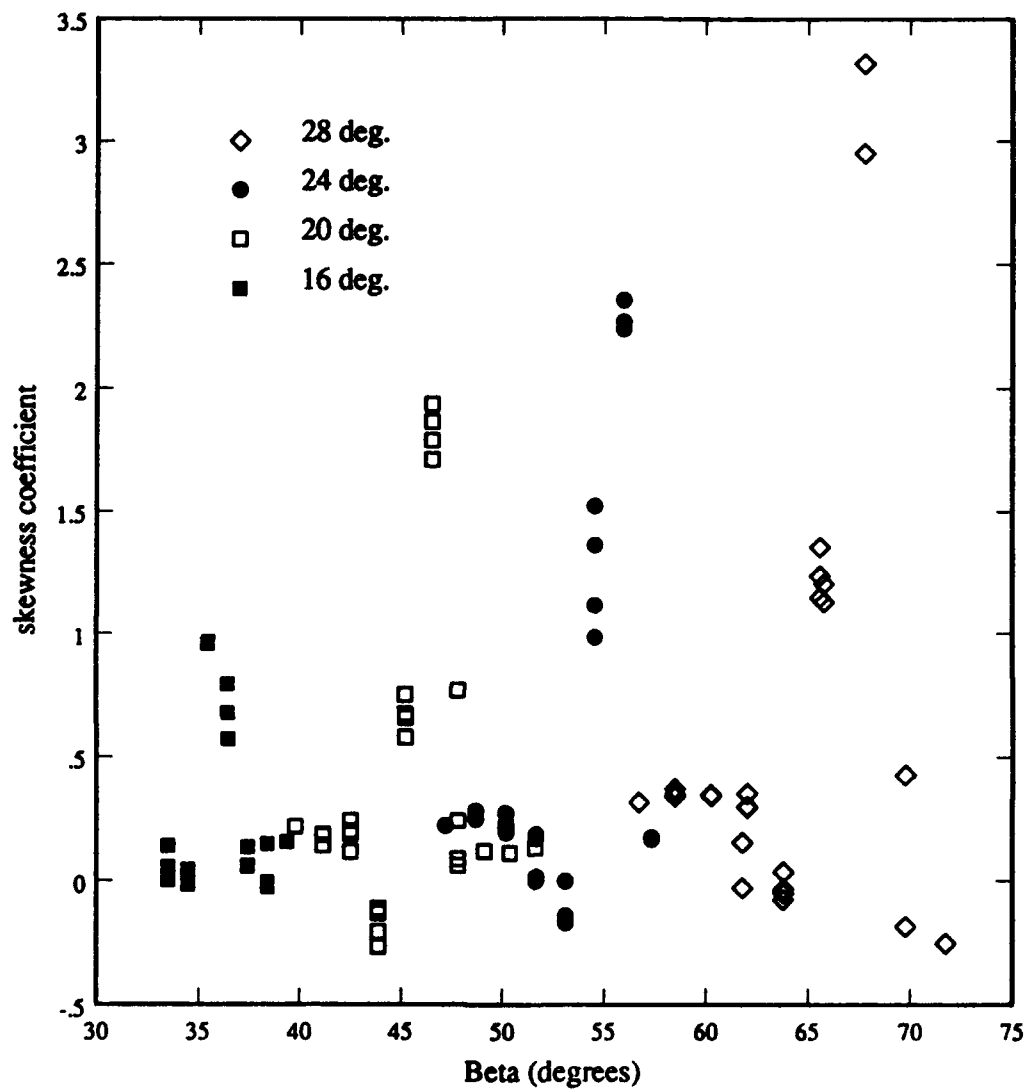
Fig. 71. Skewness Coefficient Vs. Local Conical Angle

131
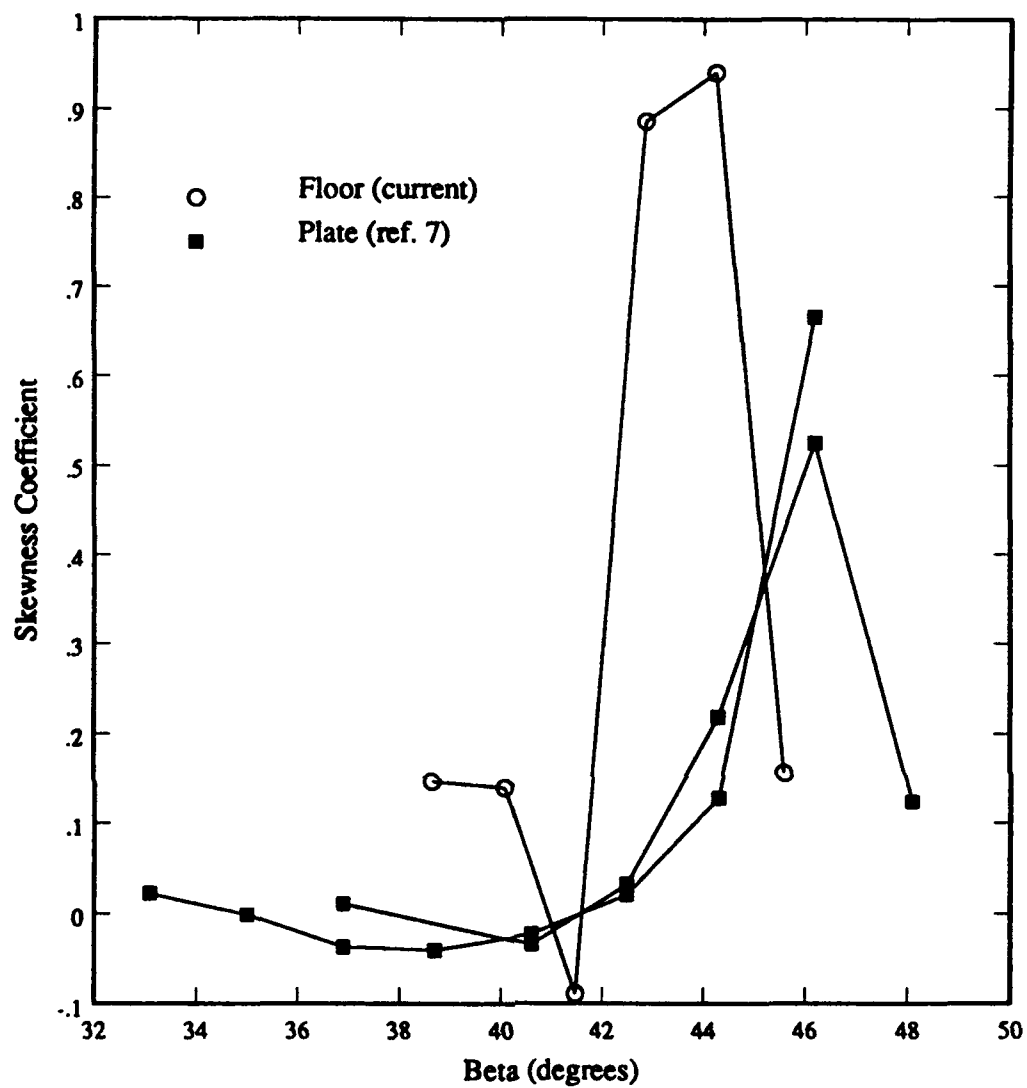
Fig. 72. Skewness Coefficient Distributions for 18 deg. Interactions
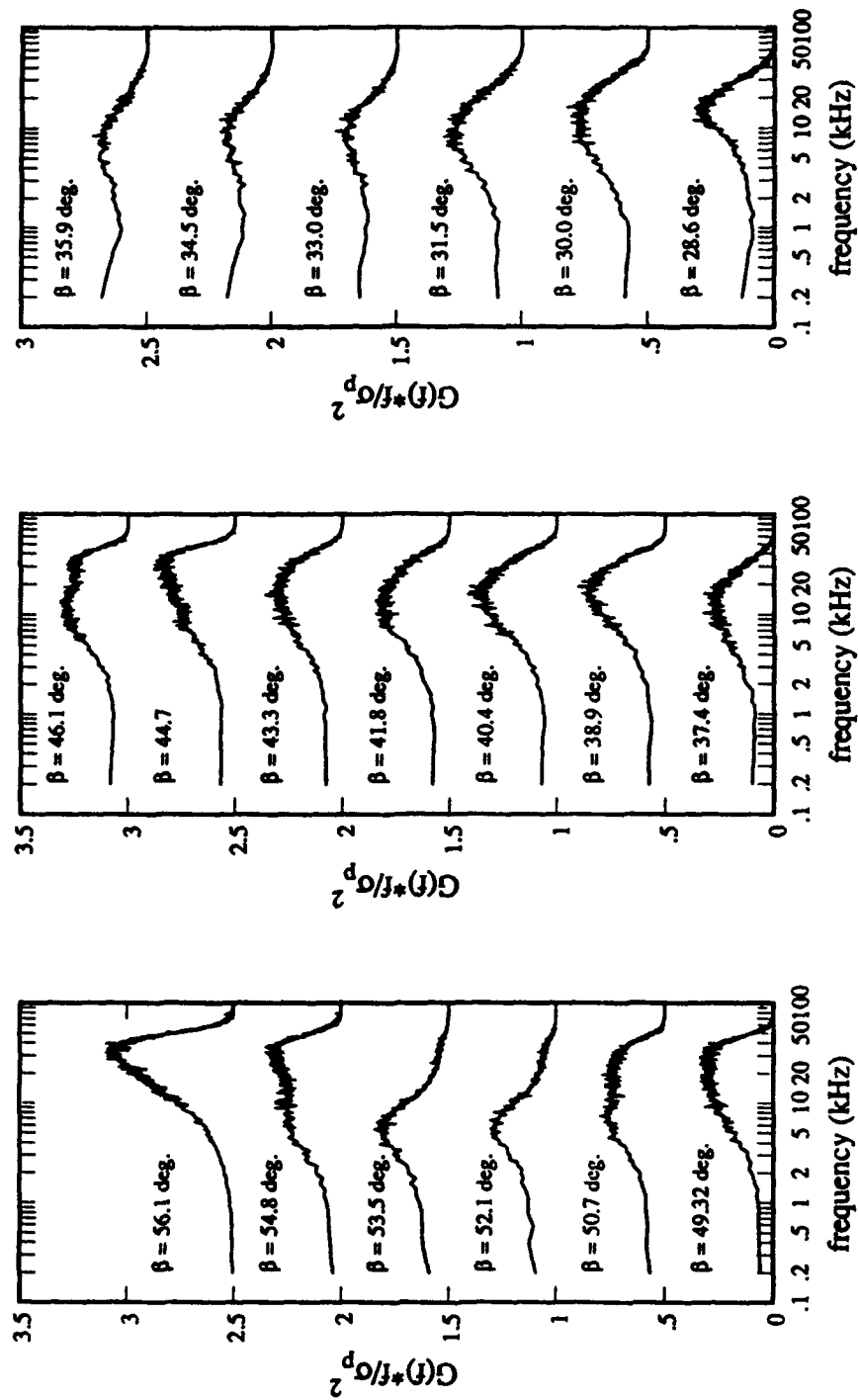
Figure 73. PSDs from the Undisturbed Boundary Layer to Near the Fin Surface

Note: Each curve is Vertically Offset 0.5 units above the curve below

133
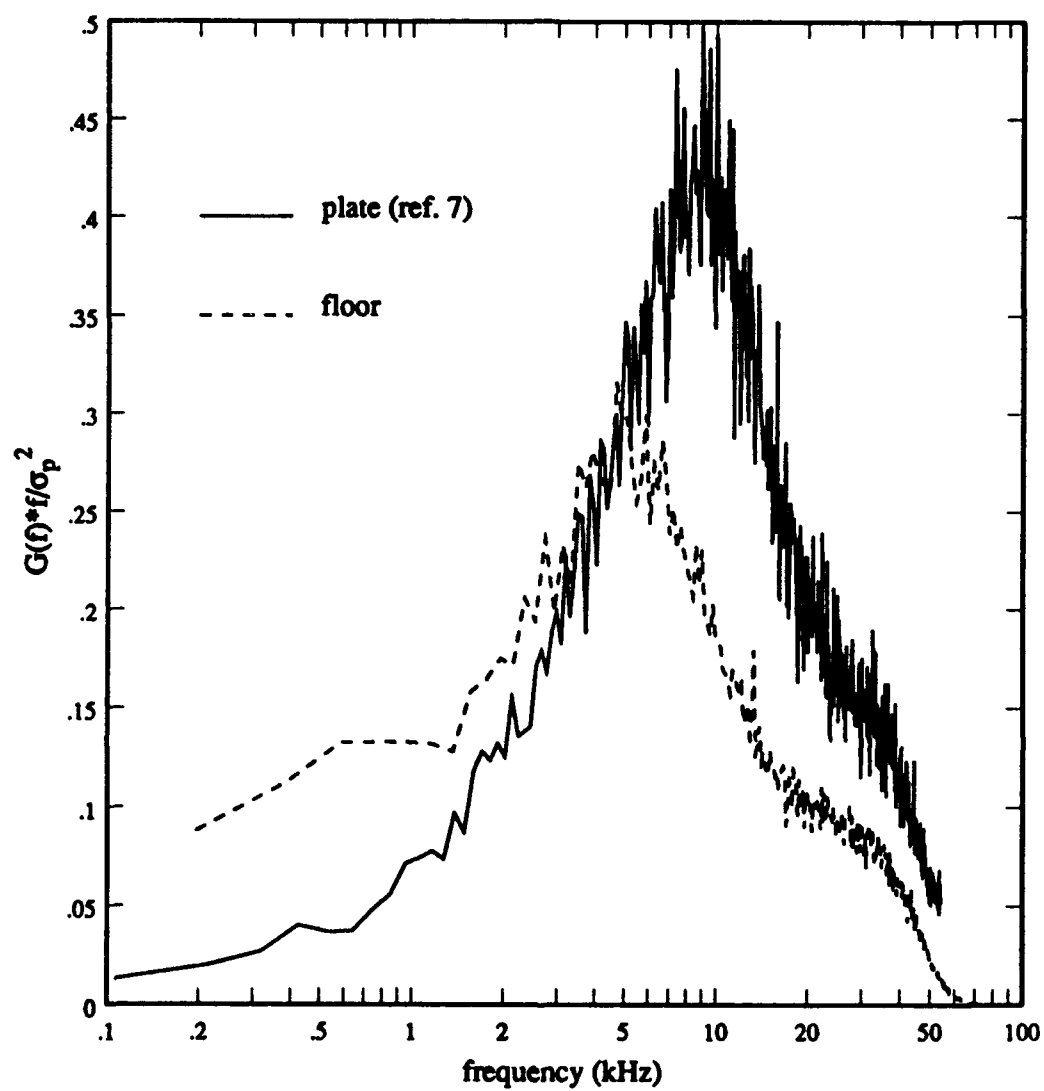
Fig. 74. PSDs at Maximum RMS for 18 deg. Interactions

134

Note: Plate data is vertically offset 0.1 units

——— plate, δ = 0.721 cm (ref. 7)
- - - - floor, δ = 1.51 cm
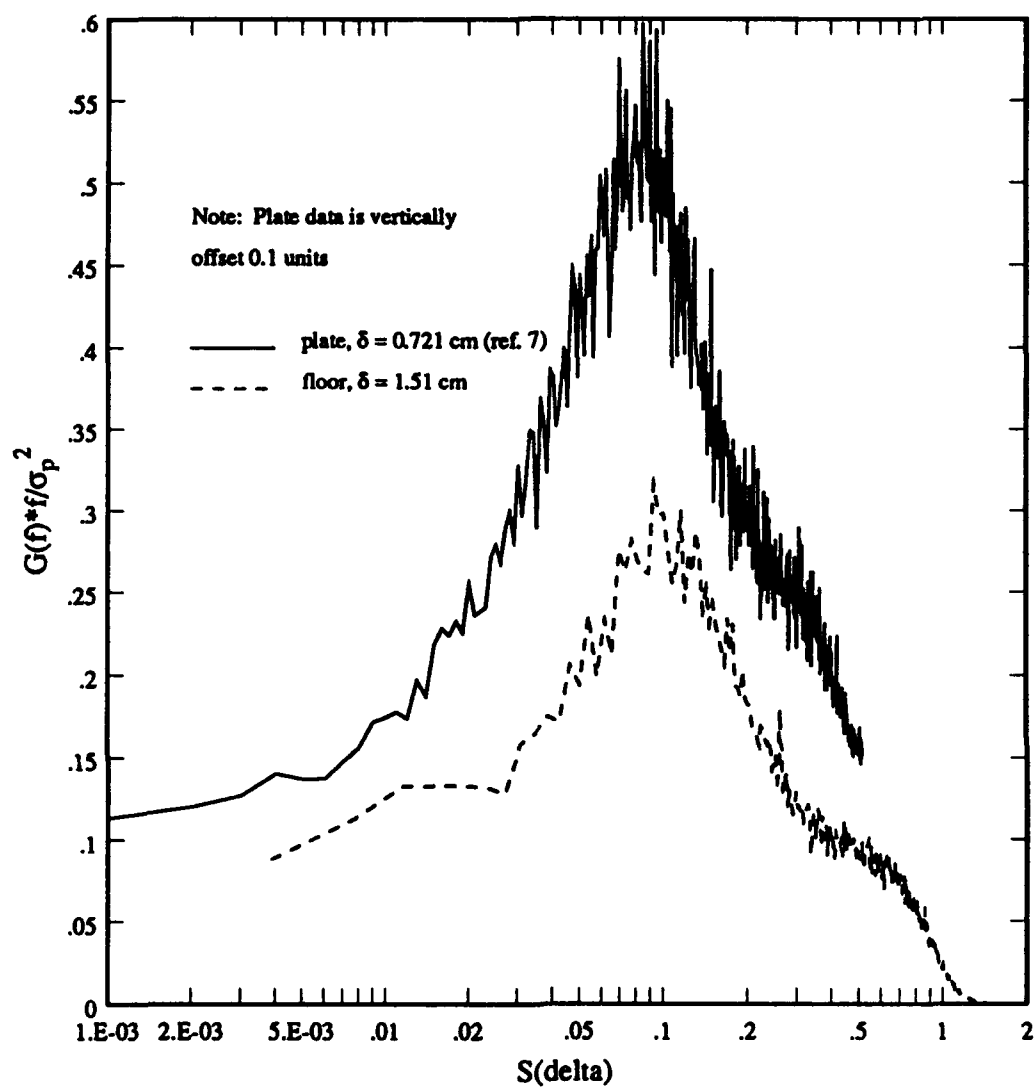
Fig. 75. Power Spectra Vs. Strouhal Number

135
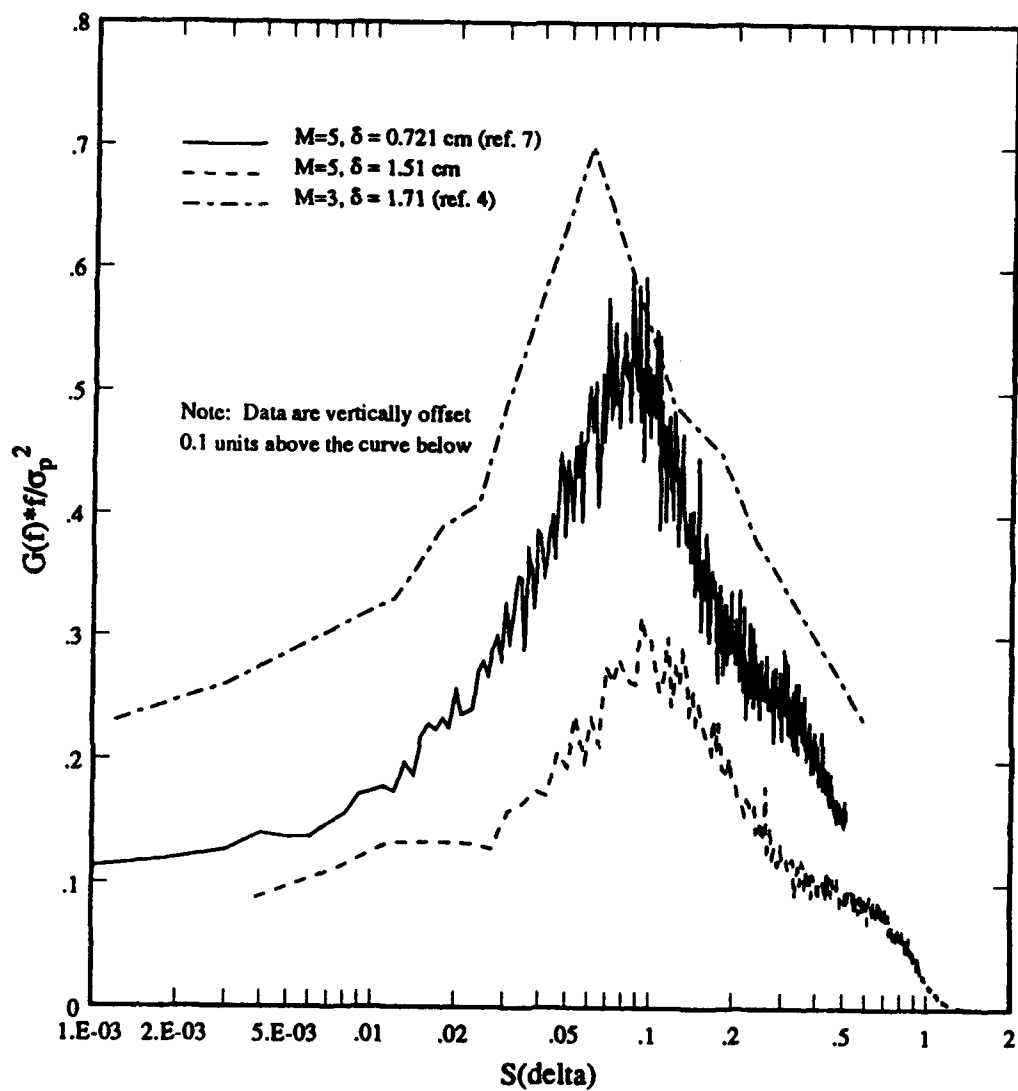
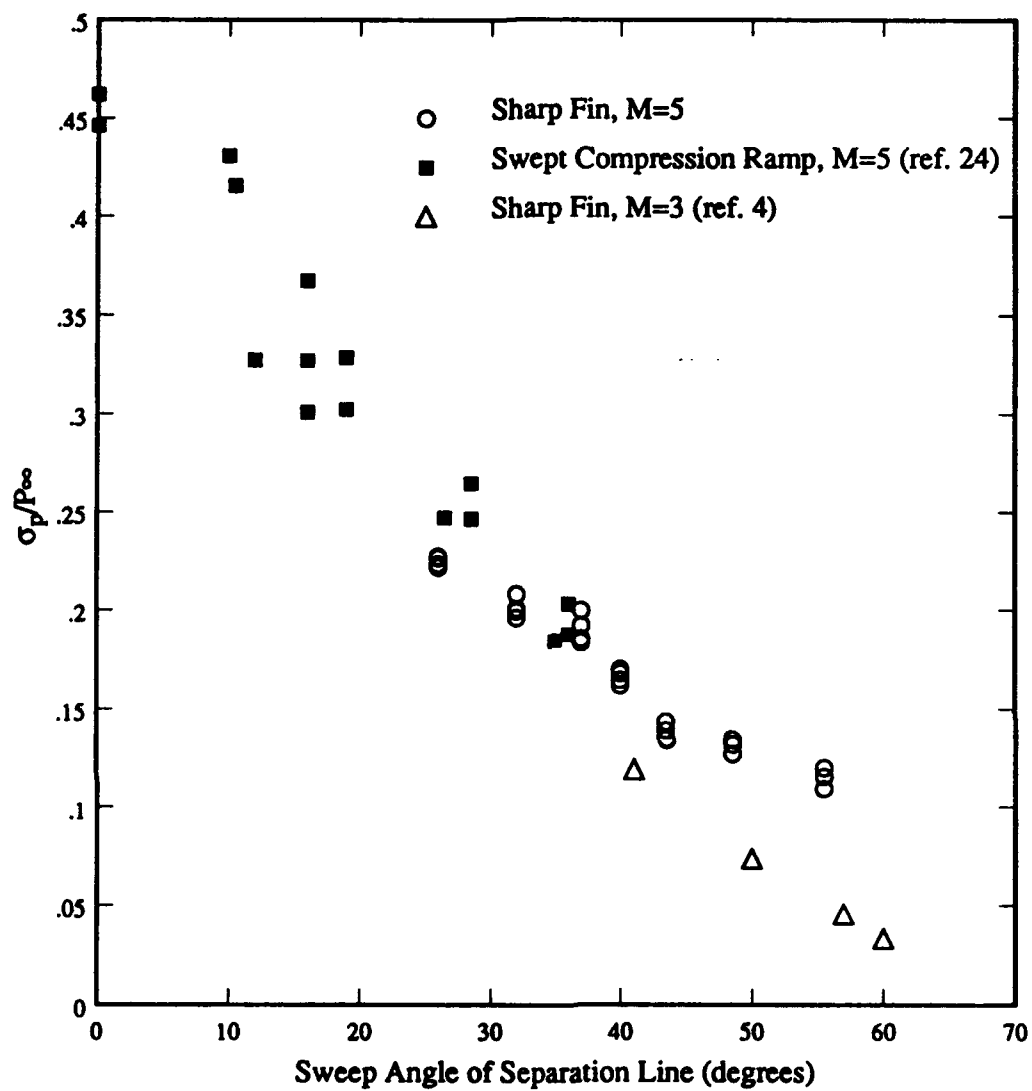Fig. 76. Power Spectra Vs. Strouhal Number at M = 3 and 5

136

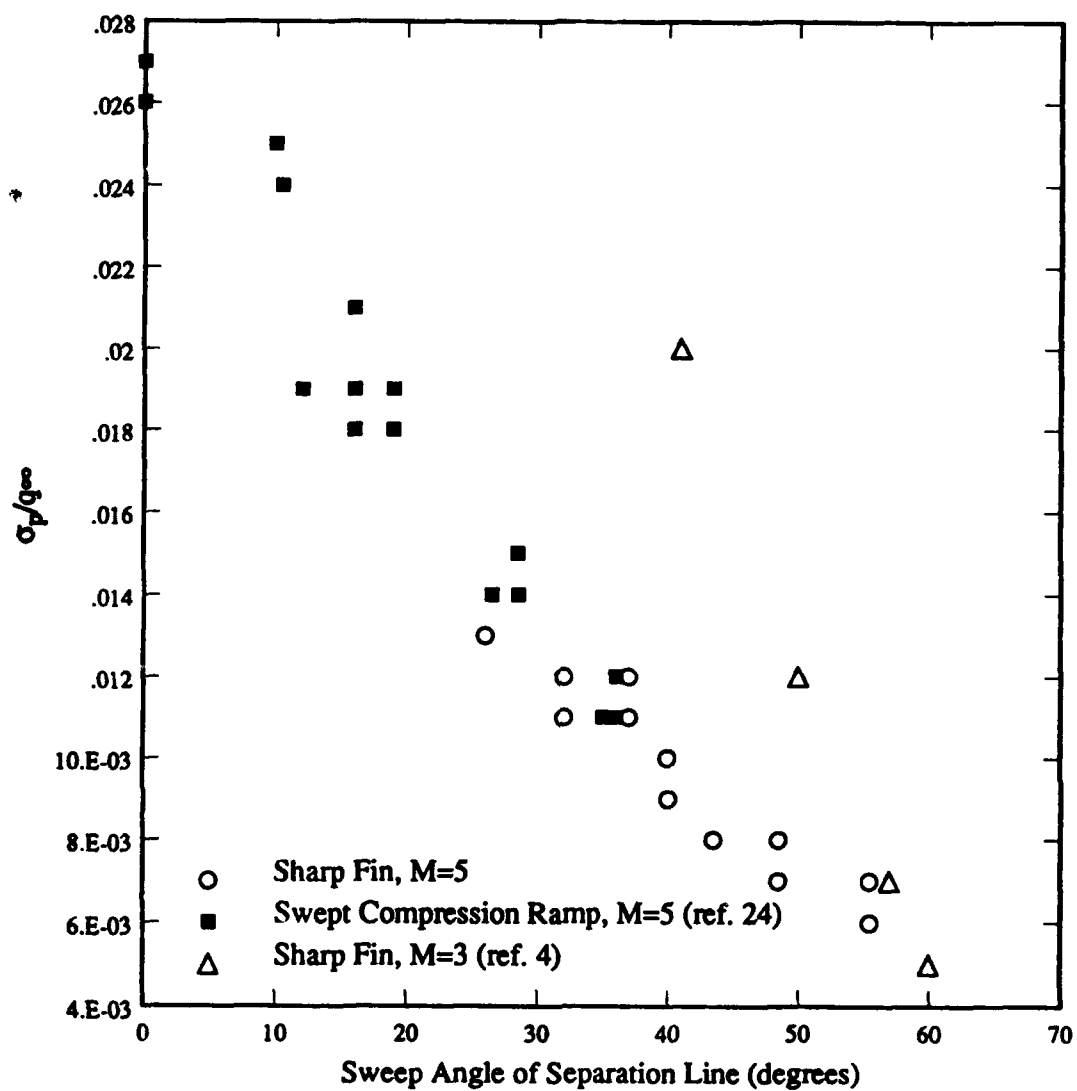Fig. 77. Maximum RMS Normalized by Freestream Static Pressure

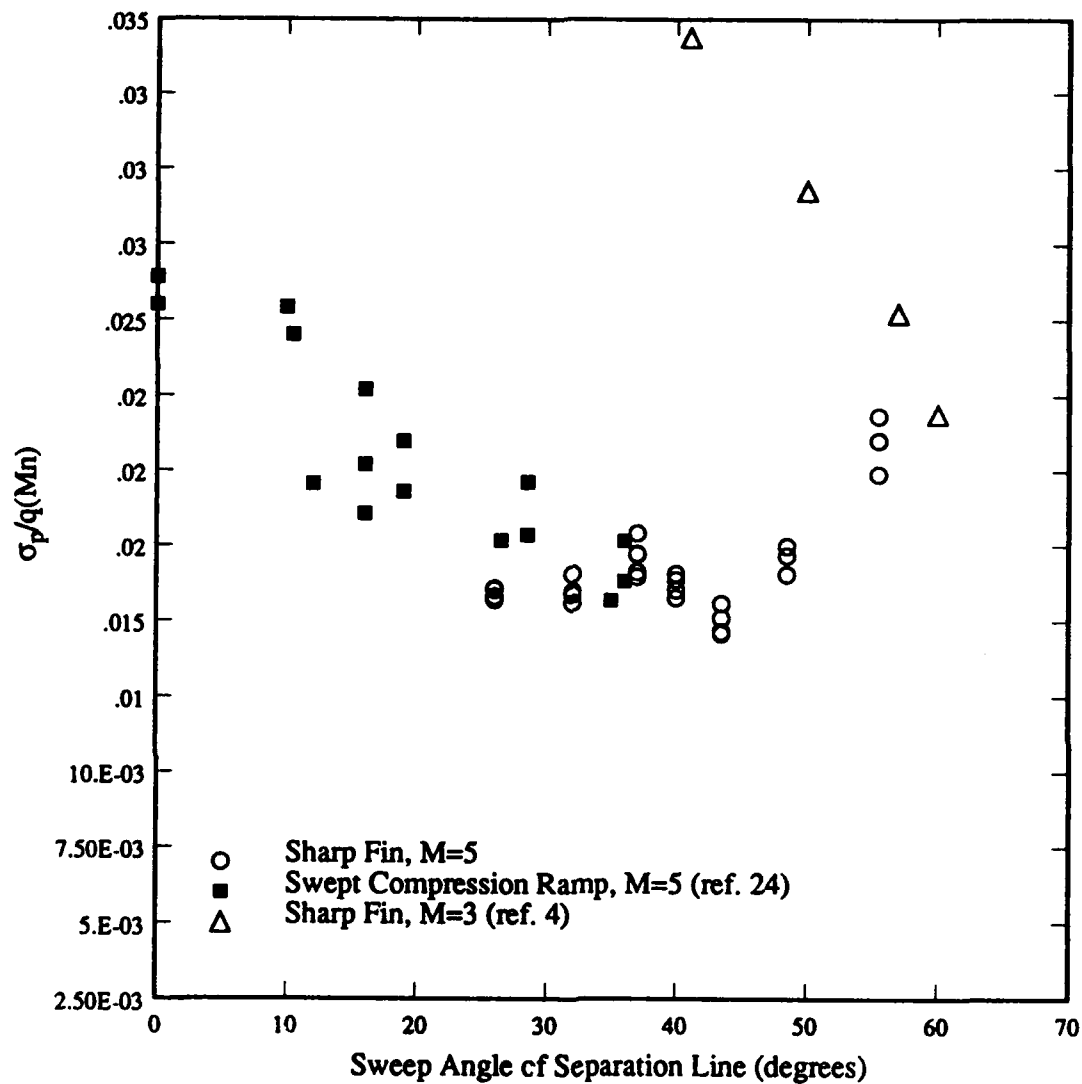Fig. 78. Maximum RMS Normalized by Freestream Dynamic Pressure

Fig. 79. Maximum RMS Normalized by Dynamic Pressure
Calculated Using Normal Mach Number

139